ISAS - INTERNATIONAL SCHOOL
FOR ADVANCED STUDIES

THE ASTROPHYSICAL ORIGIN OF THE s–ELEMENTS

Thesis submitted for the degree of
"Philosophiae Doctor"

Astrophysics Sector

Candidate:

Claudia Maria Raiteri

Supervisors:

Prof. Dennis Sciama
Prof. Roberto Gallino

October 1991

SISSA - SCUOLA INTERNAZIONALE SUPERIORE DI STUDI AVANZATI
TRIESTE
Strada Costiera 11

TRIESTE

THE ASTROPHYSICAL ORIGIN OF THE s–ELEMENTS

Thesis submitted for the degree of

"Philosophiae Doctor"

Astrophysics Sector

Candidate:

Claudia Maria Raiteri

Supervisors:

Prof. Dennis Sciama

Prof. Roberto Gallino

October 1991

Contents

Chapter 1

PREFACE

In this thesis we shall treat the astrophysical origin of the *s–process*. The subject, that can at first sight appear as very specific, is actually very wide, so that we shall concentrate on one aspect, that is we shall consider mainly the *s*–process which occurs in massive stars (MS), leading to the so–called *weak component*.

The aim is to reach a consistent picture that can explain the solar distribution of the *s*–isotopes belonging to the weak component, as well as interpret the observation of chemical abundances in the atmospheres of stars of different metallicity. The comparison with such empirical data is a way to test the validity of the theoretical predictions. Indeed, the solar abundances are in most cases well known, with typical uncertainties of about 10 %, while the latest improvements of the observational techniques using high resolution spectroscopy can provide us with abundance determinations within 0.1–0.2 dex.

In Chapter 2 we recall the main ideas on the nucleosynthesis of the heavy nuclei, with a particular care to what happens in the stellar interiors during both the hydrostatic and the explosive stages. Then, in Chapter 3, we point our attention on the *s*–process, starting with a description of its phenomenology, as given by the so–called classical analysis. It is seen how the main parameters playing in the game of neutron captures can be derived through a detailed study of the branchings on the *s*–path. In the same Chapter the possible astrophysical sites for the three components of the *s*–process are reviewed, and the contributions given by our group to model the main and the strong component are presented. These involve a detailed model for the nucleosynthesis occurring in low mass stars (LMS) in the thermally–pulsing Asymptotic Giant Branch (TP–AGB) phase of their evolution, that has proved to fairly account for the *main component* in the solar–system. Moreover, the results of such calculations are able to lead to a good interpretation of some meteoritic anomalies found in SiC grains, as well as to a satisfactory fit of the abundances observed in peculiar red giants.

We have also presented a suggestion for the possible origin of the *strong component*, that might be confirmed by the observations in the near future.

In the further Chapters of the thesis we deal with the *s*–process occurring in massive stars. We thus start by studying the evolution of a typical massive star of 25 $M_\odot$ with a hydrostatic numerical code. The calculation is followed from the Zero Age Main Sequence up to central carbon exhaustion. With the computed model we first analyze the neutron capture nucleosynthesis during convective core He burning. This is commonly believed to be the most probable site to account for the production of the *s*–nuclei from Fe to Sr. An inspection of the effects due to the variation of some critical reaction rates such as the $^{12}C(\alpha,\gamma)^{16}O$ and $^{22}Ne(\alpha,n)^{25}Mg$ ones is done, and the possibility of a propagation of uncertainties caused by some badly determined neutron–capture cross sections is underlined.

Then we investigate if subsequent nuclear stages can give some contribution to the *s*–synthesis. Since the evolutionary code we had is not able to describe what happens in the star at later stages, we considered stellar models from the current literature for a whole range of massive stars (10–50 $M_\odot$), and saw that in some cases the region where the *s*–process has occurred during He burning is swept by a convective C–burning shell. Here, an additional episode of neutron–capture synthesis can occur, giving a characteristic signature to the matter that is eventually ejected in the interstellar medium when the star explodes as a supernova.

The problem of estimating the right amount of ejected matter that has suffered He–burning or He–burning + C–burning in each star is not easy, and one has to carefully analyze the models. In particular, it is important to take into account the fact that after C–burning, other nucleosynthetic stages follow: Ne, O, Si and explosive burnings, all leading to the photodissociation of the heavy nuclei. This means that every star of given mass is characterized by its own composition of the ejecta.

The *s*–contributions from a whole generation of massive stars must then be weighted by an Initial Mass Function on the basis of a model for the galactic evolution, in order to derive the *s*–yields from massive stars. This is done in Chapter 5. But to fit the solar distribution of *s*–isotopes with atomic mass $60 < A < 90$ we also need the *s*–contributions from low mass stars, since in the atomic mass region we are concerned with both components are actually effective. Moreover, some *s*–only nuclei are also marginally produced by the *p*–process. As a conclusion, if we want to fit the solar abundances of these nuclei, we must sum all the three contributions. Despite all the uncertainties involved, it is found that our calculations can reproduce the solar values in a very satisfactory way, so that we can conclude that *massive stars can fairly account for the weak component.*

A comparison with the findings of the phenomenological approach can be performed, stressing the importance of taking into account the dynamic astrophysical prescriptions in order to have a reliable interpretation for the weak component.

The good fit to the solar *s*–abundances can be considered like a normalization point to start for an investigation of the behaviour of the weak component as a

function of metallicity. In Chapter 6 we performed calculations of neutron captures for metallicities lower than solar, and inferred the global trend of the mechanism as a function of time. It is found that the *s–process in massive stars can be considered as secondary–like down to a metallicity [Fe/H]*~ -2, but then its efficiency sharply decreases, so that no *s*–process is thought to be effective during the early evolutionary stages of the Galaxy. The observations of abundances in metal poor stars could in principle confirm this result. However, an easy confrontation is not possible and many difficulties arise, deriving from the fact that no isotopic information is available, and there are no *s*–only *elements* that can allow for a direct comparison between the observations and the theoretical predictions. Indeed, elements with mass number in the domain of the weak component receive contributions from various production mechanisms that are, besides the *s*–process from both massive stars and low mass stars, the *r*–process or equilibrium as well as explosive burning nucleosynthesis (the *e*–process). Each contribution with its own evolutionary story must be individuated if one wants to understand the behaviour of the element as a function of time.

As for the *r*–process, we can estimate the *r*–residuals by subtracting the *s*–abundances from the solar ones. The site of this process is still under debate, but the widely accepted one is attributed to the last stages of massive stars evolution, maybe in the less massive range. On the other hand, the *e*–contributions can derive from both type I and type II supernovae, and it is essential to discriminate between these two sources, because each of them has a different evolutionary timescale. Unfortunately, the available models of supernova nucleosynthesis are still affected by large uncertainties, but nonetheless they can give us first approximation indications on the production efficiency.

An interpretation of the observed abundances in stars of metal content lower than the solar one is attempted, leading to encouraging results, a more precise analysis having to rely on a detailed model of chemical evolution for the Galaxy. An analysis is presented in which our nucleosynthetic prescriptions for Cu and Zn are coupled to such a model, to see if the recent observations of these two elements can be explained by the theory. The first hand results we have now are suggesting that the picture we have settled so far has a fair degree of confidence.

Chapter 2

NUCLEOSYNTHESIS OF THE HEAVY NUCLEI

2.1 INTRODUCTION

One of the most fashinating subjects in astrophysics is the study of how and when the various nuclei which form the matter in the Universe were synthesized, and to trace the evolution of their abundances as a function of time. It involves many related topics, spanning from cosmology, to stellar evolution, to nuclear astrophysics, to stellar spectroscopy, requiring a lot of interdisciplinary effort.

Three main sources of nucleosynthesis can be envisaged:

- PRIMORDIAL NUCLEOSYNTHESIS. After $\approx$ 100 s after the Big Bang, the physical conditions of the early Universe were such as to allow the production of D, ^{3}He, ^{4}He, and ^{7}Li. The comparison between the predicted abundances of these isotopes with observational data can in principle put constraints on quantities of cosmological and particles physics interest, as the baryonic density and the number of lepton families. In fact, the possibility of the existence of one additional neutrino type beyond the known three begins to produce an overabundance of ^{4}He (Yang et al., 1984). Moreover, the ratio η between the number of baryons (protons and neutrons) and the number of photons must be confined in a narrow range in order to match all the chemical abundances (Yang et al., 1984): D/H $\approx 10^{-5}$; ^{3}He/H $\approx 10^{-5}$; ^{4}He/H ≈ 0.08; ^{7}Li/H $\approx 10^{-10}$. This range goes from 3 to 6×10^{-10} and implies a total baryon density that is lower than the critical density to close the Universe ($\Omega_B = \rho_B/\rho_c \leq 0.2$, where ρ_B is the baryon density, and ρ_c the critical one). This happens in the standard model for primordial nucleosynthesis, but an alternative scenario has recently been developed, starting from the analysis of the phase transition between normal, hadronic matter and quark–gluon matter. According to this picture, baryon density fluctuations could arise $\approx 10^{-5}$ s after the Big Bang. Neutrons and protons would separate because of the different mean

free path, leading to the fragmentation of the Universe into neutron–rich and neutron–poor regions. In this case the abundances of D, ^{3}He and ^{4}He could be reconciled with $\Omega_B = 1$, but ^{7}Li is strongly overproduced. The difficulty can be overcome when dynamic effects are considered. Indeed, if one takes into account the overlap between the proton–rich and the neutron–rich regions during the epoch of the nucleosynthesis, a late diffusion of neutrons from the neutron–rich back into the proton–rich region occurs. Such a diffusion can significantly reduce the ^{7}Li abundance to levels consistent with observations of population I and population II stars. One interesting point in this non standard model is the possibility of heavy elements production (Applegate, Hogan and Scherrer, 1988; Malaney and Fowler, 1988). Actually, a first chain of nuclear reactions leads to the synthesis of ^{14}C:

$$H(n, \gamma)^2H(n, \gamma)^3H(d, n)^4He(t, \gamma)^7Li(n, \gamma)^8Li$$

$$^8Li(\alpha, n)^{11}B(n, \gamma)^{12}B(\beta)^{12}C(n, \gamma)^{13}C(n, \gamma)^{14}C.$$

The effectiveness of this sequence has recently received a strong support by the new experimental determination of the ^{8}Li(α, n) reaction rate, which was previously very uncertain (Rolfs, 1991; private communication). ^{14}C ultimately decays into ^{14}N. However, some ^{14}C can be processed into ^{22}Ne via:

$$^{14}C(\alpha, \gamma)^{18}O(n, \gamma)^{19}O(\beta)^{19}F(n, \gamma)^{20}F(\beta)^{20}Ne(n, \gamma)^{21}Ne(n, \gamma)^{22}Ne.$$

Starting from this ^{22}Ne, a certain amount of iron–peak nuclei could be synthesized, providing the seeds for an r–process (see below), which would be sustained by a series of fission cycles. It was found that with a convenient choice of parameters, the r–abundances observed in metal–poor stars might be accounted for. The above picture for the primordial nucleosynthesis would explain why we do not observe zero–metallicity stars in our Galaxy. Although this scenario is very interesting, the bulk of the heavy elements in the Galaxy must be ascribed to the nucleosynthesis occurring inside the stars.

- GALACTIC COSMIC RAYS. Based upon simple arguments concerning the relative abundances of the elements and relevant nuclear reaction cross sections, it can be demonstrated that the synthesis of Li, Be and B is dominated by collisions of protons and α particles with ^{4}He, ^{12,13}C, ^{14}N and ^{16}O nuclei. The most likely astrophysical site in which this can happen is spallation of galactic cosmic rays on the interstellar matter (Walker, Mathews and Viola, 1985).

- STELLAR NUCLEOSYNTHESIS. The other elements are believed to be produced by nuclear reactions taking place inside the stars. In particular, the lighter elements, that is those up to Fe, are essentially synthesized through fusion reactions in different stages of stellar evolution, up to nuclear statistical equilibrium and explosive processes (the combination of these latter will

generically be called the "e–process" furtheron). On the other side, the elements heavier than Fe are chiefly obtained by neutron captures on seed nuclei (the s– and r– processes), with minor contributions by proton capture and/or photodissociation (the p–process). This idea is supported by the fact that the nuclear binding energy has a maximum for Fe, and hence Fe disruption is very energy–consuming. Moreover, energy barriers at high Z make the production of heavy nuclei through charged–particle reactions very difficult. All the material that has been synthesized inside the stars can be mixed up to the surface and chemically enrich the interstellar medium thanks to various expulsion mechanisms such as mass loss by stellar winds, ejection of a planetary nebula, or a supernova explosion.

In the next Section an outline of the most important nucleosynthetic processes occurring inside the stars will be presented, including the hydrostatic as well as the explosive stages. The main characteristics of neutron–capture processes and γ–process will also be reviewed.

2.2 STELLAR NUCLEOSYNTHESIS

2.2.1 Hydrostatic Stages

During the hydrostatic stages of thermonuclear burning, reactions occur on long time scales, involving stable nuclei. In the following we shall outline the different subsequent phases, with the main reactions involved:

- *H–burning*: conversion of H into ^{4}He through the pp–chain and/or the CNO–cycle; in this last case C, N, O seeds are needed and because of the different reaction time scales involved, they are completely converted into ^{14}N;
- *He–burning*: the main reactions are $\alpha(2\alpha,\gamma)^{12}$C and ^{12}C$(\alpha,\gamma)^{16}$O, the rate of this latter being still poorly known. As a consequecence, the ratio C/O at the end of He–burning is not well determined, and this introduces uncertainties in the further evolution of the star;
- *C–burning*: ^{12}C burns essentially through ^{12}C$(^{12}$C, $\alpha)^{20}$Ne and ^{12}C$(^{12}$C, p$)^{23}$Na, releasing α particles and protons. Most of the ^{23}Na is processed as ^{23}Na(p, $\alpha)^{20}$Ne;
- *Ne–burning*: ^{20}Ne$(\gamma,\alpha)^{16}$O; ^{20}Ne$(\alpha,\gamma)^{24}$Mg; ^{24}Mg$(\alpha,\gamma)^{28}$Si;
- *O–burning*: ^{16}O$(^{16}$O, $\alpha)^{28}$Si; ^{16}O$(^{16}$O, p$)^{31}$P; ^{16}O$(^{16}$O, n$)^{31}$S$(\beta^+)^{31}$P. Most of the ^{31}P is destroyed by (p, α) reactions to ^{28}Si;
- *Si–burning*: it involves photodissociation reactions that liberate particles which are captured again by nuclei, leading to the synthesis of iron–peak isotopes;
- *NSE*: when the temperature is high enough ($T_9 \sim 5$), a thermodynamic equilibrium is reached, with an equilibrium abundance distribution around Fe. It is common to refer to this phase as NSE (Nuclear Statistical Equilibrium); the physical conditions needed to have NSE are found either in the inner layers of a type II supernova (SNII) close to the mass cut that separates ejecta from the young neutron star, or in the interior regions of white dwarfs models exploding as type I supernovae (SNI). Model–independent calculations of NSE distributions were carried out by Hartmann, Woosley and El Eid (1985), at a typical freeze–out conditions (freeze–out is reached when nuclear transmutation stops because of the decrease of the temperature), for a variety of neutron excesses:

$$\eta = \sum_i \frac{N_i - Z_i}{A_i} X_i.$$

They found that the best situation to fit the nucleosynthesis constraints is a multizone mixing scenario where the chemical abundances are averaged over the interval $(0, \eta_{max})$ with $0.165 \leq \eta_{max} \leq 0.175$.

2.2.2 The *s*–process

The *s*–process nuclei are built up starting from Fe seeds along the valley of stability in the chart of nuclides (Figure 2.1): stable nuclei capture neutrons on long timescales ($10^2 - 10^3$ yr), while unstable isotopes usually decay, because they have beta decay rates greater than their neutron capture rates.

At some points in the chain however, there are nuclei whose rates are comparable; in this case a *branching* on the *s*–process path occurs. Here the competition between capture and decay depends upon the physical conditions, and so the study of branching points can give information on the neutron density, the temperature, and the electron density during the nucleosynthetic event, and also test the kind of neutron irradiation that was responsible for it.

In the classical scenario this "slow" neutron capture process happens when neutron densities are small ($\sim 10^8$ cm^{-3}), as it is found during the hydrostatic He–burning phases of stellar evolution. Actually, the *s*–process is a composite mechanism, that involves three components and different astrophysical sites, as will be discussed furtheron in this thesis.

If we look at the plot of the solar–system abundances versus atomic number (Figure 2.2), peaks are found when isotopes with a "magic" number of neutrons: $N = 50$, 82, 126 are considered. These nuclei have particularly stable nuclear configurations, with closed neutron shells. As a consequence, they have small cross–sections and act as bottlenecks for the neutron flow, building up large abundances when experiencing a neutron exposure. The accuracy with which these small cross sections are determined is crucial to understand how the *s*–chain develops.

2.2.3 Explosive Stages

In order to study the explosive nucleosynthesis, reaction rates on unstable nuclei have to be known. These are very difficult to measure experimentally, so that most of the cross sections are predicted on the basis of statistical model calculations, with typical errors of a factor 2. It goes without saying that the resulting picture is affected by a large uncertainty. Explosive nucleosynthesis occurs in novae and X–ray bursts, and in type I and type II supernovae.

The classical scenario for SNI deals with a CO white dwarf which is part of a binary system. The CO white dwarf is thought to be the endpoint of the evolution of a star with mass M $\leq$ 8 M$_\odot$, and is accreting mass from the companion. When the amount of transferred matter has reached a critical point, ignition will occur under degeneration conditions, and cause a thermonuclear runaway. Since the initial configuration of every SNI is the same, that is the starting mass corresponds to the Chandrasekhar's mass (M $\sim$ 1.4 M$_\odot$), the nucleosynthesis will be roughly constant. The explosion mechanism can essentially follow two paths: carbon detonation or carbon deflagration. In the first case the burning front propagates in a supersonic way, while in the second one the propagation is subsonic. The results

of the nucleosynthesis tend to favour the carbon deflagration scenario, even if some difficulties are still present, that are probably due to the fact that only parametric studies of the mechanism have been done up to now (Thielemann, 1989).

Figure 2.3 indicates the physical conditions (maximum temperature and density) attained during the propagation of the deflagration front as a function of the radial mass coordinate. Zones of different explosive burning conditions are indicated.

Figure 2.4 displays the resulting nucleosynthesis after explosive processing: in the inner 0.8 $M_\odot$ only Fe–group nuclei are produced.

In order to understand the chemical abundances in our Galaxy, we must know the composition of the supernova ejecta. Figure 2.5 shows the ratio of abundances produced in such a SNI event to solar abundances, normalized to ^{56}Fe. It is evident that Fe group nuclei are produced two times more with respect to their solar values than the intermediate nuclei from Si to Ca. The major problem in these calculations is the strong overabundance of ^{58,62}Ni and ^{54}Fe. Let us stress again that the same chemical pattern should characterize the ejecta of every SNI.

As for SNII, their progenitors are believed to be massive stars ($M \geq 8\ M_\odot$), that end their evolution with central Fe–cores. Gravitational collapse, core bounce and propagation of a shock wave are the mechanisms that lead to the explosion. We shall not enter the details of such a process, but concentrate on the explosive nucleosynthesis instead (Thielemann, 1989).

The passage of the shock front through the Si, O, Ne, C, He and H burning shells increases the temperature and density and accelerates the nuclear reactions, as well as makes possible additional reactions. In the following we shall present the case of a star with a He core of 6 $M_\odot$ studied by Nomoto and Hashimoto (1988) and by Thielemann, Hashimoto and Nomoto (1990); it corresponds to a star of roughly 20 $M_\odot$ on the Main Sequence. This is just the right mass that the SN1987A progenitor should have had.

Figure 2.6 shows the chemical structure of such a star after explosive processing, that is found to affect only the inner 2 $M_\odot$ of the star.

In Figure 2.7 the composition of the SN ejecta is displayed in comparison to solar abundances, normalized to ^{28}Si. However, in order to understand how the solar–system abundances can be reproduced, one has to perform an average of the contributions of a whole generation of massive stars over the Initial Mass Function. Anyway, Woosley and Weaver (1986) found that when dealing with the nucleosynthesis of the main species, a typical supernova can be identified, whose mass is in the range 20–30 $M_\odot$. As Figure 2.7 shows, nuclei heavier than P are on average produced by a factor of 2 to 4 less than ^{28}Si. They are due to explosive processing, while all elements lighter than P originate from hydrostatic burning. The overabundances of ^{58,61,62}Ni are strongly dependent on the position of the mass cut. The problem is that with an artificially induced shock wave we do not know where the correct mass cut between the ejecta and the neutron star remnant is. In order to match the total amount of ^{56}Ni estimated from observations of SN1987A, i.e.

0.07 ± 0.01 $M_\odot$, in the 20 $M_\odot$ model the mass cut must be at roughly 1.6 $M_\odot$.

2.2.4 The r–process

On the contrary, astrophysical sites must exist where "rapid" neutron captures on a time scale of some hundred milliseconds lead to the formation of very neutron–rich nuclei, that undergo a series of beta decays towards the stability valley as soon as the neutron irradiation stops. This is the mechanism of the r–process which requires large neutron densities ($\sim 10^{20}$ cm^{-3}) and for which three main astrophysical sites have been suggested:

- the very neutronized mass zones close to the mass cut between the neutron star and type II supernova ejecta, which obtained a high neutron to proton ratio due to electron captures during the collapse. The fact that no stellar supernova model has shown to contain regions where a sufficiently high neutron excess can be reached (Thielemann, Hashimoto and Nomoto, 1990) to reproduce the solar r–abundances has led to the suggestion that only a small range of massive stars (around 10 $M_\odot$) might actually be responsible for the r–process (Mathews and Cowan, 1990). This can have important implications from the point of view of the chemical evolution of the Galaxy, as we shall see later;

- the He–burning regions where s–processing is effective; the passage of the shock front through these regions can accelerate the neutron–producing reactions, leading to quite high neutron densities. The problem here is that the calculations made so far have found that the neutron pulse is not strong enough to explain the solar r–abundances;

- the expelled material during neutron star collisions or disruptions: during the expansion, in the neutronized matter the density decreases and neutrons can decay into protons, allowing for the build–up of heavy elements in the Fe–group. These are still sorrounded by free neutrons, and can act as seeds for the r–process.

Let us notice that the last two scenarios imply a delayed activation of the r–process, since either the production of s–seeds or the formation of neutron stars has to be awaited. On the contrary, we know that the r–process must have been active from the very early stages of galactic evolution, because there are observations of r–elements in very metal–poor stars. Indeed, the first scenario that has been presented above, implying a "primary" nature for the r–process (a concept that will be discussed in details in Chapter 6), appears to be the most likely one.

The nuclear information needed in order to perform r–process calculations includes neutron–capture cross sections, beta decays, beta–delayed neutron emission rates, and for nuclei with $Z > 80$ also beta–delayed fission and neutron–induced fission rates. Up to now there exists only very sparse experimental information about

nuclei in the r–process path, and this again implies a certain amount of uncertainty on the whole picture. Presently, the best way to determine the r–contributions to the solar–system abundances of stable isotopes is through the s–analysis. Indeed, r–residuals can be estimated by subtraction of the s–contributions from the solar values.

As for the phenomenology of the process, the r–isotopes with a magic neutron number have longer half–lives because they are more stable, so they pile up and determine the r–peaks in Figure 2.2 that slightly precede the s–peaks.

2.2.5 The p–process

There are also some proton–rich nuclei that are out of reach from both s– and r–processes. They are attributed to the so–called p–process, where *"p"* stands for proton–capture and/or photodisintegration. Since it has been demonstrated that is very difficult to produce the heaviest p–isotopes through proton–captures, the most likely scenario is the so–called *"*γ*–process"*, that is nuclear photodisintegration involving (γ , n), (γ , p), and (γ , α) reactions. The possible astrophysical sites that have been envisaged so far are the following:

- explosive H burning (Audouze and Truran, 1975);
- hydrostatic O burning in massive stars (Arnould, 1976);
- explosive O burning in type II supernovae (Woosley and Howard, 1978);
- type I (or certain type II subclasses) supernovae exploding through C deflagration (or detonation) (Howard, Meyer and Woosley, 1991).

The last three mechanisms start on s–seeds left in the interiors of the stars by the s–process that took place during He burning.

One major problem affecting the results of the p–nucleosynthesis is the strong dependence of the results on the temperature, that generally goes from 2 to 3 $\times 10^9$ K: with a low T only the heaviest p–nuclei can be obtained, while a high T can produce the low mass ones; but if T is too large, everything can be dissociated. Moreover, the process is also greatly affected by another parameter, that is the expansion time scale characterizing the explosion ($\approx$ 1 s).

In spite of the still unknown details of the process, the most recent calculations of the p–process in the oxygen burning layers of massive exploding stars by Rayet, Prantzos and Arnould (1990) have shown to fit the solar abundance p–pattern within a factor 3 for 60 % of the p–isotopes, the main difficulty concerning the underproduction of the Mo and Ru isotopes due to the lack of sufficient seeds. On the other side, the explosion of a carbon–oxygen white dwarf seems also a very promising candidate, because here we have more s–seeds. The problem of this picture is the tendency to overproduce ^{74}Se, ^{78}Kr and ^{84}Sr.

New improved calculations of the "γ–process" are still needed and are of paramount importance to estimate the p–contributions to the synthesis of the s–nuclei. At the same time, a good evaluation of the s–seeds from which the process starts is essential. In particular, Howard is now analysing the p–process from SNI using as s–seeds our prescriptions for low mass TP–AGB stars (see § 3.3).

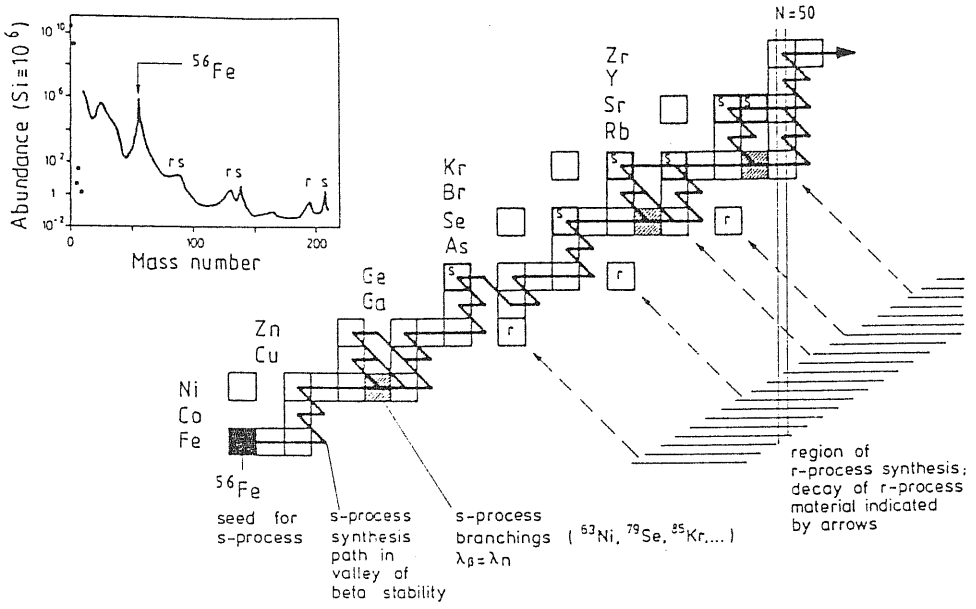

Figure 2.1: Section of the chart of nuclides for a discussion of the main features of neutron–capture nucleosynthesis

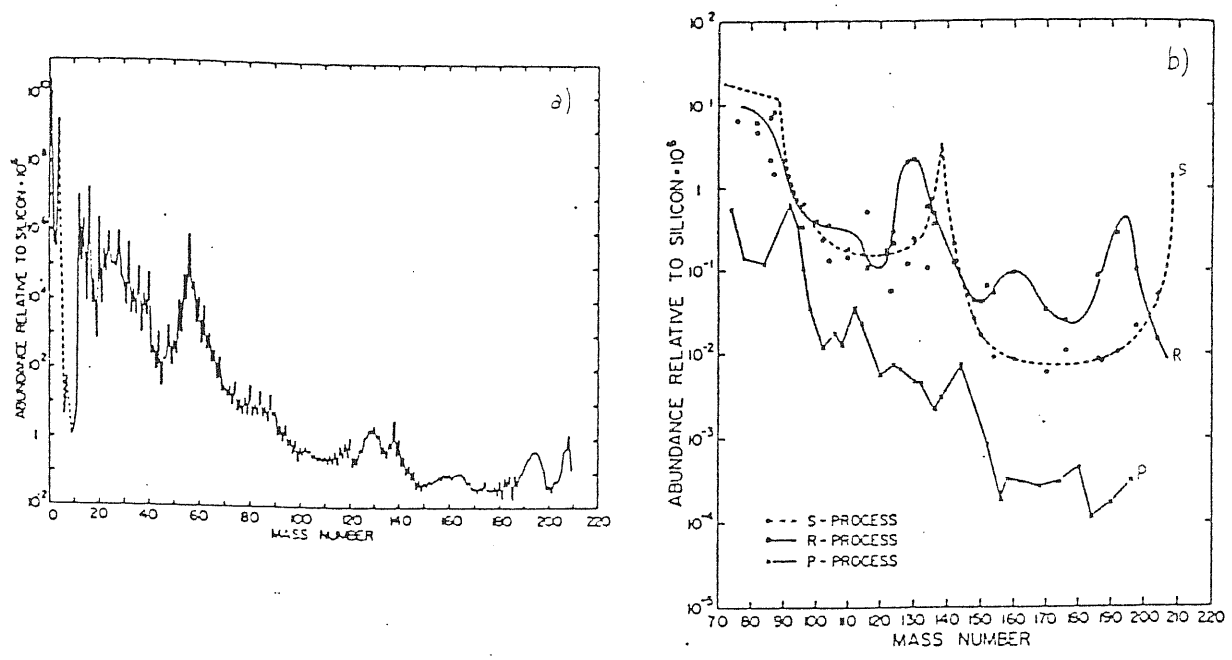

Figure 2.2: (a) Heavy–element abundances as a function of atomic mass. (b) Heavy–element abundances as a function of atomic mass approximately divided into (o)s–,(□)r– and (×)p–process contributions

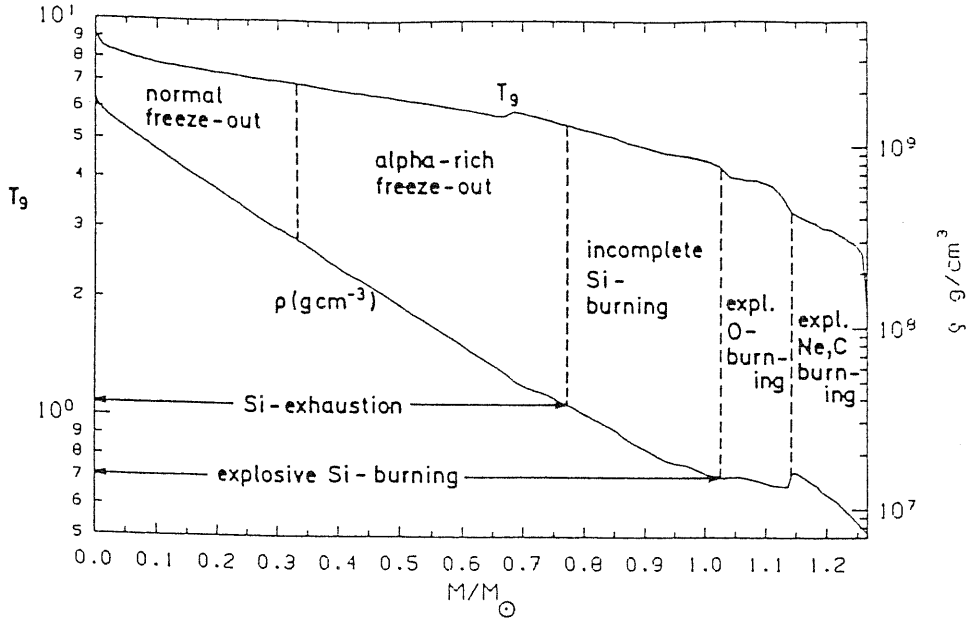

Figure 2.3: Maximum temperatures and densities attained during the propagation of the deflagration front in a SNI, as a function of the radial mass

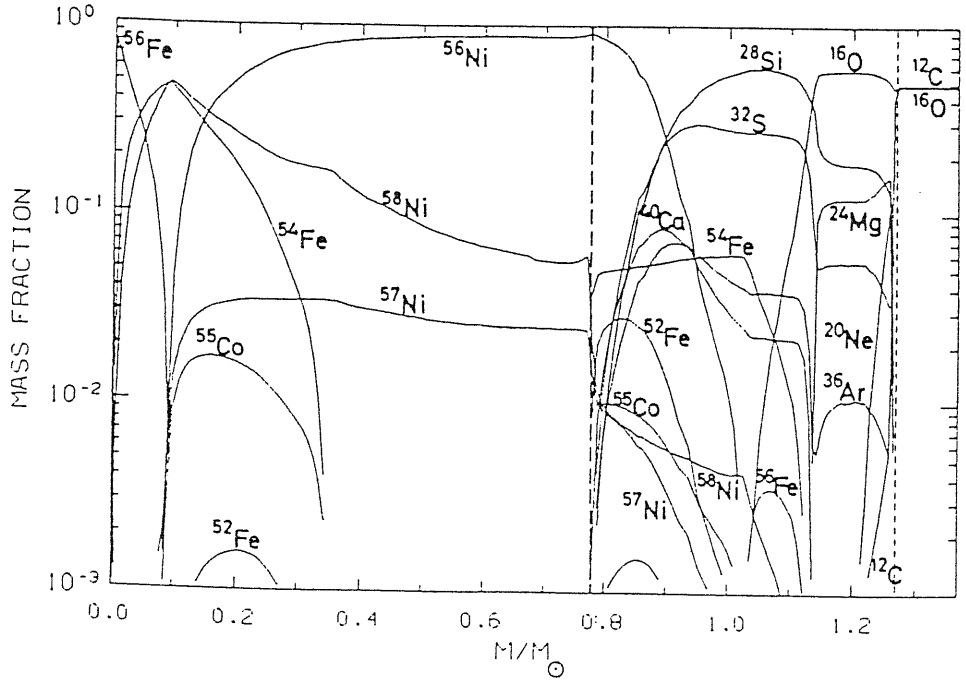

Figure 2.4: Resulting nucleosynthesis after explosive processing in a typical SNI

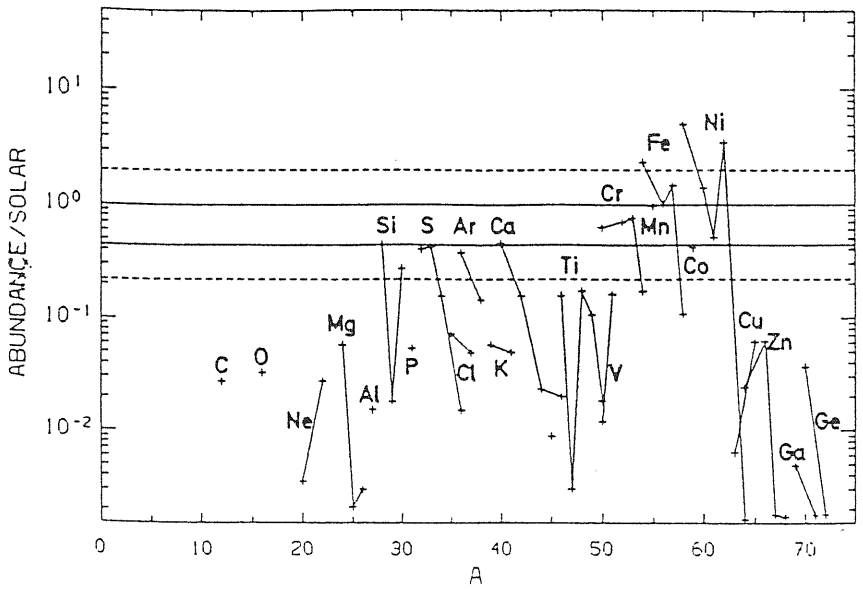

Figure 2.5: Composition of the ejecta in a typical SNI

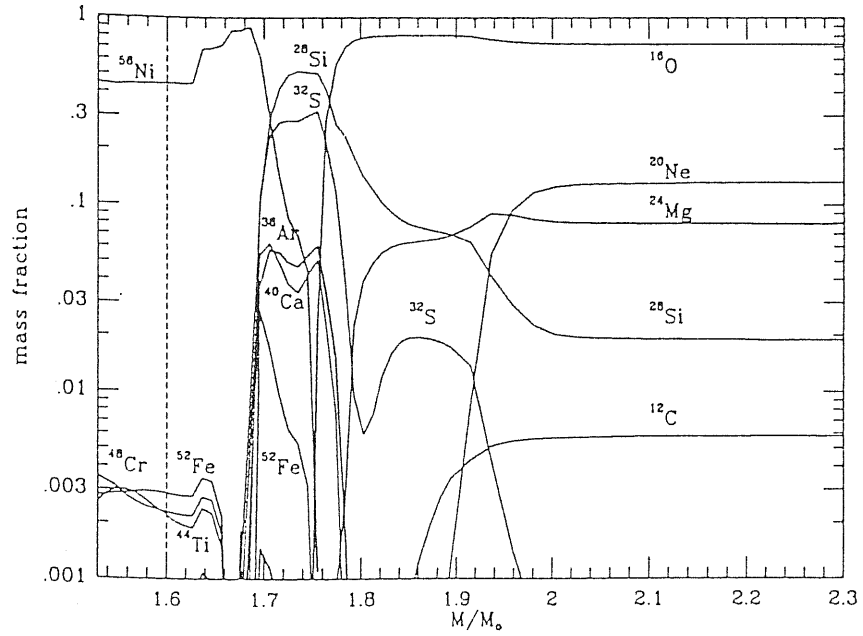

Figure 2.6: The chemical structure of the inner core of a SNII after the passage of the shock front

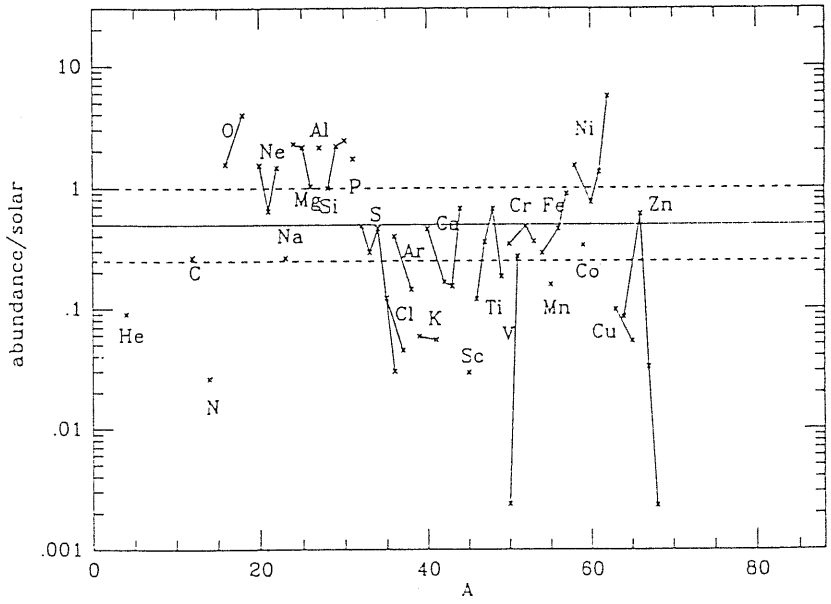

Figure 2.7: Composition of the ejecta in a typical SNII

Chapter 3

ANALYTICAL AND ASTROPHYSICAL MODELS FOR THE s–PROCESS

3.1 INTRODUCTION

In the previous Chapter we introduced the *s*–process as one of the mechanisms that can account for the production of isotopes heavier than iron. Actually, most of the heavy elements receive both *s*– and *r*–contributions, but there are specific cases of *s–only* and *r*–only isotopes. Indeed, if the cascade of beta decays following a rapid irradiation meets a stable nucleus that is out of reach for the *s*–chain, this one will be an *r*–only nucleus (see Figure 2.1). At the same time it will shield a corresponding stable isobar from the *r*–process, so that this latter will be affected only by the *s*–flow, resulting in a *s*–only isotope. The aim of *s*–process calculations in the classical context is precisely to reproduce the solar–system abundance distribution of *s*–only nuclei.

The fact that the *s*– and *r*–processes are distinct mechanisms is confirmed by the correlation existing between the product of neutron capture cross section and the solar abundance σN_s versus the atomic mass A for the *s*–isotopes, which has not the counterpart for the *r*–isotopes. Clayton et al. (1961) demonstrated that a single neutron irradiation was not suitable for reproducing the empirical σN_s curve. Some years after Seeger et al. (1965) found that an exponential distribution of neutron exposures on seed material better fitted the solar data.

With new improvements on *n*–capture cross sections and solar–system abundances, it was soon realized that three components are necessary to correctly describe the *s*–process in the solar–system (Ward and Newman, 1978):

- the *main component*, which is responsible for the synthesis of the isotopes with atomic mass number $A > 90$;

- the *weak component*, that accounts for the formation of isotopes in the atomic mass range 60–90;
- the *strong component*, that is required to reproduce the s–abundances at the lead–peak.

In the following we shall first deal with the phenomenological description of the s–process, presenting the results of the so–called *classical analysis.*

Then we shall introduce the *astrophysical models* that have been suggested so far for the three s–components. We spend only few words on s–processing in massive stars as the origin of the weak component: it will be considered in details in the following Chapters. On the contrary, the recent results obtained by our group on the main component in low mass stars on the AGB are more extensively examined. Finally, possible interpretations for the strong component are described.

3.2 THE CLASSICAL APPROACH

The classical analysis of the s–process is a phenomenological approach which treats the neutron capture mechanism according to an analytical formulation, under a set of simplified assumptions and without taking account of the astrophysical prescriptions. In the classical model any time dependence for temperature and neutron density is neglected. By this simplification, the classical approach offers an empirical tool that not only can describe the observed s–process abundances, but can also provide estimates for the mean physical conditions during the s–process. Being completely independent of stellar models, the classical analysis can be used to constrain the results obtained by them.

The first attempts to reproduce the solar–system distribution of s–only nuclei were made adopting a continuous neutron flux, with an exponential distribution of neutron exposures for all the components. Later on, single flux models for the weak and the strong components were developed.

In the following we shall briefly present the mathematical formulation on which the classical analysis is based.

3.2.1 The Exponential Exposure Distribution Model

Owing to the neutron–capture event, the abundance of an isotope with atomic weight A changes according to:

$$\frac{dN_s(A)}{dt} = \lambda_n(A-1)N_s(A-1) - [\lambda_n(A) + \lambda_\beta(A)]N_s(A), \qquad (1)$$

where $\lambda_\beta = ln2/\tau_{1/2}$ is the beta–decay rate if the nucleus A is radioactive, and λ_n is the neutron capture rate:

$$\lambda_n = n_n(t) < \sigma v >;$$

n_n is the neutron density, and $< \sigma v >$ is the product of the neutron capture cross section times the relative velocity of neutron and target, averaged over a Maxwell–Boltzmann distribution:

$$< \sigma v >= \int_0^\infty \sigma\, v\, \Phi(v)\, dv,$$

with

$$\Phi(v)\, dv = \frac{4}{(\pi)^{1/2}} \left(\frac{v}{v_T}\right)^2 exp[-\left(\frac{v}{v_T}\right)^2] \frac{dv}{v_T}.$$

v_T is the thermal neutron velocity:

$$v_T = \left(\frac{2KT}{\mu_n}\right)^{1/2},$$

with μ_n being the neutron reduced mass. Since for many nuclei the differential cross section $\sigma \sim v^{-1}$, the product σv is almost independent of the temperature, and so it is convenient to define $< \sigma >=< \sigma v > /v_T$. Usually, the maxwellian averaged neutron capture cross section is given at the reference thermal energy of 30 keV, corresponding to typical He burning conditions, where neutrons are classically believed to be released in stellar interiors. However, there are nuclei for which consistent deviations from the $1/v$ law are found. In these cases, the energy–dependence of $< \sigma >$ must be carefully examined. Recently, Beer, Voß and Winters (1991) have performed calculations of $< \sigma >$ trends for a large number of isotopes. As an illustrative example, the behaviour of ^{56}Fe cross section is shown in Figure 3.1. This kind of information is particularly important when the possibility of n–captures at temperatures far away from 30 keV is considered, as in the low temperature phase of a thermal pulse in low mass stars, or during carbon burning in massive stars (see § 3.3 and 4.4).

In order to find an analytic solution to the set of coupled differential equations (1), the classical analysis must make some assumptions:

- depending on the relative value of λ_n and λ_β, radioactive nuclei are treated as stable nuclei or they are completely neglected; branching points are treated in a separate way;
- the temperature is kept constant in order to deal with well defined cross sections and decay rates;
- a steady neutron flux is assumed.

Then, if we define the *time integrated neutron flux* τ as:

$$\tau \equiv \int n_n(t)\, v_T\, dt,$$

the system of equations becomes:

$$\frac{dN_s(A)}{d\tau} = \sigma(A-1)N_s(A-1) - \sigma(A)N_s(A), \tag{3.1}$$

and can be solved analytically in terms of an exponential distribution of neutron exposures τ of the kind:

$$\rho(\tau)\, d\tau = G\, exp(-\tau/\tau_0)\, d\tau,$$

where $\rho(\tau)d\tau$ is the number of iron seed exposed to an integrated flux τ in the interval $d\tau$. If the neutron irradiation is long enough, equilibrium between production and destruction can be reached for a large number of isotopes far from the "magic"–nuclei, and in this case equation 3.1 leads to a constant σN_s value. In a more general context, the σN_s product will be a smooth function of the atomic number, as it is found when the solar abundances are considered.

For a two–component (weak + main) distribution of the form:

$$\rho(\tau) = \frac{f_1 N_{56}}{\tau_{01}} exp(-\tau/\tau_{01}) + \frac{f_2 N_{56}}{\tau_{02}} exp(-\tau/\tau_{02}),$$

the classical (unbranched) solution is given by (Clayton and Ward, 1974):

$$\sigma(A)N_s(A) = \frac{f_1 N_{56}}{\tau_{01}} \prod_{i=56}^{A} \left[1 + \frac{1}{\sigma(i)\tau_{01}}\right]^{-1} + \frac{f_2 N_{56}}{\tau_{02}} \prod_{i=56}^{A} \left[1 + \frac{1}{\sigma(i)\tau_{02}}\right]^{-1} \qquad (3.2)$$

if α–recycling among the isotopes of lead and bismuth is neglected. f_i is the fraction of the iron seed nuclei N_{56} that have been subjected to the i–component of the exponential distribution of exposures; τ_{0i} is the mean neutron exposure. Both f_i and τ_{0i} must be determined by fitting the empirical σN_s values in the following way: the main component is determined by a least square fit in the $A > 100$ range, where the contribution of the weak component is negligible. Once the parameters f_2 and τ_{02} have been found, another fit for $A < 97$ allows f_1 and τ_{01} to be obtained.

Note that in equation 3.2 only those nuclei with small cross sections can give significant contributions and will play a major role in modelling the σN_s curve. As we said before, these are nuclei with a magic number of neutrons.

According to the best fit calculations by Käppeler, Beer and Wisshak (1989), the parameters are:

$$f_1 = 1.6\%, \qquad \tau_{01} = (0.068 \pm 0.007) \left(\frac{KT(keV)}{30}\right)^{1/2} mb^{-1}$$

for the *weak* component, and

$$f_2 = (0.043 \pm 0.002)\%, \qquad \tau_{02} = (0.30 \pm 0.01) \left(\frac{KT(keV)}{30}\right)^{1/2} mb^{-1}$$

for the *main* component. Figure 3.2 shows the resulting σN_s curve, that is now considered accurate to $\pm$ 10% : the contribution of the weak component is clearly recognizable for $A < 90$.

In the same paper, a possible exponential distribution scenario for the *strong* component was also given, where a very low fractional seed abundance

$$f = 1.2 \times 10^{-4}\%$$

experiences a neutron–capture process with a very high mean neutron exposure

$$\tau_0 = 7.0\ mb^{-1}.$$

3.2.2 The Neutron Absorption

It is important to notice that not all the neutrons that are released by the neutron source are captured by Fe seeds. Indeed, during the mechanism of neutron captures, we can distinguish two classes of neutron absorbers: the seeds, that is iron and its progeny, and the light nuclei. While the first class actually works to give rise to the *s*–process, the second one acts as *neutron poison.* The neutron economy of the process must be discussed in terms of the relative importance of neutrons released versus those captured by poisons. This is particularly true for the weak component, where it is the strong neutron absorption by light nuclei that prevents isotopes with $A > 90$ to be efficiently produced.

It is common to describe the *s*–process efficiency by calculating the number of neutrons captured per ^{56}Fe seed nucleus (Clayton et al., 1961):

$$n_c(A_{seed}) \equiv \frac{\sum_{A=A_{seed}}^{209}(A - A_{seed})N_s(A)}{fN_{56}} = \sum_{A=A_{seed}}^{209} \frac{(A - A_{seed})}{\sigma(A)\tau_0} \prod_{j=56}^{A} \left[1 + \frac{1}{\sigma(j)\tau_0}\right]^{-1},$$

where the last term results from using an exponential distribution of neutron exposures $\rho(\tau)$. Settling A_{seed}=56, typical values that were found according to the exponential exposure distribution approximation are:

$$n_c = 11.2 \pm 0.7$$

for the *main* component;

$$n_c = 1.4 \pm 0.4$$

for the *weak* component, and

$$n_c \simeq 150$$

for the *strong* one.

3.2.3 The Branching Analysis

As we already said in the previous Chapter, when an unstable nucleus on the *s*–path is found whose decay–rate is comparable with the neutron capture rate, a bifurcation of the neutron flow results. The analytic description of the *s*–nucleosynthesis occurring at these branching points is due to Ward, Newman and Clayton (1976); it is very useful to define the *branching factor*:

$$f_- = \frac{\lambda_{\beta^-}}{\lambda_{\beta^-} + \lambda_n}, \tag{3.3}$$

that is the fraction of the neutron flow that goes through the β^- decay channel instead of the neutron capture one. In the same way we can define f_+ for the β^+ (or electron capture) weak interactions. Of course, the possibility exists that both

processes are involved in a branching. In this case all the rates must appear in the denominator of 3.3.

The classical analysis describes the neutron flow through a branching nucleus by means of propagators. Let us consider a simple case in which a nucleus with atomic mass number A and Z protons (A, Z) can either capture a neutron or β^- decay into the $(A, Z+1)$ nucleus. Then, for the neutron–capture channel we have:

$$\sigma N(A,Z) = \zeta(A,Z)\sigma N(A-1,Z),$$

where

$$\zeta(A,Z) = \left[\frac{1}{1-f_-(A,Z)} + \frac{1}{\tau_0\sigma(A,Z)}\right]^{-1} \sigma N(A-1,Z)$$

is a propagator. For the beta decay channel the solution is instead:

$$\sigma N(A,Z+1) = \eta(A,Z+1)\left\{\frac{f_-(A,Z)}{1-f_-(A,Z)}\right\}\sigma N(A,Z),$$

with

$$\eta(A,Z+1) = \left[1 + \frac{1}{\tau_0\sigma(A,Z+1)}\right]^{-1}.$$

The neutron density is derived from the analysis of branchings that do not depend or very little depend on temperature. In these cases $\lambda_{\beta-}$ has a well–defined value, and f_- can be obtained by a fit to the empirical σN_s curve. Then equation 3.3 allows to infer λ_n, that is the neutron density.

Several branchings of this kind have been studied so far to derive information on the main component. It is clear that a more reliable estimate of the physical parameters involved is attained when a combination of all branchings is considered, because in this way the uncertainties are reduced. The present situation can be summarized as in Table 3.1 (see Käppeler et al., 1990a). From the Table an average of :

$$n_n = (3.4 \pm 1.0) \times 10^8 cm^{-3}$$

is obtained, which is not too far from $n_n = (2.0^{+1.4}_{-0.8}) \times 10^8$ cm^{-3} that was derived by Beer (1991) on the basis of refined calculations.

From the branchings that are sensitive to the temperature we can have an estimate of the temperature conditions that are likely to play during the s–nucleosynthesis. A summary of these thermometers is given in Table 3.2 (see Käppeler et al., 1990a). The resulting average thermal energy is:

$$KT = 29 \pm 5\ keV$$

[corresponding to an average temperature of $(3.3 \pm 0.5) \times 10^8$ K], which is a bit higher than the value of 25 keV found by Beer, using a lower neutron density.

There are also two branchings that can be studied in order to obtain the electron density during the s–process. As a matter of fact, the electron capture rates in the highly ionized stellar plasma are dominated by capture of continuum electrons, and hence depend on the electron density. Since the electron to baryon ratio is almost exactly 0.5, we can calculate the mass density from a branching whose unstable nucleus is characterized by such a density dependent electron capture rate. On the basis of the couples ^{163}Dy/^{163}Ho and ^{179}Hf/^{179}Ta, an electron density

$$n_e \simeq 2 \times 10^{27} cm^{-3}$$

is inferred, which corresponds to a matter density of $\rho \approx 6 \times 10^3$ g cm^{-3}.

As a general result of the branching analysis in the classical approach, one has to notice that, within present uncertainties, the above solutions for n_n and KT satisfy all cases, in agreement with the assumption of a steady process. However, there is one exception, which provides the only stringent evidence for a pulsed s–process (Ward and Newman, 1978; Beer, 1986): the branching at ^{85}Kr.

The criterion, whether a branching is sensitive to a pulsed s–process, is that the total lifetime of the branch point isotope,

$$\tau = (\lambda_n + \lambda_\beta)^{-1},$$

must be comparable to the pulse duration Δt. Only the lifetimes of ^{63}Ni, ^{79}Se and ^{85}Kr are sufficiently long to feel the effect of s–process pulses, if Δt is greater than 3 yr, as derived from the study of the ^{151}Sm branching (Beer and Macklin, 1988). Since ^{63}Ni and ^{79}Se essentially belong to the weak component, the necessity of using a pulsed neutron flow for the main is determined by the branching at ^{85}Kr. It is found that a problematic overproduction of ^{86}Kr and ^{87}Rb can be avoided only under the assumption of a pulsed s–process. Moreover, it is also possible to constrain the pulse duration, which must fall in the range 3–20 yr.

3.2.4 The Single Flux Model for the Weak and the Strong Components

The classical description of the weak component is very difficult, because it involves few s–only isotopes and only two branching points (at ^{79}Se and ^{85}Kr), both of which being strongly contamined by the main component. A safe analysis of branchings to derive the physical parameters of the weak component is thus not possible, and this lack of information leads to large uncertainties on the classical model.

We saw above what a description in terms of an exponential distribution of neutron exposures predicts for the weak component, but in this formulation some problems arise, because to reproduce the two s–only isotopes ^{70}Ge and ^{76}Se a strong overproduction of ^{58}Fe, ^{59}Co, ^{61,64}Ni and of the s–only isotopes ^{96}Mo, ^{100}Ru and ^{104}Pb results. As a consequence, a new model was searched for, and Beer (1986)

and Beer and Macklin (1989) found that a single–exposure s–process gives a better fit to the empirical data in the $A < 90$ range. Figure 3.3 shows the product of capture cross section and s–process abundance as a function of mass number A, when a single flux s–process is chosen for the weak component. The fit to the empirical data is clearly superior with respect to that obtained with an exponential distribution of neutron irradiations which was displayed in Figure 3.2.

The most recent calculations by Beer (1991) show that, by adjusting the model to the s–only isotopes ^{70}Ge and ^{76}Se, the parameters of the weak component that also allow to reproduce the ^{80}Kr/^{82}Kr solar ratio are:

$$n_n = 1.8 \times 10^8 cm^{-3},$$

$$\tau(KT = 30keV) = (0.194 \pm 0.028) mb^{-1},$$

$$KT = 20\ keV,$$

$$f = (0.546 \pm 0.381)\%,$$

$$n_c = 4.4 \pm 0.9.$$

Unfortunately, the whole picture is affected by many difficulties. Indeed, as we shall see later, the neutron density and temperature conditions are completely out of any astrophysical scenario. This means that the phenomenological treatment is not suited to completely determine the physical parameters involved in the process.

The strong component of the s–process, concerning only the lead–peak isotopes, is also very difficult to investigate. A single flux model has been applied to this component too, and it was found that the fraction of iron seed that is needed in order to reach the lead and bismuth atomic weights is 0.9×10^{-4}, and the time integrated neutron flux is given by $\tau \geq 2.5$ mb^{-1} (Beer, 1986).

3.3 THE ASTROPHYSICAL MODELS

3.3.1 The Neutron Sources

Observations of surface abundances in red supergiant stars have revealed correlated *s*–elements and carbon enhancements. This strongly supports the idea that the *s*–process occurs during the *helium burning* stages of stellar evolution, and that the processed material is then brought to the surface by some dredge–up or mixing mechanism. The best candidate nuclear reactions that can produce neutrons during He–burning are the ^{13}C (α , n) ^{16}O and ^{22}Ne (α , n) ^{25}Mg reactions (Cameron, 1955; Burbidge et al., 1957; Reeves, 1966).

The first one becomes efficient at relative low temperatures (T $\simeq 1.5 \times 10^8$ K), but requires some mixing of protons with carbon to be possible in order to get ^{13}C through the chain:

$$^{12}\mathrm{C}\ (\mathrm{p}\ ,\ \gamma)\ ^{13}\mathrm{N}\ (\beta^+\ \nu)\ ^{13}\mathrm{C}.$$

On the contrary, ^{22}Ne is naturally obtained at the beginning of He burning, when all the ^{14}N which was synthesized by the CNO cycle during the preceding hydrogen burning phase is transformed into ^{18}O first, and into ^{22}Ne then, via the reaction path:

$$^{14}\mathrm{N}\ (\alpha\ ,\ \gamma)\ ^{18}\mathrm{F}\ (\beta^+\ \nu)\ ^{18}\mathrm{O}\ (\alpha\ ,\ \gamma)\ ^{22}\mathrm{Ne}.$$

The ^{22}Ne neutron source starts to be effective when higher temperatures are reached (T $\geq 2.5 \times 10^8$ K). It operates also during *carbon burning*, provided that not the whole ^{22}Ne supply has been exhausted during the He burning episode. Furthermore, at the low temperatures (T$\leq 8 \times 10^8$ K) characterizing core carbon burning in stars less massive than ~ 15 M$_\odot$, Arnett and Thielemann (1985) found that the reaction sequence ^{12}C(p,γ)^{13}N (β^+)^{13}C(α ,n)^{16}O, sustained by protons and α particles from the ^{12}C+^{12}C fusion reaction, is a powerful neutron source. But as we shall see later on, this last possibility is not interesting when we want to study the chemical enrichment of the interstellar medium, since the inner core does not participate to it.

Other neutron sources could also be found in massive stars, such as the ^{12}C (^{12}C, n) ^{23}Mg reaction during carbon burning, or the ^{16}O (^{16}O, n) ^{31}S one during oxygen burning. But these reactions require such high temperatures (T $\geq 10^9$ K) that it is plausible that all the nuclei beyond Fe will be photodissociated, since the (γ , n) reaction rates begin to exceed the neutron capture rates.

3.3.2 The Weak Component

It has long been recognized that massive stars during the central He–burning stages of their lives can produce heavy nuclei up to $A \sim 90$ through the ^{22}Ne (α, n) ^{25}Mg

neutron source (Couch, Schmiedekamp and Arnett, 1974; Lamb et al., 1977; Gallino and Busso, 1985; Arnett and Thielemann, 1985; Busso and Gallino, 1985; Prantzos, Arnould and Arcoragi, 1987; Langer, Arcoragi and Arnould, 1989; Prantzos, Hashimoto and Nomoto, 1990).

The efficiency and the details of the process were not always in agreement, but this is due to the fact that the nucleosynthesis mechanism depends on so many evolutionary as well as nuclear parameters, which are continuously improving with time. In any case, it is a general result that during He burning in massive stars the neutron density is small, around 10^6 cm^{-3}, much smaller than the one which is predicted by the classical model for the weak component. The point is that such a low n_n has important consequences on the pattern followed by the neutron captures, leading in particular to a very high overabundance of the s–only isotope ^{80}Kr. This was indicated as a major difficulty of such a scenario (Prantzos, Hashimoto and Nomoto, 1990). We shall see that the problem is easily overcome when a full analysis of the s–process that includes both the weak and the main component at the same time is performed.

The possibility of neutron captures during carbon burning has been considered in the past, with no definitive answer to the question, due to the large uncertainties affecting this evolutionary phase. As a matter of fact, the way carbon burning develops depends on the stellar evolutionary code, that is on the input physics (rate of the $^{12}C(\alpha,\gamma)^{16}O$ reaction, treatment of convection, rate of neutrino losses). The result is that for a star of a given mass we can have both models in which central C burning is radiative, and models where it is convective. Generally speaking, convection is favoured by a higher C/O ratio at the end of He–burning. In any case, since we are interested in the understanding of the weak component in the solar–system, we do not care about core C burning and the possibility of s–processing there, because the region of the star where it is happening is likely to be trapped into the stellar remnant after the supernova explosion. The phase we must considered instead is shell C–burning, that according to the most updated evolutionary models (Nomoto and Hashimoto, 1988; Woosley, 1990, private communication), could spread convectively over almost all the CO core. If neutron captures can be effective during this stage, they will alter the s–process results of the previous He–burning episode.

In the following Chapters we shall discuss the weak component and its reproduction by massive stars, with a careful attention to the nuclear inputs.

3.3.3 The Main Component

The main component was traditionally ascribed to the convective thermal instabilities which develop in the He shell of intermediate mass stars ($3 \leq M/M_\odot \leq 8$), during the Asymptotic Giant Branch (AGB) phase of their evolution. Neutrons are released through the ^{22}Ne (α , n) ^{25}Mg reaction, and the overlapping of the recurrent

convective pulses provides an exponential distribution of neutron exposures as the one classically required to reproduce the solar–system distribution of the *s*–elements (Ulrich, 1973; Iben, 1975; Truran and Iben, 1977; Cosner, Iben and Truran, 1980).

This scenario has been argued against later on in the light of both theoretical and observational arguments. Indeed, the too high n_n that is found in such models leads to a nucleosynthesis path which is right–shifted in the chart of nuclides, in comparison to what would be expected for a classical *s*–process. In addition, the relative overproduction factors of some *s*–nuclei do not match the solar ratios. Moreover, the observational counterparts of such bright red supergiant models have not been found in significant number in the Magellanic Clouds, and no strong overabundances of ^{25}Mg and ^{26}Mg isotopes have been observed in those stellar atmospheres showing enhancements of *s*–process elements, as would be caused by the operation of the ^{22}Ne(α,n)^{25}Mg reaction.

All these difficulties have urged towards the search of a better candidate, and the attention has fallen on the low mass stars (LMS, $1 \leq M/M_{\odot} \leq 3$), in the same thermally–pulsing phase. But in low mass stars α–captures on ^{22}Ne cannot be the main neutron source because of the lower temperatures involved. However, Iben and Renzini (1982a,b) showed that at least for low metallicity stars ($Z = 0.001$) an alternative neutron source can be provided by the ^{13}C (α , n) ^{16}O reaction. As a matter of fact, following a thermal pulse, the outer edge of the He–processed, carbon rich zone expands to such temperatures that carbon recombination occurs. This leads to an increase of the opacity, and a semiconvective region develops just below the envelope, which mixes hydrogen–rich matter with carbon–rich material. During the subsequent evolution this region heats up and ^{12}C is converted into ^{13}C and ^{14}N by an incomplete CN cycle. A ^{13}C–rich pocket of $\approx 10^{-4}$ M$_{\odot}$ forms, which will be ingested by the next growing pulse, allowing the liberation of a neutron flux. Sometimes in between two successive thermal pulses the convective envelope penetrates inward into the stellar structure, and carries out to the surface a certain amount of matter that has seen He–burning and *s*–processing. The mechanism, that is called the *third dredge–up*, can thus explain the C and *s*–enrichments observed in some red supergiants.

A confirmation of the effectiveness of this picture was obtained by Hollowell and Iben (1988, 1989) starting from the same stellar model of Iben (1982) and Iben and Renzini (a 0.7 M$_{\odot}$, $Z = 0.001$ star), and including some overshooting and a time–dependent treatment of mixing in their code. According to Hollowell (1989; private communication), the ^{13}C–rich pocket would also form in stars of higher metallicity, up to $Z \sim 0.006$.

3.3.4 New Results of n–capture Nucleosynthesis in Low Mass Stars

An analysis as accurate as possible of the s–nucleosynthesis occurring in low mass stars using the above evolutionary models and the best nuclear inputs has been done by our group. The first results were presented in Gallino et al. (1988), Gallino (1989), and Käppeler et al. (1990a), and in the following we shall briefly outline the most important aspects of this work.

The shape of the thermal pulse is displayed in Figure 3.4 and is assumed to be constant in time. The Figure shows the point when the ^{13}C–rich pocket starts to be ingested, at a rate which is controlled by the growth of the convective instability, and whose value is about 5×10^{-5} M$_\odot$ /yr. The ^{13}C nuclei rapidly burn at a mean temperature of $T_8 = 1.4$, and a first neutron irradiation is obtained, with the mean neutron density that exhibits a rather fast rise to a plateau value of about 2×10^9 cm^{-3}. With the end of the ingestion phase, the neutron density declines according to the burnout of the residual ^{13}C. Then, after $\approx$ 20 yr, the pulse spreads up to its maximum extension, and the temperature at the base of the convective He shell increases up to $T_8 \sim 3$, so that some ^{22}Ne can burn. This allows a second neutron burst to occur, whose maximum neutron density is 9×10^8 cm^{-3}, but that rapidly dies out. The first neutron exposure has a duration of about 12 yr, while the second one is active for only about 2.5 yr. Then an interpulse period follows on a timescale of 2×10^5 yr, during which the unstable nuclei decay, until another pulse develops in the same manner as before. Every pulse involves a certain fraction of matter that has already experienced a neutron exposure in the previous pulse. The overlapping factor r between pulses depends on the core mass of the star and on the metallicity, and it increases with time. Overlapping factors in the range 0.6–0.8 must be considered. The computations are repeated for $\approx$ 20 identical pulses, to be sure that all the chemical abundances have reached asymptotic conditions.

Despite such an analysis must face a number of not well known details, it has proved to satisfactorly account for the main component in the solar–system. In Figure 3.5 we show the best fit results that we obtained for a star of metallicity $\approx$ 1/3 of the solar one, assuming that the same mechanism for the formation of the ^{13}C neutron source as was found for a metal poorer star applies. In the Figure, the s–only isotopes are indicated by stars and diamonds; the latter are not affected by branchings and can therefore be used to define the mean overabundance (solid line). Other symbols denote relative s–process contributions of $\geq$ 80 %(+), and 60 to 80 %(×), according to Käppeler, Beer and Wisshak (1989). The s–isotopes with $A < 90$ receive a minor s–contribution by the main component (particularly ^{80}Kr), but are complementary contributed by the weak s–component occurring in massive stars, as we shall see in the next Chapters. The Figure also shows that there is a clear problem for ^{86}Kr and ^{87}Rb, that are heavily overproduced.

The parameters corresponding to the Figure 3.5 are:

$$\tau_0 = 0.30 \pm 0.01 mb^{-1},$$

as the effective exposure;

$$f = (0.076 \pm 0.007)\%,$$

as the fraction of solar iron required as seed, and

$$n_c = 9.6 \pm 0.4,$$

as the number of neutrons captured per iron seed. These numbers can be compared with those characterizing the classical fit to the solar distribution of s–isotopes (see § 3.2). The agreement is particularly good for the total neutron exposure τ_0; this is why both models succeed in reproducing the solar–system composition remarkably well.

A better confrontation between the astrophysical calculations and the classical analysis can be obtained through a detailed investigation of branchings. Let us stress that the phenomenological model for the main component deals with constant temperature and neutron density, while in the astrophysical context we have strong dynamic conditions. The time dependence of both temperature and neutron density greatly influences the behaviour of chemical abundances during the thermal pulse. In order to clarify the point, we shall discuss the representative case of the Zr isotopes, which are suitable to illustrate the characteristic abundance changes as a function of n_n and T, as is illustrated in Figure 3.6. We describe the situation reached in asymptotic conditions.

Starting from ^{90}Zr, the Figure shows that it is partially depleted during the rise of the neutron density that accompanies the ingestion phase. The reason is that the rate at which it suffers neutron captures becomes faster than its production through the β^- decay of ^{90}Y. This is ultimately due to the rather long β^- half lives of ^{89}Sr and (especially) ^{90}Sr, and to the small cross sections in this region, at the neutron magic number 50. Indeed, a time delay is required to build a sufficient abundance of ^{89}Sr ($\tau_{1/2} \simeq 50$ d) and of ^{90}Sr ($\tau_{1/2} \simeq 10$ yr) from ^{88}Sr, which has a low cross section ($< \sigma_{n,\gamma}^{30keV} > = 6.2$ mb). During this time, both ^{90}Zr and its precursor, ^{89}Y, suffer neutron captures and are partially destroyed; when a sufficient flux begins to pass through the chain ^{89}Sr - ^{89}Y - ^{90}Y - ^{90}Zr, this latter increases again. A further contribution to ^{90}Zr comes on longer time scales, during the fall of the neutron density and after ^{13}C exhaustion, due to the decay chain starting from ^{90}Sr. After the remixing with 40 % of fresh matter with a composition equal to the initial one, about 20 yr after the first neutron irradiation, the neutron flux generated by the ^{22}Ne(α,n)^{25}Mg source at high temperature is so small that the final abundance cannot vary remarkably. Only after this second neutron burst ^{90}Zr receives again a sensitive contribution from the residual decay of ^{90}Sr, in the interpulse phase. From the phenomenological point of view, the behaviour of ^{90}Zr in the low temperature

phase is characteristic of those isotopes that are strongly affected by a branching involving a rather long lived nucleus, with half-life of the same order as the duration of the process (in this case, ^{90}Sr).

Coming to heavier isotopes, Figures 3.6 presents the evolution of ^{94}Zr, the abundance of which is practically fixed when the n_n of the first exposure drops below 2×10^8 cm^{-3}. Roughly the same behaviour is obtained for the isotopes ^{91,92,93}Zr, typical for cases that are not affected by s–process branchings.

The dynamic nature of the neutron irradiation is particularly evident at the branching point ^{95}Zr, despite of its relatively short half-life ($\tau_{1/2}$ = 64 d). Usually defined as an r-only nuclide, ^{96}Zr receives at peak neutron density an important contribution from neutron captures on ^{95}Zr. When n_n falls below a critical value, ^{95}Zr begins to be preferentially destroyed by β^- decays, producing ^{95}Mo. Being rather insensitive to freeze–out effects and to the second neutron burst, the ^{96}Zr abundance is a good indicator for the peak neutron density during the low temperature phase. A similar situation occurs for the ^{85}Kr branching, as will be discussed below.

Table 3.3 presents the empirical σN_s values for the s–only isotopes involved in branchings together with the respective results obtained with the classical approach and the low mass stars model. The general agreement between the two different approaches seems to suggest that the constant temperature and neutron density adopted in the classical model should correspond to some effective values of these parameters in the stellar environment (see Käppeler et al., 1990a for a more detailed discussion).

However, a noticeable difference between the classical analysis and the LMS model does occur right at the few branchings that are sensitive to the peak neutron density during the low–temperature phase of the pulse. This holds in particular for ^{85}Kr and, somewhat less pronounced, for ^{95}Zr. In case of the ^{85}Kr branching, the high neutron density during the initial low–temperature phase gives rise to a strong production of ^{86}Kr and ^{87}Rb, while the flow to ^{87}Sr, ^{86}Sr is very weak. This part of the branching receives significant contributions during the decline of the first neutron burst and reaches its final abundance during the comparably low neutron density in the final high–temperature phase. Because their abundances are only sensitive to the total neutron exposure, the ^{86}Kr and ^{87}Rb abundances are pratically frozen after the first burst, showing a 50 % overproduction compared to the average. We emphasize here that in LMS the abundances of ^{86}Kr and ^{87}Rb are not influenced by the pulsed nature of the neutron fluence in the model, contrary to the suggestion by the classical approach. Indeed, the bulk of both isotopes is produced during the first neutron peak at a neutron density of about 2×10^9 cm^{-3}, when the total life time of ^{85}Kr is only about 1.5 yr, much shorter than the duration of the first peak. This important feature should be investigated further together with complementary information from nucleosynthesis in massive stars.

A similar discrepancy is found for the branching at ^{95}Zr. Even neglecting the

r–process contribution, the LMS model yields a 30 % excess of ^{96}Zr.

The above problems with the abundances of ^{86}Kr, ^{87}Rb and ^{96}Zr seem to suggest either that the relevant cross sections are slighly different, or that the true neutron density is lower than indicated by the present models. Such a modification could be possible for instance by decreasing the ^{13}C rate of ingestion in the pulse. Indeed, improved calculations of s–nucleosynthesis in LMS, taking into account new determinations of not–$1/v$ trends for the $\sigma_{n,\gamma}$ of many isotopes, and adopting a 2 times lower ingestion rate, have proved to lead to a quite fair situation, avoiding the problems of the ^{86}Kr, ^{87}Rb and ^{96}Zr overabundances (Gallino et al., 1991).

3.3.5 Observational Constraints from Peculiar Red Giants and Meteoritic SiC Grains

From the observational point of view, there are supergiant stars showing a peculiar surface composition, with correlated carbon and s–elements enhancements. They can be divided in two classes (Lambert, 1991):

- *intrinsic* TP–AGB stars: they include MS, S and C (N–type) stars showing the unstable nucleus ^{99}Tc ($\tau_{1/2} = 2 \times 10^5$ yr) as a probe that they are presently undergoing nucleosynthetic activity;

- *extrinsic* TP–AGB stars: they include the various classes of G and K–type Ba stars and the cooler S stars not showing Tc, all of them being part of a binary system. In particular, since the Ba stars are not luminous enough to have experienced thermal pulses by their own, they are believed to have received s–processed matter through mass transfer from the companion, which was previously an AGB star.

In the following we shall summarize the main results that we have obtained using our model for the nucleosynthesis in low mass stars to fit the abundance distributions observed in the peculiar red giants (Busso, Gallino and Raiteri, 1991, and Busso et al., 1991).

In order to compare observed distributions to model predictions we performed a series of nucleosynthesis calculations using our low mass star model (see the previous Section), and assuming that the mechanism for the ^{13}C–pocket formation is effective also in population I stars.

We then followed the evolution of surface abundances as long as material from the He-shell is dredged to the surface in the interpulse periods, using simple descriptions for the dredge-up process and for mass loss, and assuming pre-AGB photospheric CNO compositions from observations of normal giants (see e.g. Lambert, 1991). The outcome of this work was a number of atmospheric evolutionary histories which start from the first pulse and proceed up to the complete erosion of the envelope by mass loss. Each case is characterized by:

i) a set of parameters (like the initial metallicity, the amount of ^{13}C burnt, the overlapping factor r between successive pulses) which specifically control the efficiency of the s-processing and hence the value of the *asymptotic neutron exposure* τ_0.
ii) a set of more general *stellar* quantities (initial mass/envelope mass, dredged-up mass, frequency of dredge up, interpulse duration, adopted law for mass loss) which control the mixing history and the atmospheric evolution.

By varying the above parameters within the limits allowed by the present knowledge of the AGB evolution we spanned a rather large interval in neutron exposures (from 0.05 up to 1 mb^{-1}), in initial metallicities (from 1/3 of solar up to solar) and in final surface enhancements (from $\simeq$ 1 to $\simeq$ 100).

Fitting intrinsic TP-AGB stars.
The observations in MS and S giants are affected by large uncertainties, due both to the high crowding of lines in the spectra, and to the incomplete knowledge of their photospheres (see Gustafsson, 1989). Among s-elements, this is particularly true for Sr abundances, which are highly sensitive to the model atmosphere and to non-LTE effects (Smith and Lambert, 1986) and hence cannot be used safely for our purposes. Concerning the other s-process elements, due to the above problems an overall cautious uncertainty of $\pm$ 0.3 dex has to be assumed. For C the uncertainty is lower (<0.2 dex), while for Tc is higher, at least 0.4 dex.

The spectroscopic measurements of C stars, especially in the case of s-process elements, are affected by even larger errors: Gustafsson (1989) evaluates them in at least 0.4 dex in the work by Utsumi (1985) (with stronger uncertainties for elements like Sc and La), while they are certainly higher in the older data by Kilston (1975).

With these limitations in mind, Tables 3.4 and 3.5 show two examples of fits to intrinsic TP-AGB stars. In view of the discussed uncertainties the agreement has to be considered as very good. From fits similar to those presented here, we derived that MS and S star abundances are consistent with an s-process efficiency similar to that responsible for the solar distribution ($0.2 \leq \tau \leq 0.4$ mb^{-1}), while C-stars (N-type) show, in average, higher neutron exposures ($0.3 \leq \tau \leq 0.6$). These results are in agreement with previous conclusions by Lambert (see e.g. Lambert, 1991).

However the effective neutron exposure is not well constrained by the observations, which sometimes allow for more than one solution, depending on how and when we mix the He-shell material, which has a composition evolving in time. Indeed, the same surface abundances can in principle result either from a process characterized by a relatively high asymptotic τ value but with an envelope dredge-up which is already efficient in the first pulses, where the s-processing is still incomplete, or from one with a lower neutron exposure but with a dredge-up which mixes the nucleosynthesis products only in the final AGB phases, when the n-captures have already built consistent abundances of s-nuclei. Conversely, different s-process distributions in the photosphere can be obtained by differently mixing the *same* He-shell material, as shown in Figure 3.7.

Fitting extrinsic TP-AGB stars

For normal Ba stars uncertainties of the order of at least 0.2 – 0.3 dex are expected for the *s*-process elements, from inspections of works by different authors. The errors in C,N,O determinations are probably lower (see e.g. Lambert, 1985).

Table 3.6 gives an example of how we can fit the observed abundances, by simply further mixing with an unperturbed secondary atmosphere the surface distribution typical of a C star with a relatively high neutron exposure ($0.4 \leq \tau_0 \leq 0.6$). The agreement is good, though some problems still remain for the abundance of Rb, whose observations give values lower than those predicted. This is a well known problem, which however depends on the large uncertainty of Rb abundance determinations. One has to underline that while models based on the ^{13}C neutron source provide expectations for Rb only a factor of 2 higher than observed, those based on the ^{22}Ne source give estimates higher by a factor of 10 and hence have clearly to be excluded (see also Malaney and Lambert, 1988).

Eventually, Table 3.7 presents a fit to the observed distribution of abundances in HR363, an MS-type giant not showing Tc. Despite the already mentioned indetermination of the τ_0 values on observational grounds only, it is clear that this star (as well as the similar source HR1105) is characterized by a neutron exposure lower than those found for classical Ba stars (see e.g. the different values of $<Ba/Y> = (N_{Ba}+N_{Nd})/(N_Y+N_{Zr})$ in HR363 and in HR774). This seems at odd with the usual interpretation, based on their binarity, that S stars not showing Tc are evolved Ba stars. As Table 3.7 shows we actually do not need this hypothesis from the purely nuclear point of view: the Tc abundance can be reduced below the observable threshold simply assuming that dredge-up occurs after a consistent number of pulses, so that we can sample our sources when Tc is almost completely decayed in the atmosphere. Hence, though the binary nature of this class of stars is clearly stated, the problem of the neutron exposure suggests an alternative scenario, in which they would be objects near the end of the AGB, which have seen dredge-up only once or twice, about $(0.8–1)\times 10^6$ yr ago.

This fact is better illustrated in Figure 3.8, where the surface abundance of ^{99}Tc and ^{93}Zr is plotted as a function of time assuming dredge-up every 9 pulses. It is clear that, while both Tc-rich and Tc-poor phases can be observed, without the need of invoking mass transfer from a companion, ^{93}Zr would be a better test, since for any reasonable duration of the AGB phase it should remain relatively high. Observations of the isotopic composition of Zr in S stars without Tc should then allow for a more decisive discrimination between the two possible evolutionary interpretations of these sources.

Interpretation of isotopic anomalies in SiC grains

Among the carriers preserving the cosmic memory of their nucleosynthetic origin, SiC grains in primitive meteorites are characterized by large anomalies in C, N, Si (Tang and Anders, 1988; Zinner, Tang and Anders, 1989) and especially noble gases (Zinner, Tang and Anders, 1987), the isotopic ratios of which are typical of

the s–process, suggesting their formation in the extended atmospheres of carbon stars. These results allow us to test our models of nucleosynthesis in low mass stars that are thermally pulsing on the AGB (Lewis, Amari and Anders, 1990; Gallino et al., 1990a).

In order to determine the chemical composition of the stellar atmosphere, where SiC grains form, the s–processed matter coming from the He shell was mixed into the envelope using the same procedure already adopted for the fit to the peculiar red giants.

The comparison between the stellar results and the meteoritic data leads to the following conclusions:

- the excess ^{22}Ne measured in the SiC samples comes from the ^{14}N chain of reactions in the He–shell zone, without the need of the generally accepted radiogenic contribution from ^{22}Na;
- the isotopic anomalies shown by SiC grains are reproduced by carbon stars of population I, with metallicity Z in the range 0.01–0.02.

The analysis of the Kr isotopes can provide further information and deserves a special discussion. The most remarkable feature shown by Kr isotopes is the large spread extrapolated for ^{86}Kr/^{82}Kr and the smaller one for ^{80}Kr/^{82}Kr. Both can in principle be accounted for by two rather different scenarios involving either many stars or a single star. A first possibility is that these spreads come from different stars with a wide range of neutron exposures, up to $\tau \simeq 0.30$ mb^{-1}. Table 3.8 shows that both ratios do vary with the neutron exposure, the agreement between theoretical expectations and SiC extrapolations being quite satisfactory.

We note that some discrepancy remains for ^{84}Kr/^{82}Kr; also this ratio varies, by up to 10 %, in models with the same overlap factor and different neutron exposure, whereas the SiC data seem to fall on a single correlation line.

A second possibility is that SiC grains reflect the conditions in one star, at different times in its AGB history. This is illustrated in Figure 3.9, where the evolution of Kr isotopic ratios in the He shell with pulse number mimics their behaviour as a function of τ. The model shown in the Figure is a TP–AGB star of [Fe/H] = –0.2, with an asymptotic neutron exposure of $\tau_0 = 0.32$ mb^{-1}. The values between pulses 4 and 10 cover almost the entire observed range for SiC. This analysis cannot be pursued further because the details of the mixing of s–process material with the envelope are not yet sufficiently known. For a single star to be the source of all the anomalies, the conditions for the formation of SiC grains must occur early enough in the TP–AGB phase to preserve the signature of various s–processed episodes, but avoid the very first pulses where the ^{84}Kr/^{82}Kr ratio is too low. Such a possibility is compatible with present results for the dredge–up mechanism. In any case, to reproduce the whole measured range by a single star means that the asymptotic exposure should be high ($\tau \simeq 0.30$), not very different

from that characterizing the solar–system main component and the S stars in the Galaxy.

Despite many uncertainties, the Kr measurements in SiC grains give us some important information. First, the low $^{80}Kr/^{82}Kr$ ratio is a clear indication of a low temperature in the He shell, which is characteristic of the ^{13}C source but not of the ^{22}Ne one. Second, the large variation of the $^{86}Kr/^{82}Kr$ suggests a range of neutron exposures in the He shell *s*–processed zone.

All these theoretical and observational positive tests would make one think that the main component is really a well known mechanism. Unfortunately the situation is not so well stated. As a matter of fact, a number of evolutionary models have been run for AGB stars of different masses and metallicities, and different prescriptions for the input physics (see Lattanzio, 1989, and Boothroyd and Sackmann, 1988), but none of them was able to find the formation of the ^{13}C–rich pocket, while only under some specific assumptions it was possible to find dredge–up of internally processed matter. This is really a drawback for the understanding of the main component.

However, observations tell us that there are low mass stars showing *s*–overabundances, so that one has to think that something is missing in our way of modelling these evolutionary stages, and a lot of effort is still needed to clarify the situation.

3.3.6 The Strong Component

At the moment, it seems that a strong *s*–process mechanism has to operate in order to give account of the 30% missing abundance of ^{208}Pb, the *s*–only isotope at the termination of the *s*–path. The most promising site for this strong component up to now was identified in the core helium flashes experienced by low mass stars ($M \leq 1\ M_\odot$) at He–ignition (Truran and Iben, 1977). This scenario has not been investigated in details yet, and we can't be sure that a single event rather than more than one is needed to best fit the empirical data. We only know that the neutron source has to be the $^{13}C\ (\alpha, n)\ ^{16}O$ reaction, since the temperature is too low for the alternative ^{22}Ne source to be effective.

Another suggestion for the synthesis of ^{208}Pb has very recently been advanced by our group (Gallino et al., 1990c): according to this scenario, the strong component might find its origin in low mass, low metallicity stars during the He–shell thermal pulses they undergo while ascending the AGB. The mechanism in a word would be the same that, for higher metallicities, allows the main component to be obtained, but now the same amount of neutrons (that depends on the ^{13}C–rich pocket which is of primary origin and thus metal independent) is to be distributed on a lower seed content. The result is that the ^{208}Pb abundance increases dramatically as the metal content goes down.

Figure 3.10 shows the overabundance of Pb isotopes as a function of metallicity [Fe/H] [we use here the spectroscopic notation $[Fe/H] = \log (Fe/H)_\star - \log (Fe/H)_\odot$] obtained by us. The large overproduction of ^{208}Pb at low [Fe/H] is quite evident.

High resolution spectroscopy of metal poor stars would be very highly desirable, in order to check if lead is actually enhanced, and test the validity of the above picture. A starting collaboration with P. François on this is presently under way.

Branching point	$n_n(10^8\ \mathrm{cm}^{-3})$
^{95}Zr	4^{+3}_{-2}
^{147}Nd, ^{147,148}Pm	3.0 ± 1.0
^{169}Er, ^{170}Tm	0.5–6.0
^{185}W, ^{186}Re	$3.5^{+1.7}_{-1.1}$
^{191}Os, ^{192}Ir	$4.3^{+3.4}_{-2.5}$

Table 3.1: Derived neutron densities for the main component

Branching point	KT(keV)
^{134,135}Cs	> 13
^{151}Sm, ^{152}Eu	29 ± 5
^{154,155}Eu	29 ± 5
^{176}Lu	27 ± 6

Table 3.2: Derived thermal energies for the main component

Characteristic s–only isotope	σN_s (Empirical)	σN_s (Classical)	σN_s (LMS)
Branching Sensitive to Neutron Density			
^{96}Mo	48.4 ± 4.4	52.0	63.0
^{148}Sm	7.73 ± 0.35	7.37	7.27
^{170}Yb	5.93 ± 0.25	5.23	5.79
^{186}Os	4.54 ± 0.34	4.56	4.80
^{192}Pt	4.07 ± 2.09	2.66	2.83
Branching Sensitive to Temperature			
^{134}Ba	23.5 ± 4.1	28.9	25.3
^{152}Gd	0.45 ± 0.12	0.44	0.30
^{154}Gd	6.63 ± 0.29	6.51	6.05
^{176}Lu	1.62 ± 0.07	2.75	1.69

Table 3.3: Comparison of empirical σN_s values with results obtained via the classical approach and the LMS model

Element	Model Abundances τ = 0.21, D.F.= 0.014 M = 1.5 $M_\odot$	Observed Abundances Wallerstein and Dominy (1988) Smith and Lambert (1985)
C/O	0.60	0.56
$^{12}C/^{13}C$	27	26
[Fe/H]	0.00	0.02 ± 0.10
[Y/Fe]	0.69	0.73 ± 0.3
[Zr/Fe]	0.60	0.78 ± 0.3
[Ba/Fe]	0.42	0.28 ± 0.3
[Nd/Fe]	0.18	0.18 ± 0.3
log(Tc/Zr)	−2.33	−2.30
log(Tc/Nb)	−0.55	−0.60
log(Zr/Nb)	1.79	1.70
<Ba/Y>	0.20	0.19

D.F. = final dilution factor of He-shell matter in the envelope

Table 3.4: Fitting o^1 Ori (M3 III S)

Element	Model Abundances τ = 0.57,D.F = 0.02 d.u. each 5 pulses, M = 1.5 $M_\odot$	Observed Abundances Utsumi (1985) Lambert et al. (1986)
C/O	1.20	1.14
$^{12}C/^{13}C$	51	52
[Fe/H]	-0.3	(-0.3 ÷ 0.0)
[Y/Fe]	1.60	1.80±0.4
[Zr/Fe]	1.60	1.50±0.4
[Ba/Fe]	1.81	1.75±0.4
[La/Fe]	1.80	2.20±0.4
[Nd/Fe]	1.56	1.40±0.4
[Sm/Fe]	1.41	1.50±0.4
<Ba/Y>	0.38	0.31

Table 3.5: Fitting X Cnc (C5,4)

Element	Model Abundances τ = 0.57,D.F = 0.02+0.63 M = 1.5 $M_\odot$	Observed Abundances Utsumi (1985) Lambert et al. (1986)
[C/Fe]	0.40	0.36±0.1
[O/Fe]	0.010	0.1±0.1
$^{12}C/^{13}C$	30	23
[Fe/H]	-0.3	−0.3±0.1
[Cu/Fe]	0.18	0.41±0.3
[Zn/Fe]	0.11	0.21±0.3
[Ge/Fe]	0.43	0.18±0.3
[Rb/Fe]	1.00	0.46±0.4
[Sr/Fe]	1.30	1.00±0.4
[Y/Fe]	1.37	1.17±0.3
[Zr/Fe]	1.40	1.14±0.3
[Nb/Fe]	1.36	1.19±0.3
[Mo/Fe]	1.28	1.24±0.3
[Ru/Fe]	1.05	0.78±0.3
[In/Fe]	1.02	0.87±0.3
[Ba/Fe]	1.60	1.35±0.3
[La/Fe]	1.51	1.39±0.3
[Ce/Fe]	1.57	1.32±0.3
[Pr/Fe]	1.37	1.62±0.3
[Nd/Fe]	1.35	1.49±0.3
[Sm/Fe]	1.20	1.30±0.3
[Eu/Fe]	0.65	0.65±0.3
[Gd/Fe]	0.98	1.08±0.3
[Dy/Fe]	0.93	0.91±0.3
[Lu/Fe]	0.20	0.11±0.3
[Hf/Fe]	1.45	1.10±0.3
<Ba/Y>	0.38	0.31

Table 3.6: Fitting HR 774 (G8III-Ba3)

Element	Model Abundances τ = 0.31, D.F.= 0.014 M = 1.5 $M_\odot$ d.u. each 9 pulses	Observed Abundances Wallerstein and Dominy (1988) Smith and Lambert (1985)
C/O	0.55	0.58
$^{12}C/^{13}C$	22	17
[Fe/H]	0.00	-0.10 ± 0.10
[Y/Fe]	0.92	0.70 ± 0.3
[Zr/Fe]	0.86	0.85 ± 0.3
[Ba/Fe]	0.75	0.64 ± 0.3
[Nd/Fe]	0.47	0.77 ± 0.3
log(Tc/Zr)	−4.36	<−4.20
<Ba/Y>	0.20	0.23

Table 3.7: Fitting HR363 (M3 II S)

Ratios	He shell, asymptotic				SiC grains
	[Fe/H]=-0.2 r=0.6, τ_0=0.17	[Fe/H]=-0.2 r=0.8, τ_0=0.32	[Fe/H]=0.0 r=0.6, τ_0=0.12	[Fe/H]=0.0 r=0.8, τ_0=0.22	
$^{80}Kr/^{82}Kr$	0.038	0.032	0.045	0.036	0.02-0.05
$^{83}Kr/^{82}Kr$	0.35	0.35	0.34	0.35	0.329
$^{84}Kr/^{82}Kr$	2.21	2.44	2.07	2.42	2.55
$^{86}Kr/^{82}Kr$	1.78	2.62	1.08	1.79	0.57-2.96

Table 3.8: Expected isotopic ratios for Kr from Pop. I AGB stars compared with those measured in SiC grains

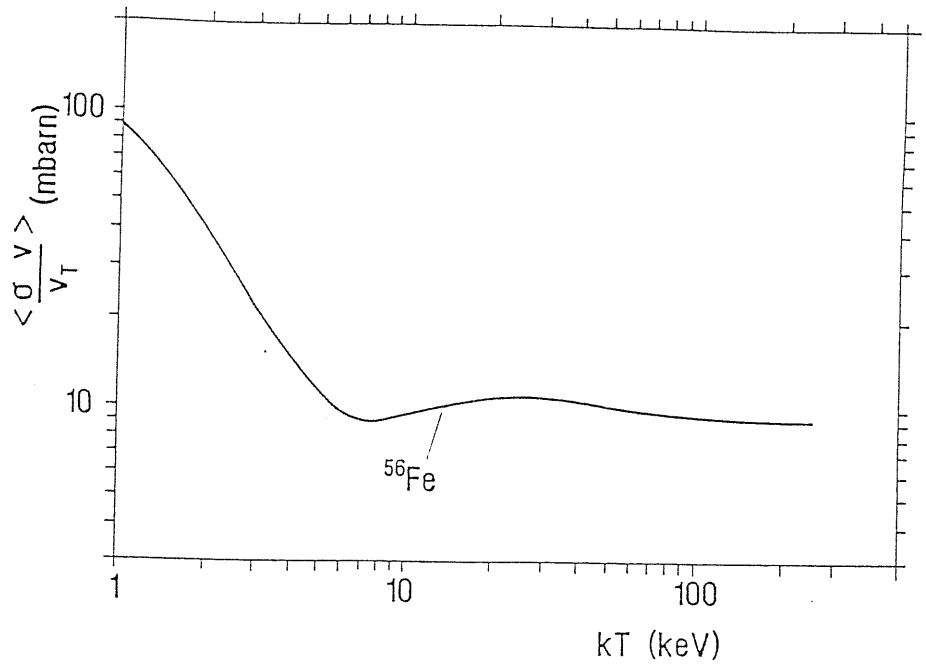

Figure 3.1: The behaviour of the neutron capture cross section of ^{56}Fe as a function of the thermal energy

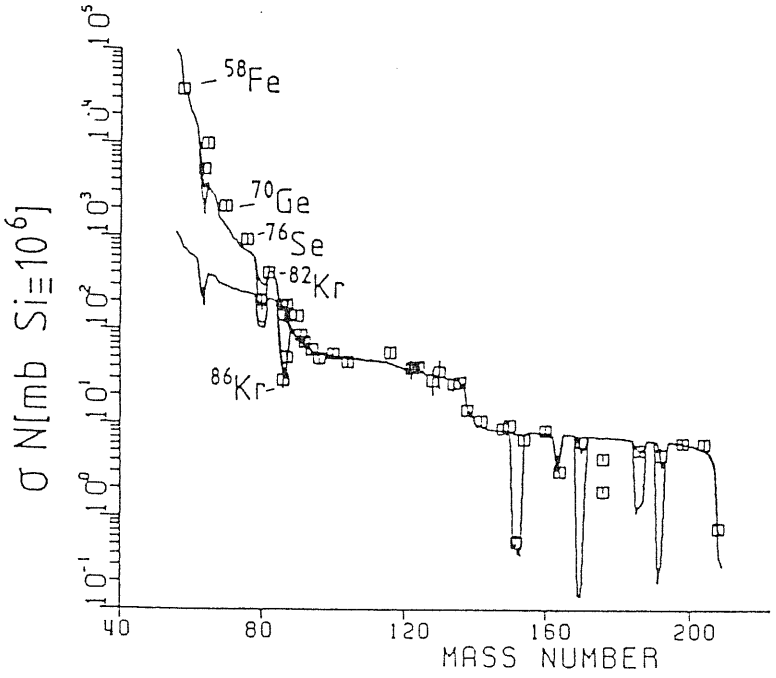

Figure 3.2: The characteristic product of cross section times s–process abundance versus mass number. Symbols are empirical data. In the range $A < 90$ the weak component is shown, as obtained with an exponential distribution of neutron exposures

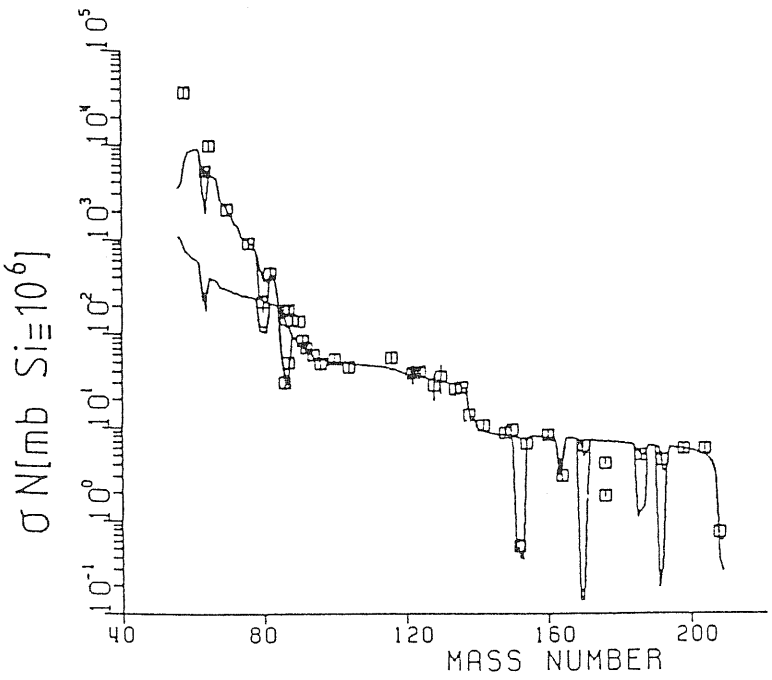

Figure 3.3: Product of capture cross section and s–process abundance as a function of mass number A. Symbols are empirical data. Below $A = 90$ the superposed weak component is effective, as given by the single flux model

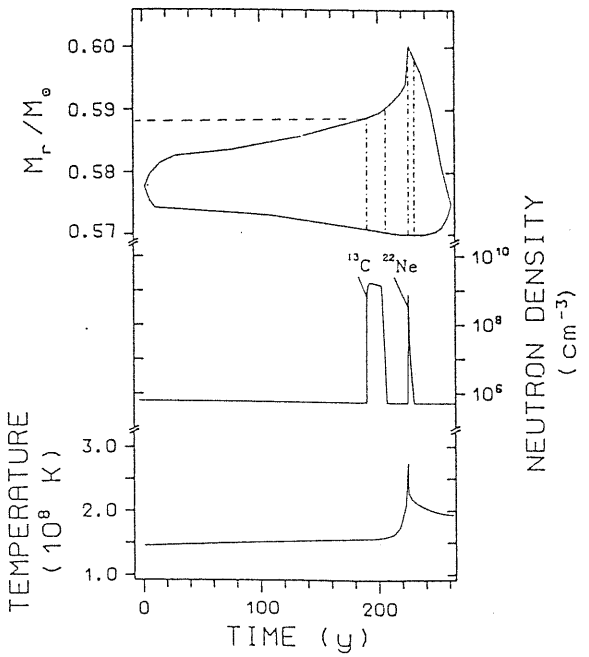

Figure 3.4: (Top) Typical development of the convective region during a thermal instability of the He–shell according to Iben (1982) (Middle) The two neutron bursts of the LMS model originating from the ^{13}C and ^{22}Ne sources (Bottom) Time behaviour of the maximum temperature in the shell

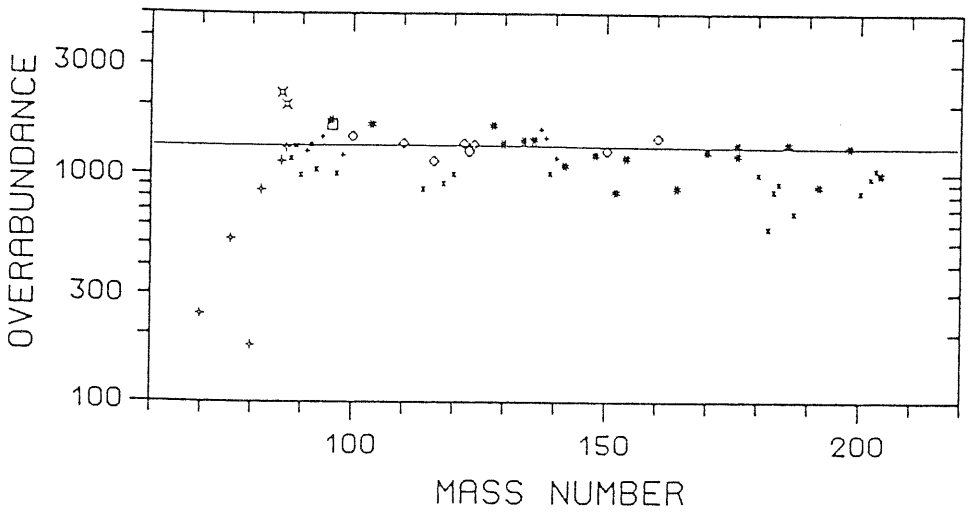

Figure 3.5: Overabundances resulting from s–processing in TP–AGB stars of low mass

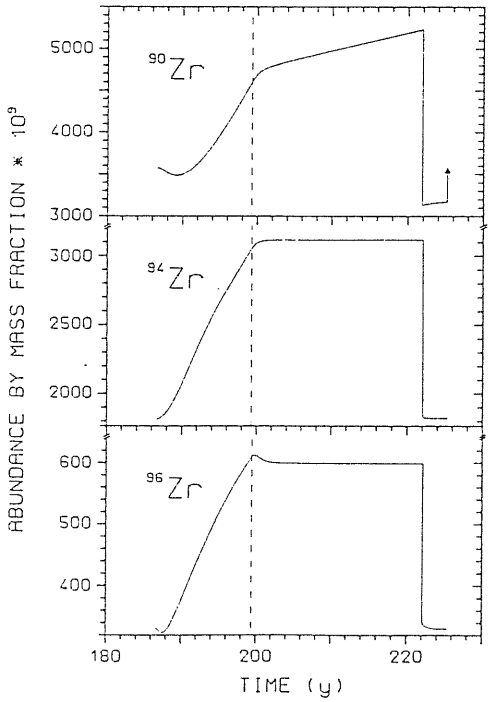

Figure 3.6: Evolution of the Zr abundances for the isotopes 90, 94 and 96 in the asymptotic limit of the LMS model; dashed line indicates the end of the ^{13}C ingestion phase

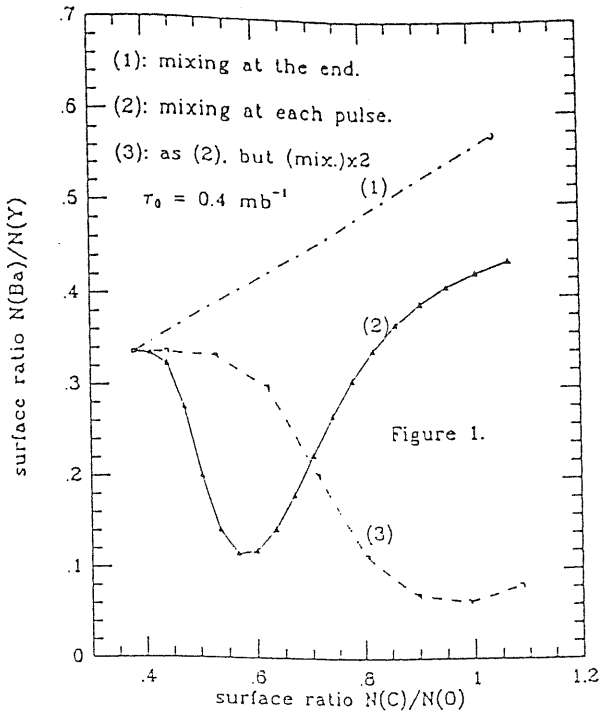

Figure 3.7: The surface ratio N(Ba)/N(Y) as a function of N(C)/N(O) for different mixing prescriptions in the low mass star model

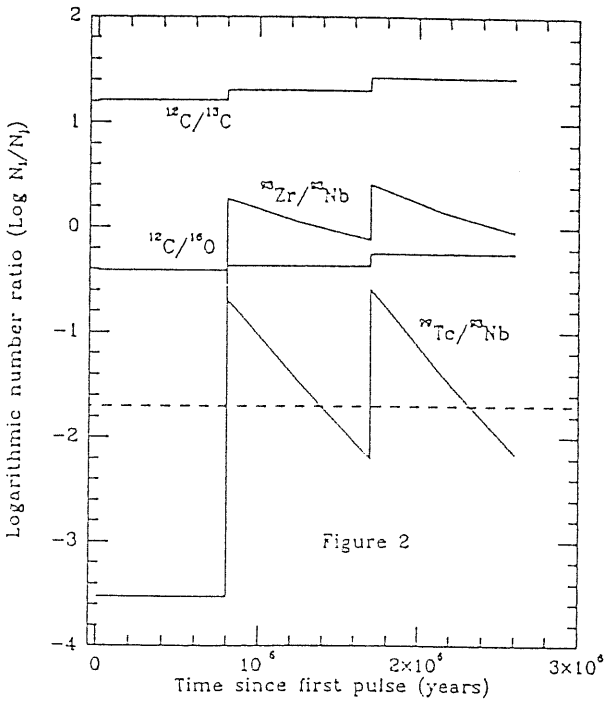

Figure 3.8: Surface ratios as a function of time since the first pulse in the low mass star model; the dredge–up is assumed to occur every 9 pulses

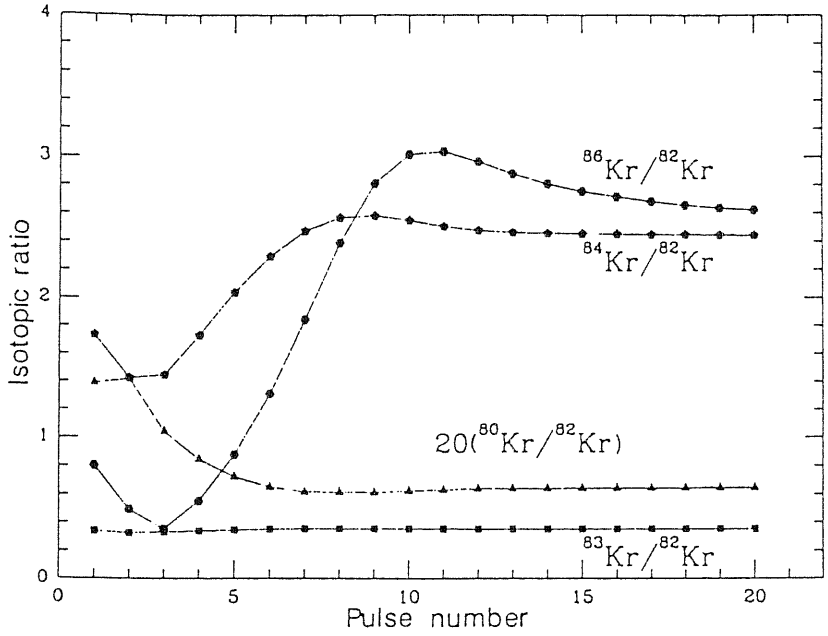

Figure 3.9: Variations with pulse number of krypton isotopic ratios with respect to ^{82}Kr for a TP–AGB star with [Fe/H] = –0.2

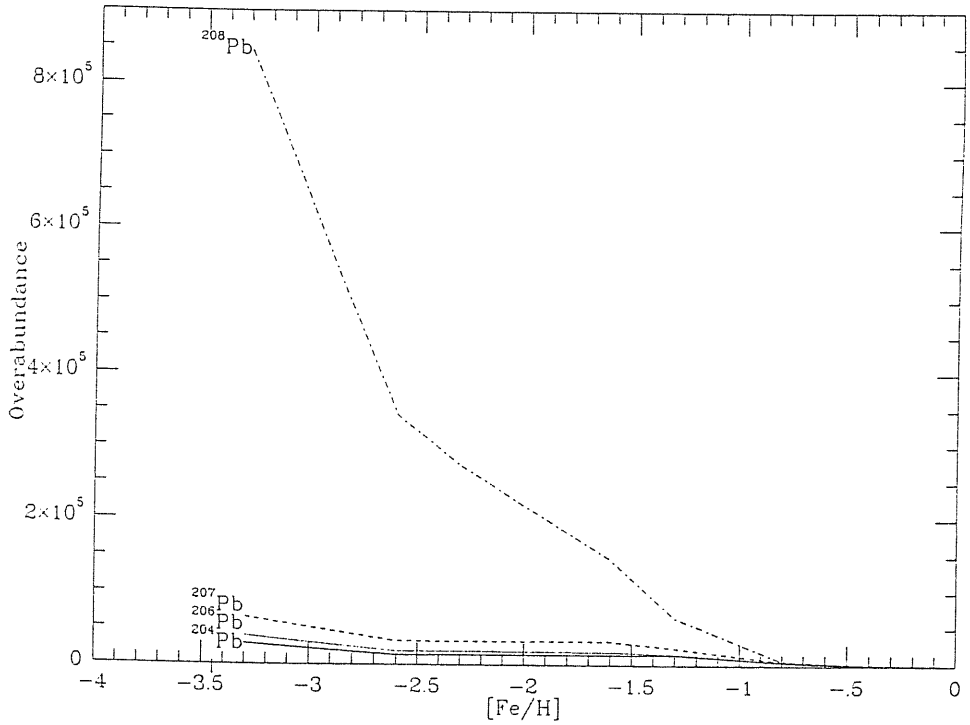

Figure 3.10: Overabundances of the Pb isotopes as a function of metallicity [Fe/H] produced by *s*–processing in low mass stars

Chapter 4

THE WEAK COMPONENT: s–PROCESSING IN A 25 $M_\odot$ STAR

4.1 INTRODUCTION

As we have previously said in § 3.3, massive stars during core He burning appear to offer the most promising scenario for the weak component, the details of the nucleosynthetic process depending on the evolutionary models and on the set of nuclear inputs adopted.

The hydrostatic stages of stellar evolution can be followed with the numerical codes that have been developed since the early calculations by Kippenhan, Weigert and Hofmeister (1967), even if there are still some physical details whose treatment is under debate. The main sources of uncertainties at present concern the correct formulation of *mass loss* and *mixing criteria.*

As for *mass loss*, even if the physical nature of the mechanism is still obscure, observations show that stars do lose mass during their lives, the phenomenon being particularly significant for the most massive and coolest ones. The mass loss rate changes with the type of star and with luminosity, and is commonly given by empirical relations of the kind $\dot{M}$ = f (L, R, M,...) (see Chiosi and Maeder, 1986 for a detailed review). Brunish and Truran (1982a,b) studied the evolution of massive stars with and without mass loss. They found that the inclusion of mass loss has the following consequences:

- the evolutionary track in the HR diagram moves at lower luminosity and effective temperature;
- since less energy must be radiated away, the Main Sequence phase is prolongued, and also the helium burning lifetime is generally increased;

- stars move faster towards the red all along the He–burning;
- during the Main Sequence, semiconvective regions are narrower and of shorter duration;
- in the next phases, the amplitude of convective regions is reduced;
- the mass fraction $q_\alpha = M_\alpha/M_{tot}$ occupied by the helium core is left unchanged when a moderate mass loss is included, because both M_α and M_{tot} are decreasing, while the maximum size the convective core reaches during He–burning is largely unaffected by mass loss (but see Maeder, 1981a, who found that in mass–losing models the growth of the convective core in this phase is greater than for constant mass evolution).

Moreover, when substantial mass loss rates are considered, nuclear processed matter can appear on the surface, and be detected spectroscopically, providing information on the correctness of our assumptions on stellar evolution and nucleosynthesis.

Finally, the lost material which comes back to the interstellar medium takes part in the chemical enrichment of the Galaxy.

Besides the rate of mass loss due to stellar winds, the basic problems in stellar modeling have their origin in the poor theoretical understanding of *mixing processes* occurring in the stellar interior. The mixing mechanisms acting in stars are still not well known, and a satisfactory theoretical treatment for them is missing. As a result, the existing stellar evolutionary codes adopt different prescriptions leading sometimes to controversial results. A detailed analysis of this subject is beyond the aims of this thesis; however, we shall briefly discuss the consequences of semiconvection on massive stars, as well as compare the classical models with those which take account of convective overshoot.

Seminconvection is likely to occur in regions which are characterized by a gradient in the mean molecular weight μ, and by their being unstable according to the Schwarzschild's criterion:

$$\nabla_{rad} \geq \nabla_{ad},$$

where ∇_{rad} is the radiative temperature gradient and $\nabla_{ad} = (d\ln T/d\ln P)_{ad}$ the adiabatic one. Situations where semiconvection may appear are found when the convective core shrinks during the Main Sequence evolution, or when the H–burning shell moves outwards during the core helium burning. In semiconvective regions the mixing timescale is slower than in convective zones, because the μ gradient fights against convection, trying to restablish equilibrium. However, a rearrangement of the chemical composition of the layers involved is obtained, until a neutrality condition is reached, which is either the Schwarzschild's one ($\nabla_{rad} = \nabla_{ad}$), or the Ledoux's one:

$$\nabla_{rad} = \nabla_{ad} + \frac{\beta}{4-3\beta}\nabla_\mu \equiv \nabla_L,$$

where $\beta = P_g/P_{tot}$ is the ratio between the gas pressure and the total pressure, and $\nabla_\mu = d\ln\mu/d\ln P$ is the mean molecular weight gradient.

By using a diffusion approximation to semiconvection, Langer, El Eid and Fricke (1985) and Langer (1986b) pointed out that while during the H–burning evolutionary phase the nuclear timescale is much greater that the semiconvective mixing timescale, so that the Schwarzschild's criterion for convection can be used, in the subsequent phases the Ledoux's criterion has to be considered and the inclusion of semiconvection implies that less mixing is allowed in comparison to the canonical treatment, which can greatly affect the evolutionary behaviour of the star. In particular Langer (1986b) found that the slowly mixed region on the top of the growing convective He–burning core, which develops because of the large μ–gradient at that point, has the effect of reducing the ^{12}C concentration at He–exhaustion and to lead to a nearly complete burning of the ^{22}Ne through the ^{22}Ne(α,n)^{25}Mg reaction in the final stages of helium burning. This is supposed to increase the s–process nucleosynthesis efficiency (see below).

Another important problem dealing with mixing processes in stars is related to the extension of convective cores. When we follow the canonical prescription to delimit a convective region (the Schwarzschild's condition), we assume the boundaries to be positioned where the acceleration of the convective bubbles goes to zero. But it seems reasonable that the convective elements would continue their travel until their velocity goes to zero, penetrating (overshooting) into the adjacent regions that are in radiative equilibrium. A correct treatment of *overshoot* has to be non–local, and can be formulated either through the mixing lenght theory, or in terms of diffusive processes. According to the former picture, the extension of convection is parametrized as a fraction Λ of the local pressure scale height H_p. When overshooting is considered, several consequences are found (Bressan, Bertelli and Chiosi, 1981; Bertelli et al., 1984, 1985, 1986; Maeder and Meynet, 1987; Alongi et al., 1991):

- the convective cores during H and He burnings are enlarged, the effect being stronger for the smaller masses, and this implies that these models have larger helium and carbon–oxygen cores, which ultimately means that the central conditions (central temperature and density) match those of more massive stars. In particular, the C/O ratio at the end of core He–burning will be affected, being lowered if some overshooting is present;

- the evolutionary tracks in the HR diagram run at higher luminosities, and a wider Main Sequence band covering a larger range of effective temperatures is obtained;

- the total stellar lifetime is enhanced; as for the core H–burning episode, it is prolongued, while the He–burning one is shortened. This is explained by the fact that the higher luminosities of these models act in the direction of a faster

evolution that during the Main Sequence phase is reversed by the availability of a greater amount of fuel (greater core mass);

- semiconvective instability does never occur in models with overshooting from the convective core.

Anyway, there are no theoretical prescriptions on the amount of overshooting which may be present in stellar interiors, and Λ has to be calibrated through a careful comparison with the observations.

Compared to those obtained from classical models, isochrones as well as synthetic C–M diagrams based on models with overshoot from the core exhibit the following features (Chiosi, Bertelli and Bressan, 1988; Maeder and Meynet, 1989; Chiosi et al., 1989; Alongi et al., 1991):

- the main sequence width increases;
- the ages determined from turn–off, red star clump and asymptotic giant branch (AGB) luminosities are longer;
- the blue loops observed in intermediate age star clusters can be matched if also a moderate overshoot of the convective envelope in intermediate mass stars is considered. Indeed, a certain amount of envelope overshoot in low mass stars, while climbing along the red giant branch (RGB) toward central He ignition, seems to be required to bring the luminosity of the bump predicted in the theoretical RGB luminosity function into agreement with the observed one;
- the number ratio of main sequence stars to post main sequence objects is enhanced;
- the upper limit for stars to experience thermal pulses on the AGB is decreased from 8–9 $M_\odot$ of the classical models to $\approx 5\ M_\odot$; as a consequence, no luminous C and M stars are expected in clusters with turn–off masses greater than $\approx 5\ M_\odot$;
- the transition from clusters exhibiting a well developed RGB to those which do not occurs at $\approx 1.6\ M_\odot$ instead of $\approx 2.2\ M_\odot$ as in the classical models.

These observational information can in principle be used to calibrate the amount of overshoot, but the situation is more complicated, so that a firm conclusion is still to be found.

An alternative way of obtaining a growth of the convective core during He burning relies on a local stability analysis, and has been called *induced semiconvection* (Castellani, Giannone and Renzini, 1971a,b; Castellani et al., 1985). In few words, the increasing chemical discontinuity that occurs at the edge of the convective core leads to a growing discontinuity in the radiative gradient, that has not physical

meaning (Schwarzschild, 1958). The difficulty is solved by mixing the core with external material from the radiative region, thus enlarging the convective region.

Finally, one has to notice that other mixing mechanisms have also been suggested to give larger convective cores, such as shear flow instabilities, meridional circulation or turbulent diffusion

The final stages of stellar evolution, on the other side, have to be studied by means of hydrodynamical codes, since the timescales of the nuclear processes involved become very short, and problems such as formation of shock waves must be faced.

As for the nuclear inputs, we have to notice that the $^{12}C(\alpha,\gamma)^{16}O$ thermonuclear reaction rate, which plays a crucial role in the stellar evolution from He burning on, has suffered significant changes in the last years. In their most recent compilation Caughlan and Fowler (1988, hereafter CF88) still give it with an uncertainty of a factor 2. Also the α–capture rate on ^{22}Ne, the neutron source, is not well determined (Barnes, 1982; Wolke et al., 1989; Bach et al., 1990). Another important input is the ^{22}Ne neutron capture cross section: the latest measurements by Winters and Macklin (1988) and by Beer et al. (1989) suggest a value of (0.06 ± 0.005) mb (at 30 keV), much lower than the one proposed by Almeida and Käppeler (1983), and close to the older estimate by Fowler, Caughlan and Zimmerman (1967). This parameter is critical for the neutron economy of the s–process, because it determines the efficiency of ^{22}Ne as a neutron absorber (Busso and Gallino, 1985; Prantzos, Arnould and Arcoragi, 1987).

Furthermore, the set of neutron capture cross sections and of β–decay rates of unstable nuclides, based on the key works by Bao and Käppeler (1987) and by Takahashi and Yokoi (1987), has been improved by a number of more recent data, whose effects on s–processing in massive stars have not yet been investigated. In the meantime, revised solar-system abundances were published by Anders and Grevesse (1989; hereafter AG89); they differ in some respects from the usually adopted compilation by Cameron (1982), particularly concerning the CNO abundances, on which the amount of ^{22}Ne present in the core H burning depends.

Taking into account the above changes, we want to re–investigate the s–process that can occur in massive stars, using the best evolutionary models and the most updated nuclear inputs. In this Chapter we first follow the evolution of a 25 $M_\odot$ star of Pop. I ($Z = 0.02$) from the Zero Age Main Sequence (ZAMS) up to carbon burning, with different prescriptions for the $^{12}C(\alpha,\gamma)^{16}O$ reaction rate. The results of the evolutionary calculations are discussed in § 4.2. The products of the n–capture nucleosynthesis are presented in § 4.3 and the influence of variations in some critical nuclear inputs is analyzed. A comparison of our results with previous calculations of s–processing during core He burning is also made.

Then we consider the subsequent evolutionary stages and see that neutron captures during shell C burning can significantly change the s–abundances (§ 4.4).

Finally, since our purpose is to study the chemical enrichment of the interstellar medium in *s*–nuclei, in § 4.5 we evaluate the composition of the *s*–processed matter which is ejected by a 25 $M_{\odot}$ star.

4.2 THE EVOLUTION OF A 25 $M_\odot$ STAR

The integration of the stellar structure was performed by means of an updated version of the FRANEC evolutionary code (Chieffi and Straniero, 1989; Straniero, 1989), based on a Newton–Raphson scheme.

The adopted criterion for convective stability is the Schwarzschild's one. Semiconvection is not included in the code; however, adopting a fine mass zoning, in the region of variable chemical composition a series of alternating, thin convective and radiative shells develop, in the same manner as described by Lamb, Iben and Howard (1976). As a consequence, a gradient of mean molecular weight results, that mimics the introduction of semiconvection. No convective overshooting is allowed; instead, during the growing of the convective He core, mixing of core material with He–rich matter from the outside is obtained as the result of an increase in the opacity, according to the so–called "induced semiconvection" discussed by Castellani et al. (1985). Finally, the surface convection is treated through the mixing length formalism, with a mixing length to pressure scale height ratio $\alpha = l/H_p = 1.6$, as derived by best fitting the Sun.

The nuclear energy generation is followed through a network that includes 20 nuclides from H up to Si. Concerning the $^{12}C(\alpha,\gamma)^{16}O$ reaction rate, as already mentioned, the latest recommended value by CF88 is given within a factor-of-two uncertainty. It is intermediate between those previously quoted by Caughlan et al. (1985; hereafter CFHZ85, which is 2 times higher), and by Fowler, Caughlan and Zimmerman (1975; hereafter FCZ75, which is 1.5 times smaller). A first evolutionary computation was made adopting the thermonuclear reaction rates by CFHZ85; a second run was made using for the $^{12}C(\alpha,\gamma)^{16}O$ reaction the older rate by FCZ75. Finally, a third track was run adopting the CF88 set of thermonuclear reaction rates; in this case it was prolonged until central carbon exhaustion. Since the analysis by Thielemann, Hashimoto and Nomoto (1990) on the elemental observations of SN1987A tends to confirm the CFHZ85 choice, we shall consider the results of the first run as our standard case.

We followed the evolution of a 25 $M_\odot$ star with a helium abundance $Y = 0.28$ and a metallicity $Z = 0.02$. The evolutionary track in the HR diagram is shown in Figure 4.1, while Figure 4.2 gives a picture of the evolution of the central conditions.

4.2.1 The Core Hydrogen Burning Phase

Our model sets up on the ZAMS with $\log(L/L_\odot) = 4.882$ and $\log T_e = 4.582$. The convective core mass is 12.705 $M_\odot$, and the central temperature and density are $\log T_c = 7.565$ and $\log \rho_c = 0.584$.

The transmutation of H into He through the CNO cycle makes the opacity decrease and the convective core recede; above the convective core a region of variable steplike chemical profiles is present (see Figure 4.3). In this figure, as in the following figures of this kind, *L, R, P, T, D* stand for luminosity ($L_\odot$), radius ($R_\odot$),

pressure (dyne/cm^2), temperature (K) and density (g cm^{-3}) respectively; *En* is the rate of nuclear energy generation (erg/g/s); K the opacity (cm^2/g); *Rad* and *Ad* are the radiative and adiabatic gradients. The physical parameters are normalized to their maximum value, shown on the right of the figure. The core H burning phase lasts for 6.101 Myr. At central H exhaustion the central temperature and density are: $\log T_c = 7.901$ and $\log \rho_c = 1.675$, and the photospheric values are $\log T_e = 4.523$ and $\log(L/\mathrm{L}_\odot) = 5.227$. The star is left with a He core $\mathrm{M}_\alpha = 6.772\ \mathrm{M}_\odot$.

4.2.2 The Shell Hydrogen Burning Phase

The H shell starts at a mass $M_r \sim 6.9\ \mathrm{M}_\odot$ and has an extension of $\sim 5.4\ \mathrm{M}_\odot$. The temperature corresponding to the peak of the shell energy generation is $\sim 4.07 \times 10^7$ K, high enough to produce the CNO equilibrium at once. This can be seen by looking at the N and C profiles in Figure 4.4, that show sharp peaks at a stellar mass fraction $M_r/M_{tot} \sim 0.29$. The star spends 1.117×10^4 yr in this H–shell–energy supported, radiative core phase.

4.2.3 The Core Helium Burning Phase

He ignition takes place when $\log(L/\mathrm{L}_\odot) = 5.246$, $\log T_e = 4.310$; the values of the central temperature and density are: $\log T_c = 8.164$ and $\log \rho_c = 2.668$. A convective core forms again, which grows very rapidly to include $\sim 16\%$ of the stellar mass (see Figure 4.5). The structure of the star at the point of maximum penetration of the convective envelope is shown in Figure 4.6.

When the central helium content Y_c falls below ~ 0.26, the $^{12}\mathrm{C}(\alpha,\gamma)^{16}\mathrm{O}$ reaction becomes effective, and carbon starts to be consumed. At this time the central temperature and density are 2.128×10^8 K and 7.980×10^2 g/cm^3, respectively.

At the end of core He burning, the values of the photospheric parameters are $\log(L/\mathrm{L}_\odot) = 5.343$, and $\log T_e = 3.567$, while the central ones are $\log T_c = 8.539$ and $\log \rho_c = 3.524$. The star is left with a carbon–oxygen core $M_{CO} = 6.295\ \mathrm{M}_\odot$ where carbon and oxygen mass fractions are $X_C \simeq 0.17$ and $X_O \simeq 0.80$, inside a H–exhausted core $\mathrm{M}_\alpha = 8.876\ \mathrm{M}_\odot$. The He core mass has increased by $\sim 31\%$ since the end of core H burning. The whole He–burning phase lasts 0.635 Myr; the ratio between core He burning and core H burning durations is $\Delta t_{He}/\Delta t_H = 0.104$.

4.2.4 Effects of Variations in the $^{12}\mathrm{C}(\alpha,\gamma)^{16}\mathrm{O}$ Reaction Rate

As discussed above, we made two other different runs, with the FCZ75 rate for the $^{12}\mathrm{C}(\alpha,\gamma)^{16}\mathrm{O}$ reaction and by updating the code with the whole CF88 set of thermonuclear rates. Table 4.1 points out the main differences among the various cases at He exhaustion: the higher the rate, the lower is the final C/O ratio and the longer the He–burning phase. This is due to the fact that $^{12}\mathrm{C}(\alpha,\gamma)^{16}\mathrm{O}$ releases about the same energy as the 3α reaction, with only one α–particle being involved

instead of three. On the contrary, the CO core mass near He exhaustion and the T and ρ stratification, on which the s–process nucleosynthesis critically depends, are only marginally affected, as already noticed by Arnett (1972a). In particular, the core models obtained with the rates by CF88 and by FCZ75 are almost identical.

4.2.5 Comparison with Previous Works

We followed a canonical model, that is a model without mass loss and convective overshooting. Stellar models of 15 and 25 $M_\odot$ of solar composition were calculated by a number of authors, among whom Lamb, Iben and Howard (1976), Weaver, Zimmerman and Woosley (1978), Woosley and Weaver (1988), with different prescriptions concerning the treatment of convection and other physical inputs. Evolution of pure He stars were calculated by Arnett (1972a, b; 1977) and by Nomoto and Hashimoto (1988). A whole series of presupernova stellar models were analyzed by Maeder (1981a,b) with and without mass loss. Evolutionary sequences for $M = 15$, 30 and 40 $M_\odot$ stars were run by Brunish and Truran (1982a), who also considered the effects of mass loss. Finally, Bressan, Bertelli and Chiosi (1981), Maeder and Meynet (1987; 1989), and Langer, Arcoragi and Arnould (1989) computed models taking into account both mass loss and overshooting.

For stars less massive than $M \leq 30$ $M_\odot$ mass loss has a negligible effect on the core structure. The introduction of overshooting tends to produce larger core masses, leading the star to evolve at higher central temperatures and lower densities. Nevertheless, the only relevant change concerns the relation between the initial mass and the CO core mass (see e.g. Chiosi and Maeder, 1986): for a fixed core mass, the central structure and hence the s–processing do not depend on overshooting, as already stressed by Langer, Arcoragi and Arnould (1989).

Substantial differences in the outer stellar physical conditions affecting the evolutionary track in the HR diagram are found by the various authors. However, concerning the structure of the convective He core, a general consistency is found between the above models and our findings; in particular, our T and ρ stratification is in close agreement with the results by Lamb, Iben and Howard (1976).

4.3 NEUTRON CAPTURES DURING He BURNING IN A 25 $M_\odot$ STAR

The computational method we used to follow the s–nucleosynthesis is discussed in the papers by Busso and Gallino (1985) and Busso et al. (1988).

The differential equations governing the abundance changes of light ($A < 28$) nuclei are:

$$dY_i/dt = \rho Y_4 \sum(R_{ij}Y_j - R_{ji}Y_i) + \sum(Y_j\lambda_{ji} - Y_i\lambda_{ij}) + n_n(< \sigma v >_{jn} Y_j - < \sigma v >_{in} Y_i), \quad (4.1)$$

where $Y_i = X_i/A_i$. Here X_i is the abundance by mass of the element i, A_i is its atomic mass, n_n is the number density of neutrons and $< \sigma v >_{in}$ is the Maxwellian averaged product of the n–capture cross section and of velocity. In equation 4.1, $R_{ij} = N_A < \sigma v >_{j\alpha}$ is the rate of production of the element i via α–captures on the element j; λ_{ij} is the probability of a beta decay from the element j to the element i.

The first term of equation 4.1 takes into account (α , n) and (α , γ) reactions, the second one describes weak interactions, and, in the third one, the n–captures, including (n, p) and (n, α) reactions, are considered.

In the above conditions, the neutron density is determined by assuming equilibrium between production and destruction in the equation:

$$dn_n/dt = \rho^2 N_A Y_\alpha R_j^{\alpha,n} Y_j - \rho N_A n_n \sum < \sigma v >_{kn} Y_k. \quad (4.2)$$

The neutron flux generated by (α , n) reactions in equation 4.1 is distributed over the seed nuclei proportionally to their n–capture cross sections.

The numerical calculations were performed taking into account, for each element, all the competing reaction channels whose probability of occurrence is higher than some percent. In particular, a relevant number of unstable nuclei had to be explicitly inserted in the network to account for the competition between n–captures and beta decays.

We divided the core mass of our 25 $M_\odot$ model into different meshes (at maximum mass extension we have 60 meshes), and derived the temperature and density gradients from the evolutionary data, as well as the temporal evolution of the convective core mass and of the central temperature and density.

We started from that point during core He burning when n–captures begin to be effective. The isotopic abundance distribution is taken from the evolutionary calculations. In particular, ^{14}N and ^{18}O have been completely converted into ^{22}Ne through α–captures. To all the isotopes that have not been processed in the previous evolution, solar–system abundances were assigned according to AG89.

The s–processing takes place near core He exhaustion, when the central temperature increases from $\sim$ 2.2 up to $\sim$ 3.5 $\times 10^8$ K, and the central density from $\sim$

1000 up to $\sim$ 3000 g/cm^3. We followed the neutron captures with a nuclear network including 450 isotopes and 41 branchings along the s–process path.

To determine the weak interaction rates of unstable nuclides included in the network, we started from the data by Takahashi and Yokoi (1987). Given the temperature and density stratification, we interpolated among the Takahashi and Yokoi's grid points in order to give for every nuclide the beta decay rates corresponding to each mesh. They were then averaged in mass over the whole convective core. The β–decay rate for ^{79}Se was taken from the most recent investigation by Klay and Käppeler (1988), and the rates for the lighter nuclei ($Z < 26$) from Cosner and Truran (1981) and from Fuller, Fowler and Newman (1982).

For the choice of the neutron capture cross sections we refer to the paper by Käppeler et al. (1990a); they are essentially based on the compilation by Bao and Käppeler (1987), implemented by a number of more recent data. In particular, in the range $56 \leq A \leq 90$, we have introduced the small corrections by Ratynski and Käppeler (1988), together with the new measurements on ^{86}Kr and Rb isotopes by Beer and Macklin (1989). As for ^{84}Kr, according to the analysis by Käppeler et al. (1990a), we choose for its n–capture cross section a value of 30 mb, which is close to the present lower limit: indeed, in low mass stars this choice was found to greatly improve the fit to solar ^{86}Kr and ^{87}Rb. As for ^{22}Ne, we adopted the 30 keV neutron capture cross section of 0.060 mb (Beer et al., 1989). An analysis of the isomeric states was performed according to the discussion of Käppeler et al. (1990a); due to the rather high temperature conditions in massive stars, the majority of these states turn out to be thermalized; exceptions are ^{85}Kr^m and possibly ^{180}Ta^m. Moreover, we also properly considered those isotopes whose n–capture cross section does not follow the usual $1/v$ law, among which ^{24,26}Mg, ^{28,30}Si, ^{56,57}Fe, ^{86}Sr, ^{87}Sr, ^{85,87}Rb, and ^{89}Y (Walter and Beer, 1985; Bao and Käppeler, 1987; Beer and Macklin, 1989; Käppeler et al., 1990b).

4.3.1 General Features of the Standard Case

Table 4.2 shows the values at central He exhaustion of the most important parameters describing the s–nucleosynthesis. The first one is the maximum value of the mean neutron density, while the second one is the peak value of the central density. The typical ratio between central and mean neutron density is $\sim$ 30. Then the value of the neutron exposure τ at 30 keV follows:

$$\tau(30keV) = \int \overline{n}_n(t) v_T dt,$$

where v_T is the thermal velocity at 30 keV. Table 4.2 also gives the value of n_c, and the ^{22}Ne mass fraction which is burnt during s–processing, starting from an initial value of 2.02×10^{-2}.

Figure 4.7 shows the temporal behaviour of the mean neutron density $\overline{n}_n$; it strongly increases with time up to its maximum value, and then abruptly decreases

when α-particles disappear. During the irradiation, the mean neutron density remains always very low, never exceeding 10^6 n cm^{-3}. The time history of the neutron exposure is illustrated in Figure 4.8.

The overabundances at He exhaustion are shown in Figure 4.9 as a function of the atomic mass; they are also reported in Table 4.2, selecting those isotopes whose overabundance is greater than 10. The following main features can be recognized:

- For $A < 70$ the highest production factor is found for ^{40}K. However, this very long lived isotope decays into ^{40}Ca with a half–life of 1.25×10^9 yr, so that its abundance will be further modified in the interstellar medium. Also ^{64}Ni, ^{65}Cu, ^{66}Zn, ^{67}Zn, ^{68}Zn, and ^{69}Ga have production factors greater than 100. Other isotopes which are efficiently produced are ^{22}Ne, ^{25}Mg, ^{26}Mg, ^{36}S, ^{58}Fe, ^{61}Ni, ^{63}Cu, whose overabundances are higher than 70.

- For $70 \leq A \leq 90$, the dominant nucleus is ^{80}Kr followed by ^{71}Ga, ^{70}Ge, ^{76}Se, ^{72}Ge, ^{82}Kr, ^{78}Se, ^{86}Sr, ^{73}Ge, ^{87}Sr. The overabundances of these isotopes are all greater than 100.

- For $A \geq 90$ the curve shows a cutoff, the heavy s–only isotopes having enhancements that average around 5. There are two exceptions: ^{152}Gd and ^{180}Ta, with overabundances of 39 and 23 respectively. As far as ^{180}Ta is concerned, its way of production is under debate. According to the analysis by Käppeler, Beer and Wisshak (1989), we followed the suggestion by Yokoi and Takahashi (1983) that in He–burning conditions the isomeric state is not thermalized. Hence, in our network the isomeric state (stable) and the ground state (unstable) are treated as separate nuclei, with a neutron capture production ratio from ^{179}Ta of 1:5.

The fall of the distribution beyond $A = 90$ is a known feature: it is due to the poisoning action of the light elements, first of all the ^{22}Ne daughter nucleus ^{25}Mg, which allows only $\sim 1/3$ of the neutrons to be captured by iron seeds. The s–only isotopes we are more interested in are ^{70}Ge, ^{76}Se, ^{80}Kr, ^{82}Kr, and ^{86}Sr, ^{87}Sr: among them, only ^{70}Ge and ^{76}Se are branching–independent. By looking at Figure 4.9 one sees that their overabundances are spread over a rather wide interval. However, we must recall that each of these isotopes receives a different contribution by the main component. This problem will be analyzed in detail in the next Chapter. Also the production of ^{58}Fe is worth a discussion: though it is not an s–only nucleus, Käppeler et al. (1982) stressed that it is hardly synthesized by other processes.

4.3.2 Sensitivity to Variations of α–capture Rates

When the CF88 rates are used, the s–process occurring during core He burning gives results close to the one obtained with the CFHZ85 rates, but the overabundances are slightly enhanced, the neutron exposure increasing from 0.206 to 0.219 mb^{-1}.

A lower α–capture rate on ^{12}C means that its competition with respect to the ^{22}Ne(α,n)^{25}Mg reaction decreases, allowing more α–particles to be captured by ^{22}Ne, thus enhancing the release of neutrons.

More important are the changes due to a possible variation of the ^{22}Ne(α,n)^{25}Mg rate. The recent paper by Wolke et al. (1989) shows how this rate is affected by a very large uncertainty in the low temperature regime which characterizes He burning conditions (below $T_9 \sim 0.35$), while there is a clear indication in favour of a higher efficiency of the ^{22}Ne(α , γ)^{26}Mg reaction with respect to the FCZ75 recommended value (notice that both in CFHZ85 and in CF88 the same FCZ75 rate for the α–captures on ^{22}Ne is quoted). In particular, at $T_9 = 0.3$, its enhancement factor may be between 2 and 50 (see Figure 4.10). Table 4.3 presents a preliminary analysis of the problem, showing the situation at He exhaustion. The quantity $\overline{n}_n^{max}$ is the maximum of the average neutron density, while n_n^{peak} is the maximum central value. The second column shows the results obtained with the FCZ75 choice. As we shall see in Chapter 5, this case gives the right overproduction factors for the s–isotopes, that allow to reach a good picture for the chemical enrichment of the Galaxy. Columns 3, 4 and 5 show cases where the (α ,γ) rate is multiplied by 5, while the (α ,n) one is allowed to vary. It is easy to recognize that only when the latter rate is two times higher than in FCZ75, the amount of s–processing is close to the FCZ75 case. Other positive solutions are found for other choices of the (α ,γ) rate, by properly varying the (α ,n) one: for instance, those in the last two columns of Table 4.3. Higher values of the (α ,γ) rate are not acceptable, since ^{22}Ne would be consumed before providing a convenient exposure.

In summary, we found that the higher (α , γ) rate suggested by Wolke et al. (1989) can still give an acceptable result concerning the s–process, provided the (α , n) rate at low temperature ($T_9 \simeq 0.3$) be slightly higher than the FCZ75 estimate.

4.3.3 Sensitivity to Other Uncertainties

Concerning the adopted set of n–capture cross sections from Fe up to Sr, one must consider that the experimental determinations have a fairly large uncertainty, of the order of 10% in the average. In addition, a few stable isotopes lying on the flow, ^{72,73}Ge and ^{77,78}Se, have only a theoretical estimate, which is uncertain by 50%. It results that, owing to the low neutron exposure, a number of isotopes having small cross sections with respect to nearby nuclides, and correspondingly larger abundances, e.g. ^{68}Zn, ^{70,72,74}Ge, ^{78}Se, let their uncertainty propagate along the s–process path. For example, a decrease by 13% of the cross section of ^{74}Ge implies a corresponding increase of its abundance by roughly the same amount, but also a decrease by about 5% of all heavier isotopes up to Sr. Consequently, with the present state of the art, one is not allowed to deduce too stringent conclusions on the s–nucleosynthesis occurring in massive stars. Of course, better evaluations of crucial cross sections in this atomic mass range are higly desirable.

4.3.4 Comparison With Previous s–Process Calculations.

The comparison between our results and previous works (Lamb et al., 1977; Arnett and Thielemann, 1985; Busso and Gallino, 1985) is some hard to perform because the evolutionary models have been improved in the meantime and a lot of nuclear parameters have been revised. A remarkable source of differences comes also from the adoption of the solar AG89 abundance distribution, which is characterized by a higher CNO content with respect to the compilations by Cameron (1973, 1982), implying that a larger ^{22}Ne abundance results and more neutrons can be released. Anyway, the main feature of s–processing in massive stars is preserved: a good efficiency in reproducing the s–only isotopes up to $A \simeq 90$, even if the production ratios among the various isotopes did show large variations in the past, owing to the more uncertain choice of cross sections.

More recently, Langer, Arcoragi and Arnould (1989) computed the evolution of a 15 $M_\odot$ star and a 30 $M_\odot$ one with initial composition $X = 0.70$, $Z = 0.03$, using the Cameron's (1982) solar–system abundances. Their models include mass loss according to the formulation by Lamers (1981) for hot stars ($T_e > 6500$ K) and by Reimers (1975) for the cooler ones; the 30 $M_\odot$ star was also run introducing a core overshoot of $l = 0.4H_p$. As for the nucleosynthetic calculations, they used the higher (but very uncertain) Almeida and Käppeler (1983) neutron cross section of 0.9 $\pm$ 0.2 mb for ^{22}Ne. The different n_c value and final overabundances are completely explained by the different assumptions in the above physical parameters.

4.3.5 Shell He Burning

During the last stages of core helium burning, the shrinkage in mass of the convective core leaves matter with variable chemical composition. However, owing to the steep shrinkage of the convective core, the actual inhomogeneity is confined only to the outer 0.5 $M_\odot$ zone, because at this time the integrated neutron exposure is practically frozen (see Figure 4.11).

In some of the past studies on this subject the subsequent formation of a radiative He shell was found to affect a mass zone already involved in core He burning; its effect would be to smooth out the composition gradient left behind in the C–O core. Investigations of the neutron capture nucleosynthesis occurring during the He shell phase were done by Arcoragi (1986), and by Busso et al. (1987). Arcoragi followed this process in a 15 and in a 30 $M_\odot$ star evolved by Langer (1986a), concluding that no significant s–processing occurs during shell He burning. Busso et al. (1987) studied helium core masses of 4 and 8 $M_\odot$ in the framework of Arnett (1972a,b) bare–core models, in which the radiative shell actually affects a mass region previously spanned by the convective He core. They found that, in the M_α = 8 $M_\odot$ model, due to the rather high temperature left after central exhaustion, some s–process nucleosynthesis resulted during the rapid initial rise of the He shell.

We followed the development of the radiative He shell in our 25 $M_\odot$ model

under both CFHZ85 and CF88 prescriptions. The shell temperature is always low ($T_8 = 1.5$), so that ^{22}Ne burning is never activated. We then conclude that the helium shell phase cannot change the abundances obtained during the previous core helium burning, and in evaluating the s–isotopes yields the material from the He–processed zone must be averaged over the n_c profile. The effect is a decrease of the s–process efficiency, the more important the less He–only processed region is left by the subsequent nuclear stages.

4.4 NEUTRON CAPTURES DURING C BURNING IN A 25 $M_\odot$ STAR

When the central temperature reaches a value of $\sim 7 \times 10^8$ K, carbon burning is ignited, whose features strongly depend upon the choice of the $^{12}C(\alpha,\gamma)^{16}O$ reaction rate, the specific treatment of convection, neutrino losses and on an appropriate determination of the equation of state. This leads to difficulties in modelling the most advanced phases and the supernova event.

With the FRANEC evolutionary code, core carbon burning develops as a radiative stage in a 25 $M_\odot$ star, both when the initial carbon content is low ($\sim$ 20%) as a consequence of a high rate for the $^{12}C(\alpha,\gamma)^{16}O$ reaction (CFHZ85), and when it is high ($\sim$ 40%), because a lower rate is used (CF88). As for the previous results, Lamb, Iben and Howard (1976) saw that while in a 15 $M_\odot$ star a small convective core develops, in a 25 $M_\odot$ star with $X_c = 0.20$ at He exhaustion carbon burns radiatively, similar to what is found in our calculations. In any case we are not interested in what happens in the core, because it will not participate to the galactic chemical enrichment, being trapped in the stellar remnant left by the supernova explosion. Moreover, all the inner region will suffer photodissociation reactions during O–burning that destroy the *s*–isotopes (Thielemann and Arnett, 1985). The problem is then to study the C–shell phase in order to see to what extent it can affect the CO core and how much *s*–processing can take place. A first evaluation of the *s*–process during shell C burning has been made by Thielemann and Arnett (1985). Since the typical temperature is of the order of 1–2 $\times 10^9$ K, the possibility of a strong *s*–process contribution by the chain $^{12}C(p,\gamma)^{13}N(\beta^+)^{13}C(\alpha,n)^{16}O$ is to be discarded, because it may only arise during central C burning operating at lower temperatures. On the other hand, the shell temperature is not high enough for the direct opening of the $^{12}C(^{12}C,n)^{23}Mg$ channel, that works only for $T_9 \geq 1.75$ (CF88). Consequently, only the $^{20}Ne(p,\gamma)^{21}Na(\beta^+)^{21}Ne(p,\gamma)^{22}Na(\beta^+)^{22}Ne(\alpha,n)^{25}Mg$ chain provides a source of neutrons, even if the ^{22}Ne nuclides are prevailingly destroyed by *p*–captures. From the work of Thielemann and Arnett (1985) one can infer that the contribution by shell C–burning to the neutron exposure is of the order of few 10^{-2} mb^{-1}.

Unfortunately, we could not follow the evolution of massive stars during shell C burning directly, because the FRANEC code has not yet been implemented to follow the more advanced evolutionary stages; nevertheless we can evaluate the *s*–nucleosynthesis during this phase relying on the presupernova models by NH88 and Woosley and Weaver (1988).

Woosley and Weaver (1988), adopting the CFHZ85 rate and introducing both semiconvection and overshooting, found that stars more massive than about 20 $M_\odot$ produce so little carbon during helium burning ($X_c = 0.12$ at He exhaustion for $M = 25$ $M_\odot$) that the following carbon and neon nuclear stages of stellar evolution are essentially skipped. However, the radiative C–burning shell shifts away rapidly,

affecting a large fraction of the CO core at the onset of the gravitational collapse. On the other hand, NH88, following a He star of $M_\alpha = 8$ with the same CFHZ85 rate but no overshooting, found $X_c = 0.19$ at He exhaustion, and a small convective C–burning core of 0.31 $M_\odot$, followed by two stages of convective shell C–burning. The second of them spreads from 1.79 up to 5.75 $M_\odot$ just before the core starts to collapse. A similar trend was found in the models by Arnett (1972b) for $M_\alpha = 8$, with initial $X_c = 0.36$. Summing up, the products of carbon nucleosynthesis are found inside a large part of the O–rich zone, both when the C shell burns radiatively and when it burns convectively. How can the C shell modify the *s*–processed matter left behind by He burning?

In the shell carbon burns typically at a constant temperature of $\simeq 1 \times 10^9$ K and a constant density of $\simeq 10^5$ g cm^{-3}. The duration of the process, as inferred from NH88, is 2×10^7 s in the M_α =8 model. The main nuclear network includes, besides the $^{12}C + {}^{12}C$ reaction, a number of $\alpha-$ and *p*–captures that are shown in Table 4.4. In order to follow the *s*–process nucleosynthesis during shell C burning, the neutron–capture network was completely revised with respect to the one constructed for He burning. Indeed the very different physical conditions and a higher initial n_n induce a different behavior of the neutron flow at the branching points, and some important β–decay rates as well as the astrophysical factors to be applied to the *n*–capture cross sections (Holmes et al., 1976) change. This in particular affects the ^{79}Se and ^{85}Kr branchings, and the production of ^{180}Ta: at the high temperature considered, the isomeric states of both ^{85}Kr and ^{180}Ta are assumed to be thermalized. We have also made a careful analysis of the behavior of neutron capture cross sections with stellar temperature. In particular, for Ne and Mg isotopes we derived the $< \sigma v > / v_{30keV}$ values at T_9= 1.0 shown in Table 4.5 (column 2). From the comparison with the 30 keV values of column 3 it appears that the effect of Ne and Mg isotopes as neutron poison is considerably enhanced during C burning.

The results of the calculation are presented in Table 4.6, where the most interesting isotopes are listed. The neutron exposure achieved is quite small: τ= 0.06 mb^{-1}, while the number of neutrons captured per iron seed is 2.35, so that the total n_c value goes from 5.67 at He exhaustion, up to $\simeq$ 8 at the end of the shell C–burning phase. Figure 4.12 shows the evolution of n_c as a function of time, and Figure 4.13 the temporal history of the average neutron density: it starts from a quite high initial value of $\sim 10^{11}$ cm^{-3} and then decreases exponentially. A similar behavior was predicted by the preliminary analysis of neutron captures during C burning by Arnett and Truran (1969). The consequence is that the neutron flow follows a different path with respect to the He burning stage and the abundance ratios between the *s*–isotopes are noticeably changed. The evolution of overabundances as a function of time is shown in Figure 4.14. As can be seen, ^{80}Kr and ^{82}Kr are first depleted, but then rise again. This is due to the initial very high value of the neutron density, that makes all the neutron flow arriving at the ^{79}Se branching go to ^{80}Se. This isotope has a low neutron capture cross section, and acts as a bottleneck, causing a decrease of ^{82}Kr. But then the neutron density goes down,

and the branching factor at ^{79}Se favors the production of krypton. A plot of the overabundances at the end of shell C–burning for all the stable nuclei involved is drawn in Figure 4.15 as a function of the atomic mass.

With respect to the results at He exhaustion, several features can be recognized: ^{58}Fe is lowered, while ^{76}Se is considerably enhanced becoming the most produced nucleus; ^{80}Kr is still high, but the ratio between its overabundance and that of ^{82}Kr has decreased, because of the different behavior of the neutron flow at the ^{79}Se branching; ^{86}Sr is left almost unchanged, while ^{87}Sr is much reduced. An important effect is the production of a consistent amount of ^{86}Kr and ^{87}Rb, which are crucial isotopes in the general scenario of the *s*–process, as already stressed in § 3.3. Interestingly, there is also a good production of ^{180}W, as the result of a fast decay of ^{180}Ta, whose isomeric state is now thermalized. The isotope ^{180}Ta itself is very much produced during the *n*–irradiation, but it completely decays before the final explosion, while ^{152}Gd is only slightly depleted. Together with ^{20}Ne, ^{24}Mg and ^{23}Na (the products of the ^{12}C+^{12}C reaction), also ^{25}Mg, created by the ^{22}Ne(α,n)^{25}Mg reaction, is largely enhanced. All these nuclei participate in a different way to the process of neutron absorption. As for the other light nuclei, good overproduction factors are obtained for ^{21}Ne, ^{36}S and ^{40}Ar, while ^{26}Mg and ^{40}K are more than half depleted with respect to He exhaustion. Finally, at higher atomic mass number, consistent production of ^{64}Ni, ^{75}As, ^{81}Br, ^{85}Rb as well as of some isotopes of Cu, Zn, Ga, Ge, Se and Kr are found.

A short comment on the way the C shell operates should be added. According to the NH88 prescriptions, three different convective C burning zones develop, that do not overlap each other. Were such an overlap effective, as indicated by previous models of Ikeuchi et al. (1971), Arnett (1972b), and Habets (1986), a more complex process of *s*–nucleosynthesis would occur, as sketched by Gallino and Busso (1985).

4.5 *s*–PROCESSED EJECTA FROM A 25 $M_\odot$ STAR

We saw that C burning affects the chemical composition of the CO core. We still have to evaluate how much He–processed matter is ejected unaltered by the supernova.

The discussion made in § 4.3 led to the conclusion that He burning enhancements for the *s*–isotopes must be calculated by performing an appropriate average over the n_c stratification left by the shrinkage of the convective core. This stratification is clearly illustrated in Figure 4.11, which shows how the number of neutrons captured per iron seed increases going towards the center of the star. One can recognize that the effect of the shrinkage is confined to the outer $\sim$ 0.5 $M_\odot$ of the CO core.

Table 4.7 gives the overabundances of the interesting isotopes and the mean n_c value after this average has been computed including different amounts of stellar mass, M_{shrink}, starting from the outer border of the CO core. The last column shows the same quantities in the center of the star at He exhaustion. The results of Table 4.7 can be understood by looking at the behavior of overabundances as a function of n_c, as in Figure 4.16. It can be seen that, while ^{58}Fe first increases, reaches a plateau and then smoothly decreases, ^{70}Ge, ^{76}Se, ^{80}Kr, ^{82}Kr, ^{86}Sr and ^{87}Sr suffer a monotonic enhancement with n_c. When the n_c value characterizing the situation of the center is reached, the spread among the overproduction factors is large. In particular ^{80}Kr is quite high with respect to all other *s*–isotopes. On the base of the M_α =8 presupernova model by NH88 (see Figure 4.17) we can infer that only the outer $\sim$ 0.25 $M_\odot$ of the CO core will be ejected by the supernova unaltered, so that for a 25 $M_\odot$ star the overabundances of the He–processed *s*–isotopes are those of column 3 of Table 4.7. The remaining part of the CO core has also seen C burning. However, in the inner core of massive stars, after carbon burning, Ne, O and Si burnings take place, followed by explosive nucleosynthesis episodes, when the shock wave leading to the supernova explosion moves across the nuclear shells. This shock front is not expected to modify the chemical composition of matter external to about 2.3 $M_\odot$ in the M_α =8 model by NH88 (Thielemann, Hashimoto and Nomoto, 1990). However, the mass limit is very uncertain, and detailed calculations of the explosion mechanism in a 25 $M_\odot$ star show that the composition is changed up to $\sim$ 3.8 $M_\odot$ (see figure 17 in Woosley, 1986). The temperatures involved are so high that the *s*–isotopes are completely destroyed by photodissociation.

As a conclusion, we can evaluate that a 25 $M_\odot$ star ejects $\sim$ 0.25 $M_\odot$ of material that has experienced *s*–processing during core He burning, and $\sim$ 2.5 $M_\odot$ of material that bears the signature of the *s*–process in the C shell phase.

$^{12}C(\alpha,\gamma)^{16}O$ rate	FCZ75	CFHZ85	CF88
α-captures	CFHZ85	CFHZ85	CF88
Δt_{He}(Myr)	0.560	0.635	0.568
$\Delta t_{He}/\Delta t_H$	0.092	0.104	0.092
$M_{CO}^{max}(M_\odot)$	6.037	6.295	6.037
X_C^{final}	0.47	0.17	0.40
X_O^{final}	0.50	0.80	0.56
$\log T_c^{final}$ (K)	8.540	8.539	8.539
$\log \rho_c^{final}$ (g cm^{-3})	3.533	3.524	3.523

Table 4.1: He–burning conditions with different prescriptions for reaction rates.

$\overline{n}_n^{max}$ (cm^{-3})	6.785 $\times 10^5$
n_n^{peak}(cm^{-3})	1.802 $\times 10^7$
τ (mb^{-1})	0.206
n_c	5.665
X_{22}^{burnt}	1.062 $\times 10^{-2}$

OVERABUNDANCES			
^{12}C	57.0	^{69}Ga	208.6
^{16}O	84.9	^{71}Ga	263.9
^{22}Ne	74.9	^{70}Ge	253.7
^{25}Mg	76.6	^{72}Ge	190.7
^{26}Mg	96.6	^{73}Ge	128.8
^{31}P	28.2	^{74}Ge	99.3
^{36}S	85.5	^{75}As	59.6
^{37}Cl	65.8	^{76}Se	212.2
^{40}Ar	47.9	^{77}Se	88.6
^{40}K	291.7	^{78}Se	108.9
^{50}Ti	15.9	^{79}Br	36.6
^{54}Cr	16.5	^{80}Kr	480.7
^{58}Fe	84.2	^{82}Kr	210.3
^{59}Co	35.9	^{83}Kr	63.0
^{61}Ni	84.6	^{84}Kr	52.6
^{62}Ni	49.9	^{85}Rb	28.6
^{64}Ni	164.5	^{86}Sr	147.3
^{63}Cu	91.8	^{87}Sr	129.2
^{65}Cu	226.3	^{88}Sr	34.8
^{64}Zn	41.0	^{89}Y	22.3
^{66}Zn	118.9	^{152}Gd	38.6
^{67}Zn	171.7	^{180}Ta	22.9
^{68}Zn	164.7		

Table 4.2: Results of the s–process calculations at the end of core He burning.

	FCZ75 FCZ75	(α,γ)*5 $(\alpha,n)/5$	(α,γ)*5 (α,n)*5	(α,γ)*5 (α,n)*2	(α,γ)*10 (α,n)*3	(α,γ)*20 (α,n)*7
$\overline{n}_n^{max}$ ($\times 10^5$ cm^{-3})	6.79	1.77	3.23	3.47	2.27	3.06
n_n^{peak} ($\times 10^7$ cm^{-3})	1.80	0.47	1.10	1.02	0.77	1.18
τ (mb^{-1})	0.21	0.05	0.29	0.21	0.20	0.20
n_c	5.66	0.97	9.36	6.00	5.28	5.39
^{58}Fe	84.2	72.4	48.9	80.4	89.1	88.0
^{70}Ge	253.7	4.3	717.2	292.9	212.2	223.1
^{76}Se	212.2	3.3	943.9	256.9	167.3	178.3
^{80}Kr	480.7	9.4	2539.8	593.5	372.4	398.9
^{82}Kr	210.3	5.8	1243.0	261.5	160.1	172.0
^{86}Sr	147.3	7.9	1172.7	186.1	110.0	118.1
^{87}Sr	129.2	7.5	1085.2	163.6	97.3	104.5

Table 4.3: Results of the s–process at He exhaustion when the α–capture rates on ^{22}Ne are varied. The lower part of the Table gives the enhancement factors for the isotopes indicated.

α–captures	p–captures
^{16}O(α,γ)^{20}Ne	^{16}O(p,γ)^{17}F
^{20}Ne(α,γ)^{24}Mg	^{20}Ne(p,γ)^{21}Na
^{21}Ne(α, n)^{24}Mg	^{21}Ne(p,γ)^{22}Na
^{22}Ne(α, n)^{25}Mg	^{22}Ne(p,γ)^{23}Na
^{22}Ne(α, γ)^{26}Mg	^{23}Na(p, γ)^{24}Mg
^{24}Mg(α, γ)^{28}Si	^{23}Na(p, α)^{20}Ne
^{25}Mg(α, n)^{28}Si	^{24}Mg(p, γ)^{25}Al
^{26}Mg(α, n)^{29}Si	^{25}Mg(p, γ)^{26}Al
	^{26}Mg(p, γ)^{27}Al

Table 4.4: Charged particle network during shell C burning

	$< \sigma v > / v_{30keV}$	σ_{30keV}
$^{20}Ne^a$	0.461	0.0767
$^{22}Ne^a$	0.159	0.06
$^{24}Mg^b$	5.5	4.2
$^{25}Mg^b$	7.3	6.5
$^{26}Mg^b$	0.6	0.084

[a] Winters and Macklin (1989)
[b] Weigmann et al. (1976)

Table 4.5: Neutron capture cross sections for Ne and Mg isotopes

$\overline{n}_n^{max}$ ($\times 10^{11}$ cm^{-3})	1.672
τ (mb^{-1})	0.059
n_c	2.354
^{58}Fe	56.7
^{70}Ge	527.1
^{76}Se	763.1
^{80}Kr	675.6
^{82}Kr	495.9
^{86}Kr	224.3
^{87}Rb	292.3
^{86}Sr	147.4
^{87}Sr	57.3
^{152}Gd	29.2
^{180}Ta	1184.5
^{180}W	102.7

Table 4.6: Results of the shell C burning

M_{shrink} ($M_\odot$)	0.10	0.25	0.50	3.1	6.0	center
^{58}Fe	75.6	94.5	100.5	87.8	86.0	84.2
^{70}Ge	5.0	11.0	46.8	212.4	232.6	253.7
^{76}Se	3.8	7.1	31.3	174.2	192.8	212.2
^{80}Kr	10.2	17.0	67.4	391.7	435.2	480.7
^{82}Kr	6.1	8.5	29.8	171.2	190.3	210.3
^{86}Sr	8.2	10.8	24.6	120.0	133.3	147.3
^{87}Sr	8.0	10.9	23.1	105.6	117.2	129.2
^{152}Gd	20.6	19.6	21.7	34.5	36.6	38.6
^{180}Ta	5.1	3.6	32.5	18.8	20.8	22.9
$\overline{n_c}$	1.053	1.597	2.577	5.097	5.375	5.665

Table 4.7: Results of the shrinkage of the He convective core.

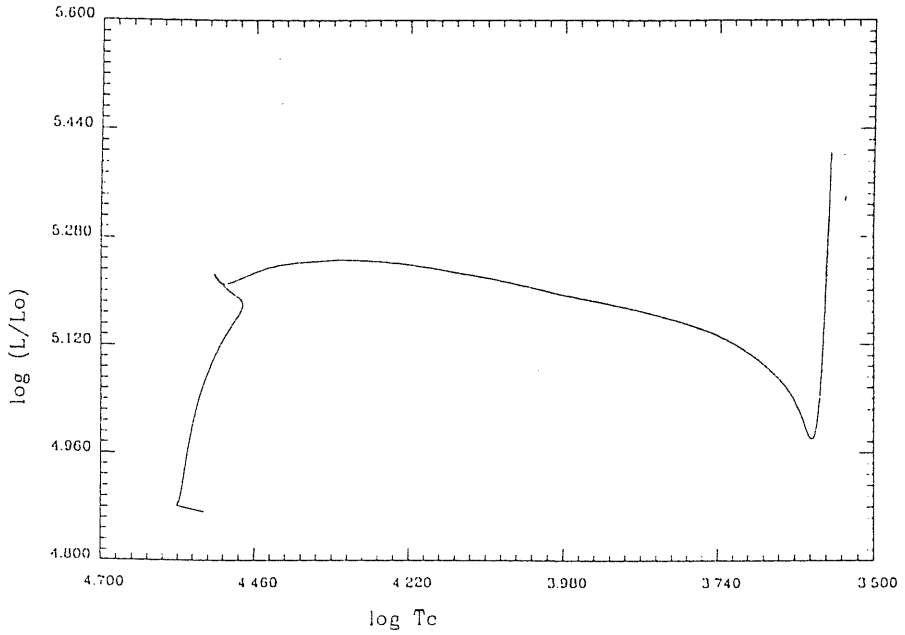

Figure 4.1: The evolutionary track in the HR diagram for the 25 $M_\odot$ star with the CFHZ85 choice of thermonuclear reaction rates.

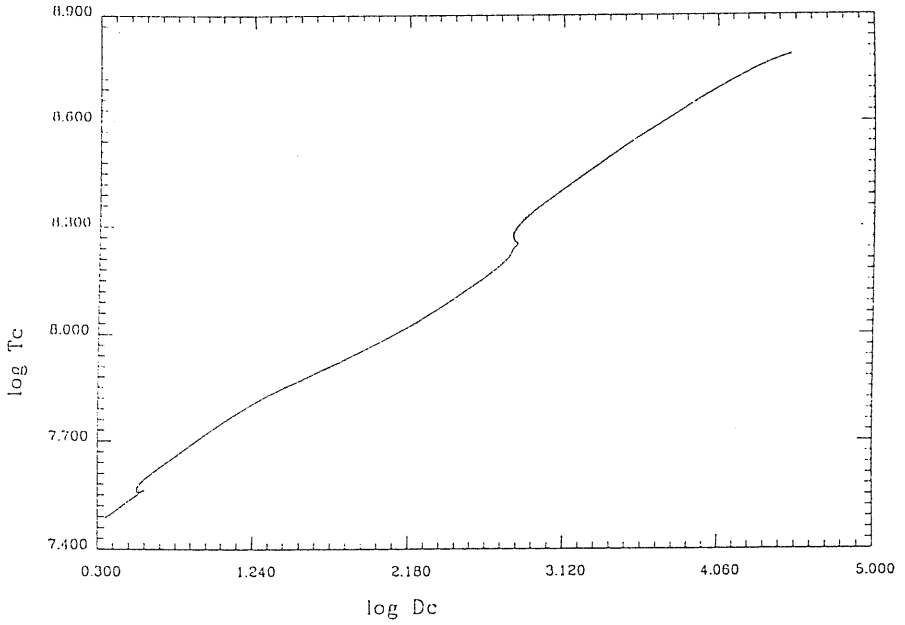

Figure 4.2: The evolution of the central conditions.

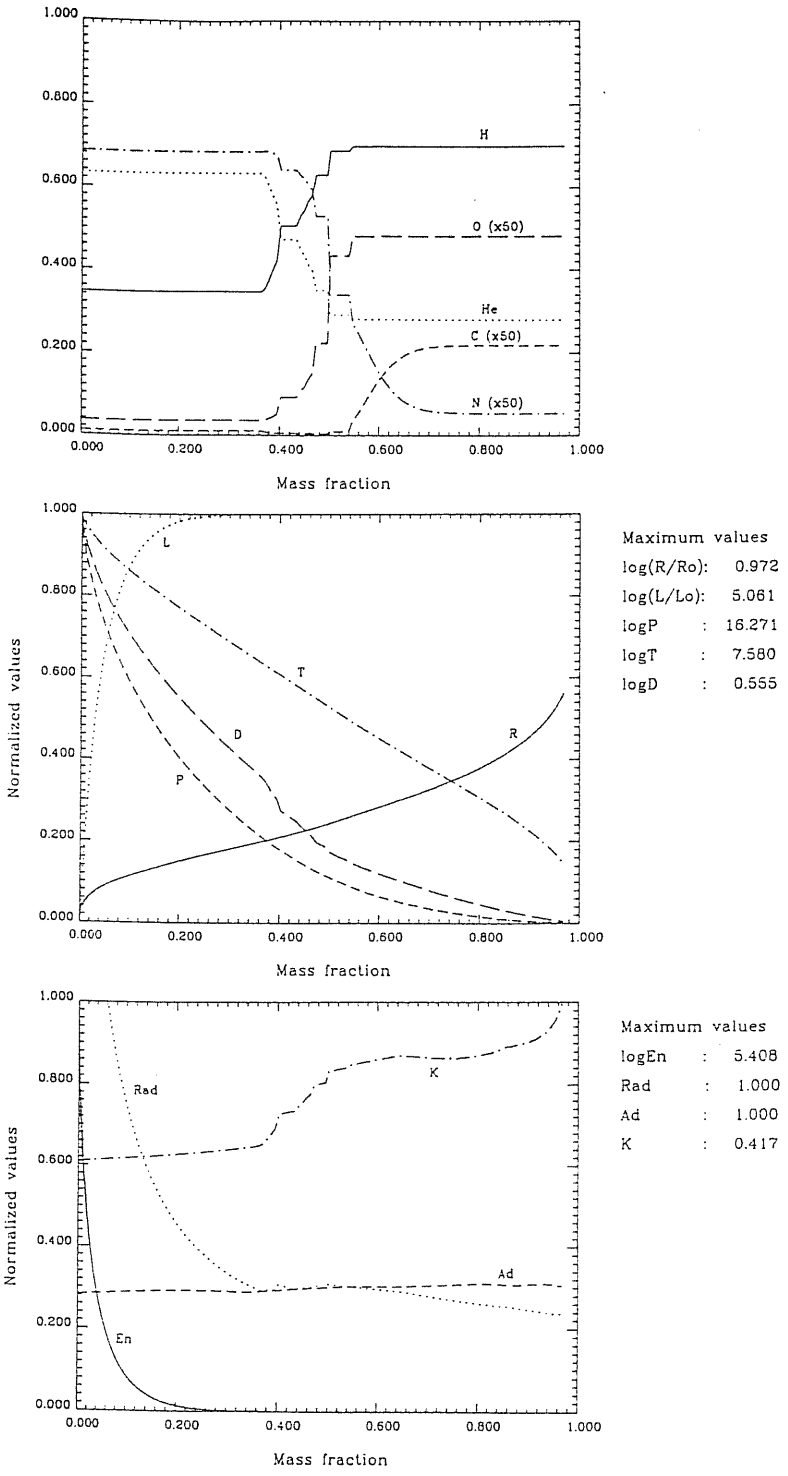

Figure 4.3: The chemical and physical structure during hydrogen burning.

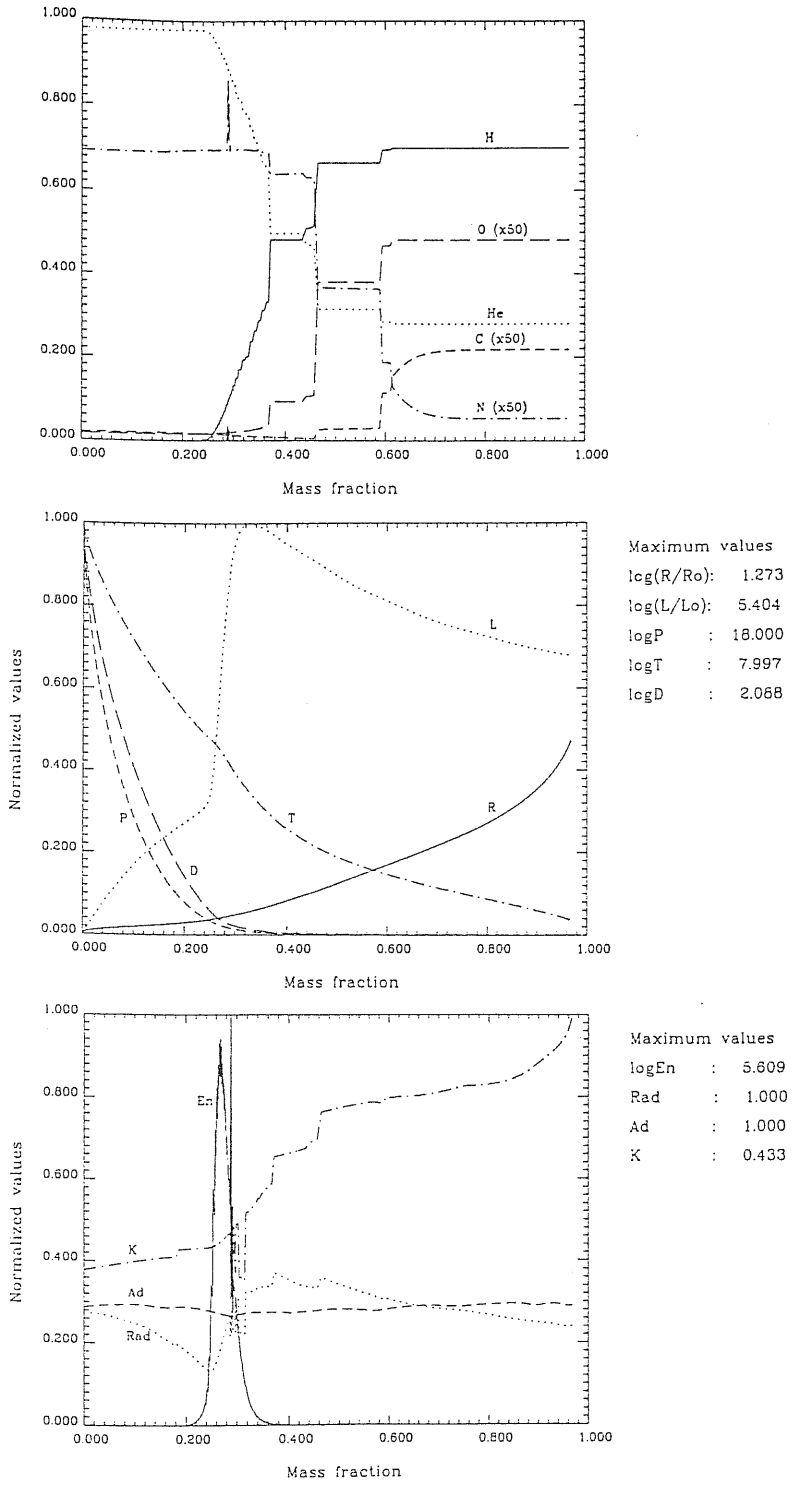

Figure 4.4: The chemical and physical structure during the shell hydrogen burning phase.

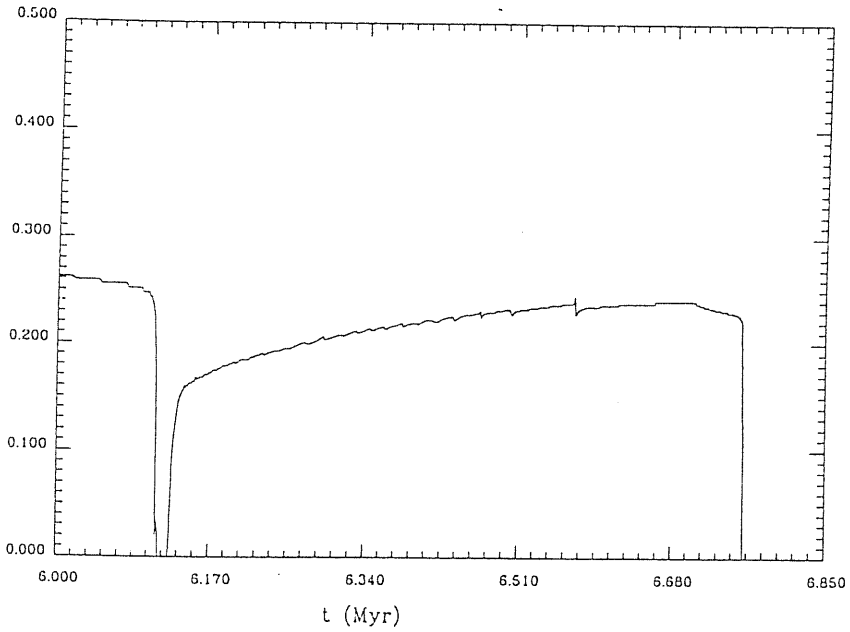

Figure 4.5: The growth of the convective core during He burning.

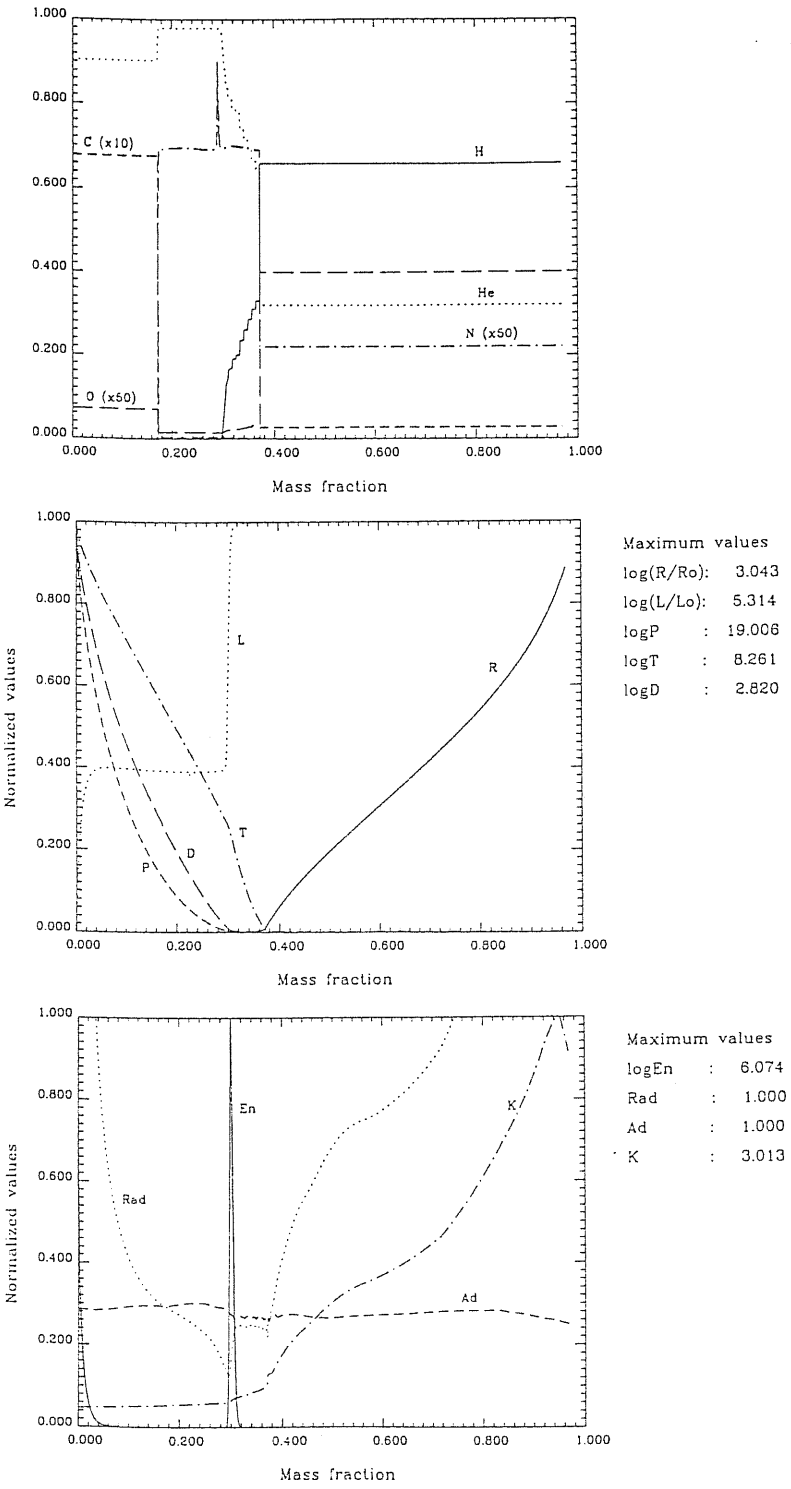

Figure 4.6: The chemical and physical structure during core He burning, when the convective envelope has reached its maximum extension.

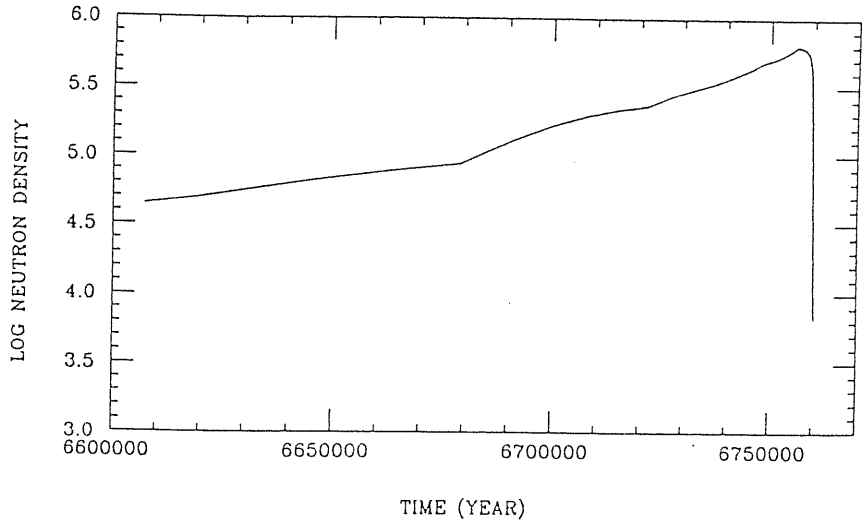

Figure 4.7: The evolution with time of the mean neutron density during core He burning.

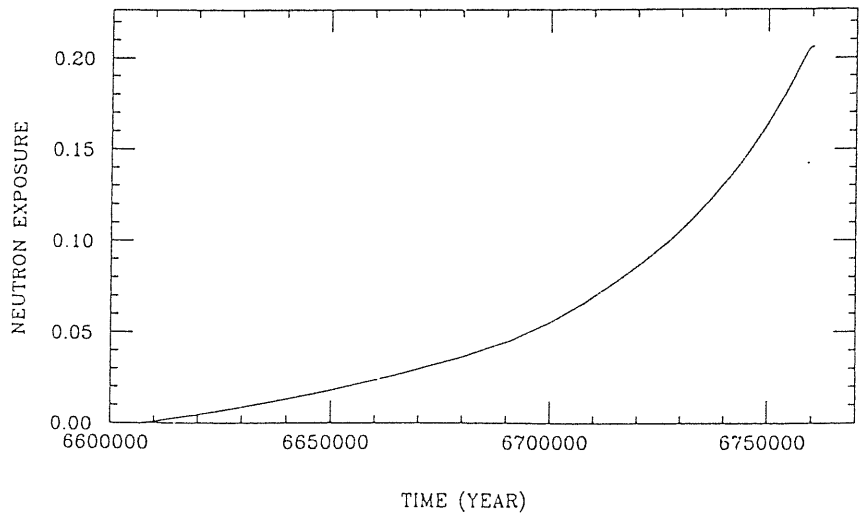

Figure 4.8: The neutron exposure as a function of time during core He burning.

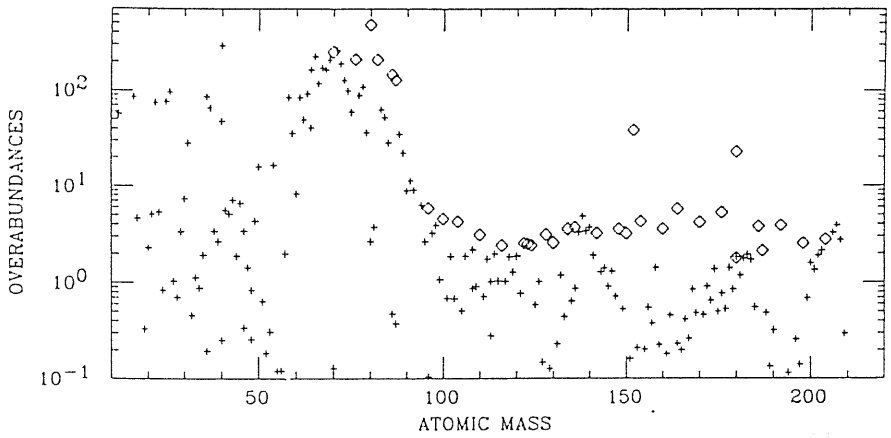

Figure 4.9: Overabundances as a function of the atomic mass number at central He exhaustion. The *s*–only isotopes (diamonds) are distinguished by the others (crosses).

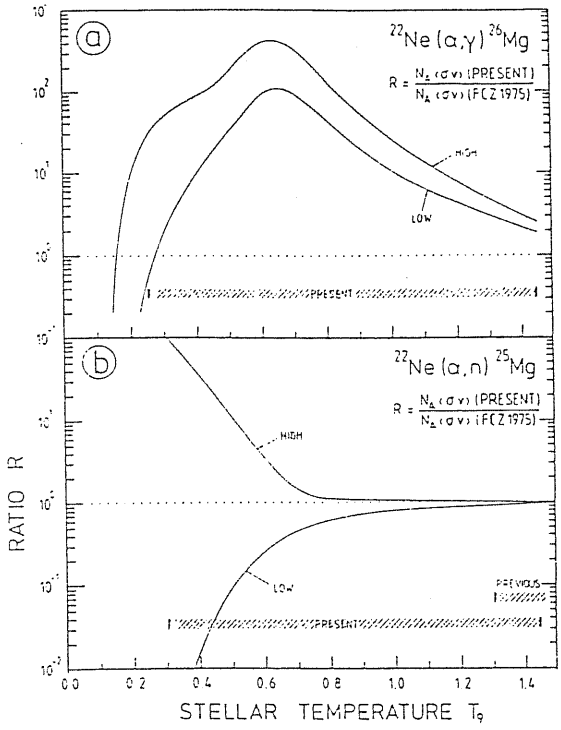

Figure 4.10: The temperature dependence of the stellar reaction rates of (a) ^{22}Ne(α, γ)^{26}Mg and (b) ^{22}Ne(α,n)^{25}Mg compared with the previous evaluations by FCZ75 (Wolke et al., 1989).

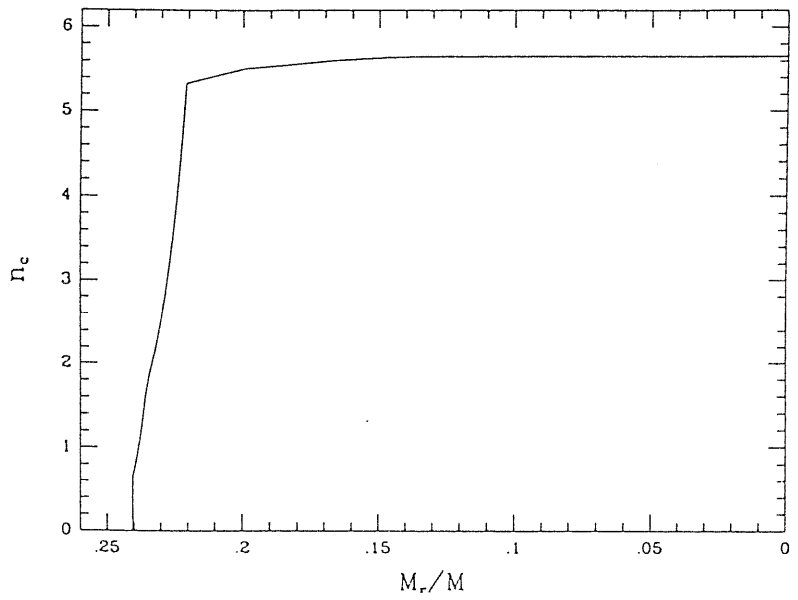

Figure 4.11: The behaviour of n_c at He exhaustion as a function of mass fraction in the CO core.

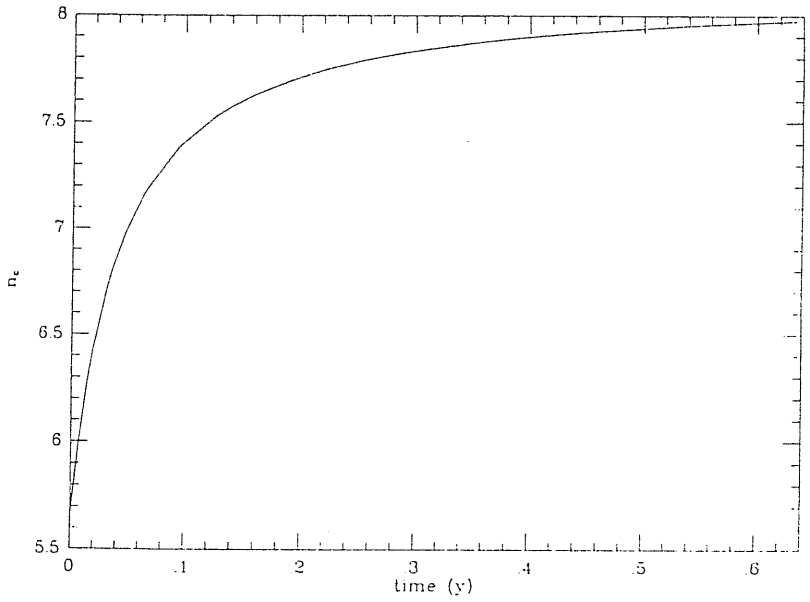

Figure 4.12: Evolution of n_c with time during shell carbon burning.

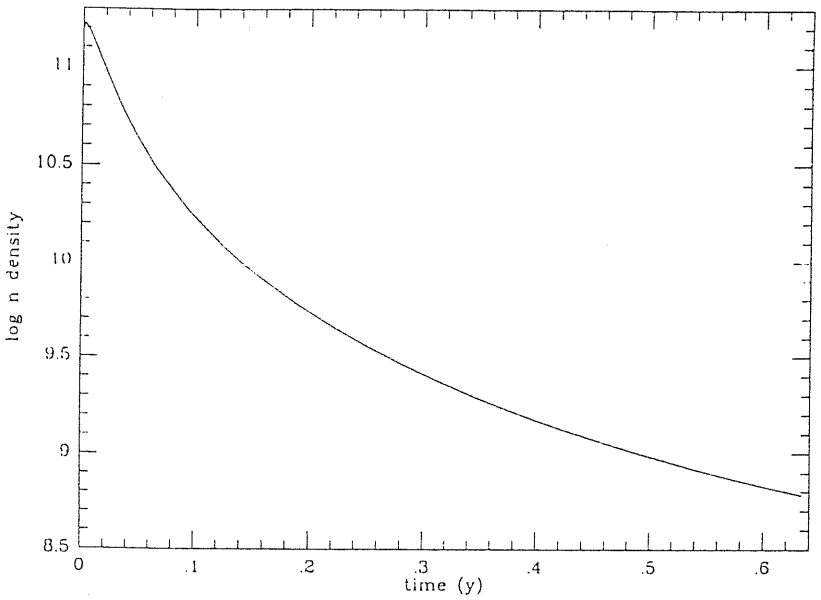

Figure 4.13: Average neutron density during shell C burning.

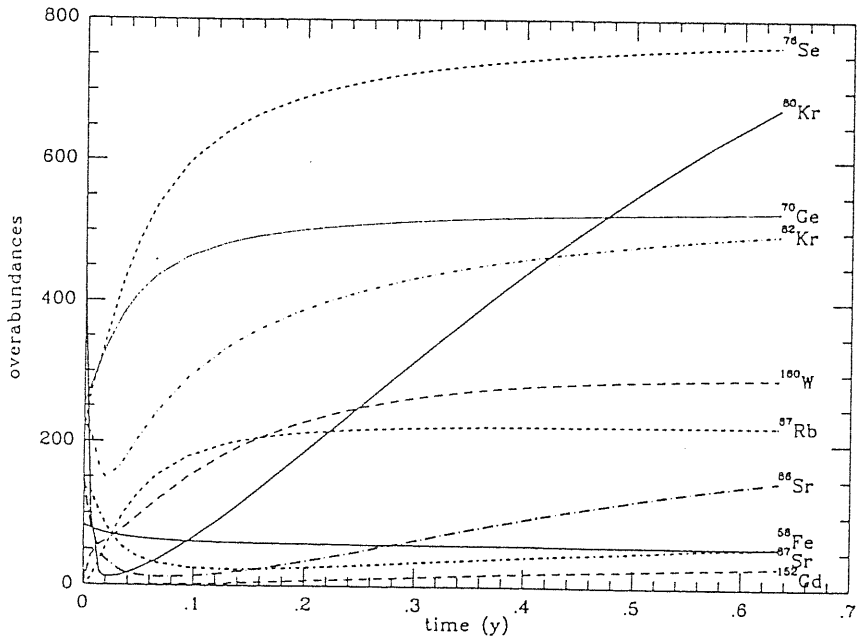

Figure 4.14: Temporal evolution of some overabundances during shell C burning.

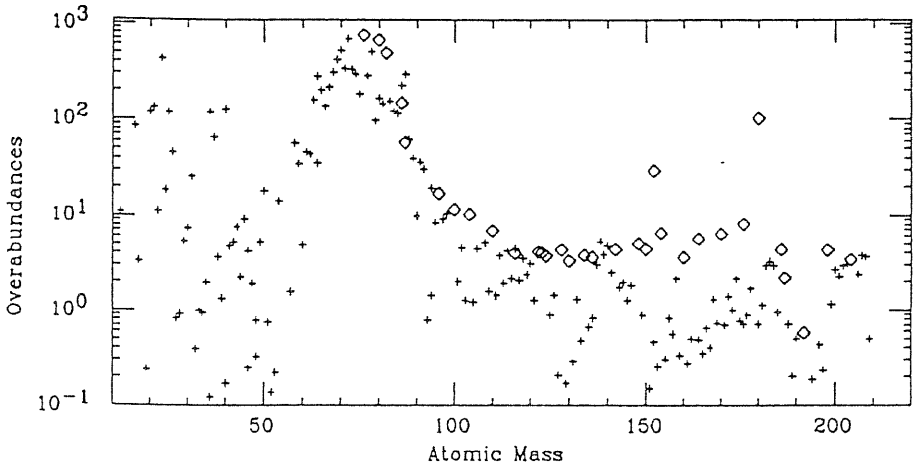

Figure 4.15: Overabundances as a function of atomic mass at the end of shell C burning. The s–only isotopes (diamonds) are distinguished from the others (crosses).

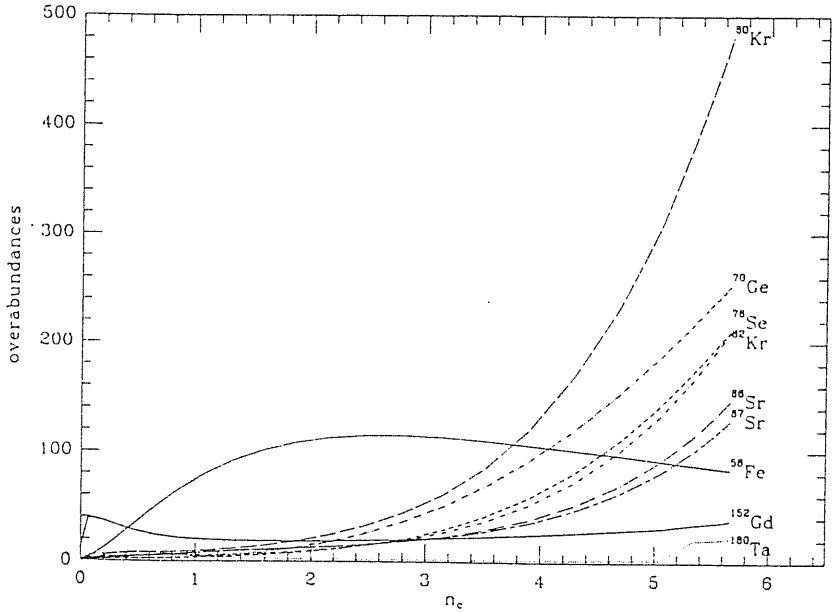

Figure 4.16: Overabundances as a function of n_c during core He burning.

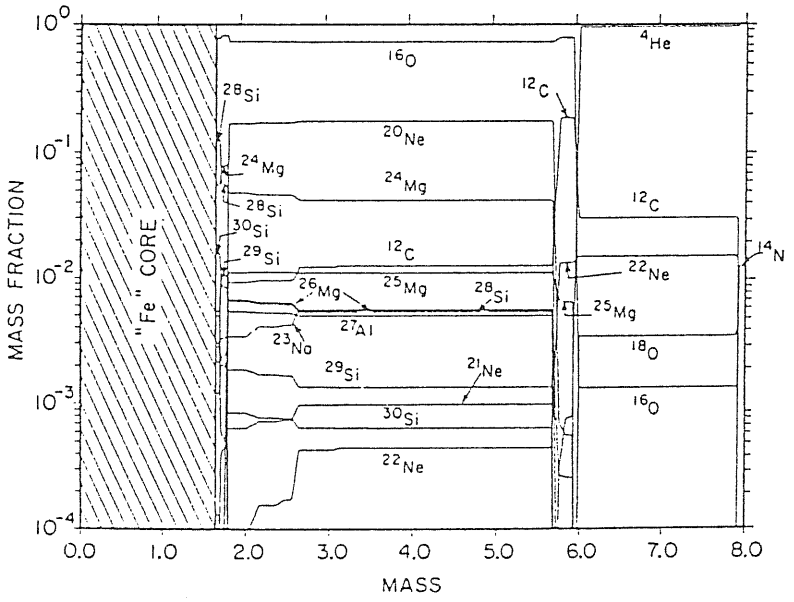

Figure 4.17: Composition of the 8 $M_\odot$ helium star by NH88, at the beginning of iron core collapse.

Chapter 5

THE WEAK COMPONENT: THE REPRODUCTION OF THE SOLAR–SYSTEM s–DISTRIBUTION

5.1 INTRODUCTION

The purpose of this Chapter is to understand under which assumptions the weak (and the main) component in the solar–system can be reproduced. In the atomic mass range that we shall consider ($70 < A < 90$) the s–theory suffers from difficulties deriving from the complex structure of the neutron path at the branching points ^{79}Se and ^{85}Kr, and from the present poor knowledge of the nuclear parameters involved (Käppeler, Beer and Wisshak, 1989; Beer and Macklin, 1989; Gallino et al., 1991). In particular, under standard prescriptions, ^{86}Kr and ^{87}Rb are overproduced by the main component, whereas the weak component is not well determined in the framework of the classical analysis, since no good prescriptions for the neutron density, temperature, and for the type of irradiation can be foreseen (see § 3.2). However, a detailed study of the s–process in massive stars can better clarify the two astrophysical processes that give rise to the weak and the main component.

In the previous Chapter we calculated the s–process nucleosynthesis that occurs during both core He and shell C burning in a 25 $M_\odot$ star, and evaluated the composition of the s–processed material which is ejected by this stellar model.

Now we want to analyze the chemical enrichment of the interstellar medium in s–nuclei. In order to do this, in § 5.2 we shall introduce basic concepts concerning the chemical evolution of the Galaxy, and estimate the contributions of massive stars in the framework of the Simple Model theory. The s–yields from a whole stellar generation are derived by requiring that the solar abundance of ^{16}O is reproduced. Indeed, oxygen is supposed to be entirely produced by massive stars in the same

stellar regions where the s–nuclei are synthesized.

In § 5.3 the s–contributions to the solar composition from TP–AGB low mass stars and from the p–process are then taken into account, and the possibility to match the solar distribution of the s–isotopes produced by the weak component is investigated.

We shall show that, despite the complexity coming from the uncertainties introduced by C burning, an overall good fit can be achieved. This result brings important consequences for the galactic chemical enrichment, showing that stars more massive than 50 $M_{\odot}$ cannot participate to the s–enrichment with contributions from the CO core: they are supposed to suffer strong stellar winds, their cores likely collapsing into black holes.

Finally, a comparison with the results of the phenomenologic approach is attempted in § 5.4, underlining how the different conditions in neutron density and temperature play in determining the shape of the neutron flow.

5.2 *s*–YIELDS FROM A GENERATION OF MASSIVE STARS

In order to calculate the contributions to the chemical enrichment of the interstellar medium in *s*–nuclei coming from massive stars, we first need to review some basic concepts of galactic chemical evolution. (Talbot and Arnett, 1973; Tinsley, 1980; Chiosi and Matteucci, 1984).

The chemical evolution of a galaxy is governed by the evolution of individual stars as well as collective processes such as star formation rate, stellar mass function and dynamics of the gas–stars system.

Each generation of stars contributes to the chemical enrichment by processing new material in the stellar interiors, and returning to the interstellar gas a fraction of the mass containing both processed and unprocessed matter during the various stages of mass ejection (stellar wind, planetary nebula, SN explosion). What we need is a complete specification as a function of the stellar mass of the fractionary amount of each elemental species i returned to the interstellar medium as well as the fraction of mass going into a remnant, thus subtracted for ever to further nuclear processing. These data can be derived from calculations of stellar models up to the very final stages. The basic quantities required to follow the evolution of a chemical species can be specified in the framework of the Simple Model (see next Chapter), following the formalism by Talbot and Arnett (1973). This has the advantage that many important conclusions can be reached without having to consider detailed chemical models.

According to this formalism, the evolution with metallicity Z of the abundance of the species i can be described by:

$$X_i^p \sim p_i \, y,$$

if i is a *primary* element, and

$$X_i^s \sim 0.5 \, p_i(Z) \, y,$$

if i is a *secondary* element, where $y = ln[M_g(0)/M_g(t)]$ and M_g is the mass of the galactic gas. Let us remind that, depending on the process of nucleosynthesis taking place inside a star, an element is considered as *primary* if it is built through thermonuclear reactions starting from H burning, without the need of seed nuclei synthesized in a previous generation of stars. On the other side, an element is considered as *secondary* if it is built starting from chemical species already present in the star at its birth. The quantity p_i is the so–called *yield* of species i, and is defined as the mass of that element newly created and ejected by a generation of stars, relative to the mass locked up in long–lived dwarf stars and compact remnant. In the formalism of Talbot and Arnett (1973), the yields are defined through a

production matrix Q_{ij} involving all elemental species:

$$p_i = \frac{\sum_{j \neq i} q_{ij} X_j}{1 - f},$$

f being the fraction of mass ejected from a generation of stars, and

$$q_{ij} = \int_0^\infty \Psi(m) Q_{ij}(m) dm.$$

$Q_{ij}(m)X_j$ is the fraction of stellar mass initially in the form of species j which is eventually ejected as species i and $\Psi(m)$ is the initial mass function. For primary elements p_i are constants, while for secondary species as the s–isotopes are generally assumed to be, they are proportional to the metallicity $[p_i(Z) \propto Z]$. At this stage we shall adopt such general point of view, considering the s–nuclei that are produced in massive stars as secondary species. A more detailed investigation on this point will be performed in the next Chapter. In evaluating q_{ij} we have to consider that due to their long evolutionary times, stars less massive than about 1 $M_\odot$ do not participate in the recycling of the interstellar gas.

In order to predict the massive star contributions to the solar abundances of the s–only isotopes we must consider that stars more massive than a certain limit may collapse into black holes without experiencing a supernova explosion, thus not contributing to the chemical enrichment of the Galaxy. The problem of the limiting mass has been investigated by many authors in the framework of studies on the chemical evolution of the Galaxy (Twarog and Wheeler, 1987; Matteucci, 1986; Olive, Thielemann and Truran, 1987; Wheeler, Sneden and Truran, 1989). They must explain why theory predicts too large an amount of oxygen if all stars between 10 and 100 $M_\odot$ are included in the computation of yields. The limiting mass is not well established; in particular, a higher slope of the initial mass function can lower the contribution by the most massive stars. In our calculations the slope of the initial mass function was set equal to -2, while we chose the value 50 $M_\odot$ for the limiting mass (see discussion in Chiosi and Maeder, 1986), calibrating the galactic model in such a way as to *reproduce the solar oxygen abundance*. Indeed, it is in the O–rich region that the s–only isotopes are synthesized. To correctly reproduce the solar oxygen implies that also the s–contributions from massive stars to the solar distribution are fixed. Let us recall that a 25 $M_\odot$ star is currently considered as a typical nucleosynthetic site for primary elements produced by massive stars (Woosley and Weaver, 1986). However, this is not true for the s–elements, and we want to discuss this point in some more detail. A simple inspection of the overabundances achieved by an s–only isotope such as ^{82}Kr at He exhaustion and after C burning, provides us a very useful information about the relative role played by s–processing inside the O–rich zone. While O is thought to be produced entirely by massive stars, the solar abundance of ^{82}Kr already receives about a 50 % contribution from the main component of the s–process, so that the average ratio $(^{82}\mathrm{Kr}/\ ^{16}\mathrm{O})/(^{82}\mathrm{Kr}/\ ^{16}\mathrm{O})_\odot$ should be 1/2; since in the oxygen rich zone we have

$^{16}O/\ ^{16}O_{\odot} \approx 80$, final overabundances for ^{82}Kr such high as 200 (in the He processed zone) or 500 (in the C processed one) necessarily imply that only 1/5 to 1/10 of the O–rich region can contribute to the production of the *s*–elements. However, one has to take into account that *s*–processing is contributed very differently in stars of various masses, and if the above criterion is not true for a given star, it must be true when a whole generation of massive stars is considered. In order to make this analysis we derived the Q_{ij} of primary species and the remnant masses from Woosley (1986), while the fractional masses with which every burning stage contribute to the final yield of an *s*–isotope were estimated by carefully analysing the works by NH88, Thielemann, Nomoto and Hashimoto (1990), and Woosley and Weaver (1988). In particular, the 25 $M_{\odot}$ model contributes to the *s*–abundances with both He and C processed matter; the amount of He processed matter ejected is 0.25 $M_{\odot}$ (on which the shrinkage of the convective He core has acted), while the C processed matter is 2.5 $M_{\odot}$. Let us specify that, in defining the limit up to where the passage of the shock front destroys all the *s*–nuclei, we have chosen an intermediate solution between the results by Thielemann, Nomoto and Hashimoto (1990) and those of Woosley (1986). Stars in the mass range from 25 to 50 $M_{\odot}$ are likely to behave in a different way: indeed, in these stars either ^{22}Ne goes to exhaustion at the end of core He burning, or C burning is radiative (Arnett, 1972b). As a result, the O–rich zone ejected is hardly affected by *s*–processing during C burning. Recent models of such massive stars are lacking, and new evolutionary calculations are highly desirable. Finally, as far as stars between 10 and 25 $M_{\odot}$ are concerned, the models by NH88 show that the C processed region suffers some kind of a partial O burning, with the consequent dissociation of the *s*–nuclei; moreover, at least in the less massive ones, this zone is surely locked inside the neutron star that forms during the explosion. Thus the *s*–process that occurs during C burning is found to be important only for a small interval of stellar masses around 25 $M_{\odot}$. The scenario just depicted proves to be able to satisfy the $^{82}Kr/\ ^{16}O$ criterion discussed above.

For stars of different masses, the *s*–abundances at He–exhaustion were calculated using a distribution of exposures that produces a central n_c parameter following the law:

$$n_c = 10.3[1 - \exp(-M_{\alpha}/10)],$$

which has been calibrated to our results of the 25 $M_{\odot}$ star and which agrees well with the results found by Prantzos, Hashimoto and Nomoto (1990). Moreover, we calculated for each mass the effect of the shrinkage of the He core mass, according to the results by NH88; the effect is particularly important for the stars of lower mass.

For M>50 $M_{\odot}$, following the above discussion, we let all the CO core mass be locked into black holes: these stars can contribute only through stellar wind to the galactic enrichment. The wind has been characterized by a distribution of *s*–isotopes as found in our models during He burning when $n_c = 2.6$, which agrees well with indications from Prantzos, Arnould and Arcoragi (1987).

Having defined the parameter space of our problem, we calculated the contributions that massive stars give to the solar–system abundances of the s–only nuclei produced by the weak component (plus ^{58}Fe). The calculation was performed by considering the operation of the s–process first during He burning alone, and then during both He and shell C burning, whenever it is effective. Table 5.1 shows the results in term of ratios to the solar abundances (Anders and Grevesse, 1989): column 2 presents the case where only He burning is included, while the case of column 3 takes into account both He and C burnings. It is easy to recognize that in both cases massive star contributions are quite different for the various isotopes: in particular, the inclusion of C burning makes the spread even more pronounced.

5.3 CONTRIBUTIONS TO THE SOLAR–SYSTEM ABUNDANCES

The spread of our calculated s–contributions from massive stars to the solar abundances shown in Table 5.1 was actually expected, since each nuclide that appears in the Table is also produced by two other mechanisms. The first one is the s–process taking place in the He convective shell of low mass stars climbing up the Asymptotic Giant Branch (see § 3.3). The secondary nucleosynthesis occurring in these stars has recently been demonstrated to fit the main component of the s–process (Gallino et al., 1988; Gallino, 1989; Käppeler et al., 1990a). LMS contributions to the isotopes we are concerned with are shown in column 4 of Table 5.1; they are taken from the best fit case of Gallino et al. (1990b).

The second mechanism is the p–process. Despite recent investigations (Howard, Meyer and Woosley, 1991; Rayet, Prantzos and Arnould, 1990), the site for the process to operate and the way it operates is still uncertain (see Chapter 2). The adopted set of p–contributions was taken from Käppeler, Beer and Wisshak (1989), following a semiempirical analysis by Beer (1985); we can attribute a 50% uncertainty to them. These values are presented in Table 5.1 (column 5). As can be seen, the abundances of ^{80}Kr and chiefly ^{152}Gd are greatly affected by the p–process. In the last two columns of the Table the total contributions to the solar abundances are shown, both in the case where massive stars are supposed to give only He–burning contributions and in the case where also the C–shell burning products are considered.

At this stage, it is important to stress that the overabundances we obtained are affected by various sources of uncertainties. First of all, we can expect some uncertainty in the stellar model, depending on the physical inputs we chose and on the procedure we adopted to perform the calculations. This could affect in particular the ^{80}Kr abundance, that critically depends on the final stages of C burning, as shown in Figure 4.14. Moreover, a certain degree of imprecision is naturally related to the determination of both the neutron capture cross sections and the solar abundances. Table 5.2 shows the neutron capture cross sections adopted for our s–only isotopes, together with the uncertainties on their values (Käppeler, Beer and Wisshak, 1989), the solar–system number densities with their uncertainties (Anders and Grevesse, 1989), and the resulting $\Delta(\sigma N_{\odot} p)$ when a 50 % indetermination on the p–corrections is taken into account. Finally, as already discussed in § 4.3, there is an effect of propagation of the n–capture cross section uncertainties on the flow. It derives in particular from ^{68}Zn, ^{72}Ge, and ^{78}Se, and introduces an overall uncertainty of the order of 10 % or more on the final abundances of the s–only isotopes up to $A = 90$.

Apart for the case of ^{58}Fe, which however is not an s–only isotope, the last column of Table 5.1 shows that solar values can be reproduced inside the range of present uncertainties in the case where both He and C burning conditions are taken

into account (case "He+C"). The s–only isotope ^{70}Ge appears somewhat underproduced; however Anders and Grevesse (1989) noticed that the determination of the solar abundance of this isotope is uncertain, the meteoritic value we used considerably differing from the photospheric one. Adopting an average value between the two, the solar abundance determination would be lowered by $\sim$ 20 %, providing a good fit for this isotope too.

When only He burning is considered in massive stars (Table 5.1, column 6) a general agreement is found for all s–only isotopes but ^{70}Ge and ^{76}Se, that are underproduced. This is an argument in favour of the operation of carbon burning.

As a conclusion of the above discussion we can state that the good agreement of the results of Table 5.1 with the solar distribution of s–isotopes implies that the *s–process in massive stars is actually able to account for the weak component.*

An alternative picture for the galactic chemical enrichment was also analyzed, by assuming that stars more massive than 50 $M_\odot$ participate in the s–enrichment with CO core contributions corresponding to processed matter with an n_c value of 9.51 (see also Prantzos, Arnould and Arcoragi, 1987). The contributions from such massive stars are derived from He burning alone since, due to the high temperatures reached, at the end of this phase ^{22}Ne is completely depleted. No s–processing in the C shell is thus expected in these stars. Table 5.3 shows the resulting MS (column 2) as well as total (column 3) contributions to the solar values. The calibration criterion was again to adjust the free parameters in order to match the solar abundance of oxygen. It is interesting to notice that the same quantities are obtained independently of the inclusion of matter infall to the disk. In comparison to the MS contributions shown in Table 5.1 the situation is much worse, except for ^{152}Gd. The values of Table 5.3 put severe constraints on the chemical evolution of the Galaxy, firmly stating that very massive stars cannot give carbon–oxygen core contributions, unless the s–isotopes are destroyed by photodissociations in the entire O–rich region by the passage of a supernova shock front (which is unlikely). Their CO cores are presumably collapsing into black holes.

5.4 COMPARISON WITH THE PHENOMENOLOGICAL APPROACH

We saw in Chapter 3 that the phenomenological description of the weak component suffers from many difficulties. In particular, it strongly depends from the treatment of the main component, and its neutron density and temperature are assumed in analogy with this latter, without any consideration to the astrophysical prescriptions.

In Table 5.4 the contributions to the solar–system abundances of the isotopes we are interested in coming from the classical main and weak components are shown.

In the first three columns the data are taken from Käppeler, Beer and Wisshak (1989; KBW89); both the results of the model with an exponential distribution of neutron exposures (ee) and of the single flux model (sf) for the weak component are presented. The neutron density adopted is 1.3×10^8 cm^{-3} for the main component, and 1.7×10^8 cm^{-3} for the weak; the thermal energy is 23 keV for the main, and 18 keV for the weak (see also Beer and Macklin, 1989).

As can be seen, when the main and the weak contributions are added, the (ee) case shows an overabundance of ^{58}Fe and a too low abundance of ^{70}Ge and ^{76}Se. With the (sf) model, instead, ^{58}Fe is less produced, and ^{70}Ge and ^{76}Se are better fitted, but the heavier isotopes are too low.

In the last two columns the more updated results from Beer, Walter and Käppeler (1991; BWK91) are shown. Here the main component has been revised with respect to the one of 1989: a pulsed model is used, together with a refined analytic treatment of the best fit procedure. The physical parameters characterizing the main are: $n_n = 2 \times 10^8$ cm^{-3}, and $KT = 25$ keV. On the other side, in this paper the weak component has been formulated considering the astrophysical implications: BWK91 refer to the results obtained by us following the s–process in both core He and shell C burning in massive stars, which have been presented in Chapter 4. In the BWK91 model the weak component is thus a superposition of two different exposures: the first one is to mimick the conditions playing during core He burning in massive stars, with a mean neutron density of 10^6 cm^{-3}, and a temperature of 25 keV; the second one takes into account the operation of shell C burning, with a $n_n^{max} = 1.6 \times 10^{11}$ cm^{-3}, and $KT = 86$ keV. According to the authors, a best fit solution is found when it is assumed that the 82 % of the matter that experienced the first neutron exposure sees also the second one. The confrontation between this new model for the weak component and the single flux one shows a general rearrangement of the contributions, with a particularly heavy variation of ^{86}Kr.

The results of Table 5.4 can be compared with the one we obtained by performing computations in a true astrophysical environment, and that are shown in Table 5.1. Let us notice first of all that very different contributions are found for ^{80}Kr: while from the phenomenologic point of view this isotope is produced by both the main and the weak component, according to the astrophysical scenario its synthesis

must be ascribed to massive stars. This is essentially due to the fact that the classical main component has a higher temperature (and a lower neutron density) with respect to the s–process occurring in TP–AGB stars, so that the production of ^{80}Kr at the ^{79}Se branching is favoured. As for the weak component, the analytic approach by BWK91 gives a greater weight to the high–temperature, high–neutron density phase (which corresponds to our C burning), during which ^{80}Kr (but also ^{82}Kr) is not so heavily produced.

The effect of the different conditions playing at the ^{85}Kr branching is then affecting the abundances of ^{86}Sr, ^{87}Sr, ^{86}Kr and ^{87}Rb. A higher neutron density for the main component as in the astrophysical case means that the neutron flow essentially goes to ^{86}Kr and ^{87}Rb, avoiding a too strong production of ^{86}Sr and ^{87}Sr. Indeed, one of the major problems in the astrophysical picture for the main component is the overproduction of ^{86}Kr (see also § 3.3, and Käppeler et al., 1990a). Let us recall that, in order to overcome the same problem, the classical analysis assumes a pulsed model for the main component, with a pulse duration of 3–20 yr (see § 3.2). On the other side, we saw that C burning can produce some ^{86}Kr and ^{87}Rb, so that it is explained why the analytic description of the weak component by BWK91 finds a larger contribution to these isotopes (and a lower one for ^{86}Sr and ^{87}Sr) than we do.

A more detailed critical comparison between our results and the findings of the phenomenologic approach is presently under way, and will be the topic of a forthcoming paper.

	MS(He)	MS(He+C)	LMS	p-PROC.	TOT(He)	TOT(He+C)
^{58}Fe	0.32	0.35	0.02	0.00	0.34	0.37
^{70}Ge	0.41	0.57	0.14	0.10	0.65	0.81
^{76}Se	0.34	0.71	0.29	0.10	0.73	1.10
^{80}Kr	0.76	0.83	0.10	0.15	1.01	1.08
^{82}Kr	0.33	0.51	0.52	0.03	0.88	1.06
^{86}Kr	0.00	0.17	1.03	0.00	1.03	1.20
^{87}Rb	0.00	0.22	0.88	0.00	0.88	1.10
^{86}Sr	0.24	0.21	0.66	0.06	0.96	0.93
^{87}Sr	0.21	0.13	0.76	0.00	0.97	0.89
^{152}Gd	0.08	0.06	0.45	0.33	0.86	0.84
^{180}Ta	0.04	0.02	0.94	0.00	0.98	0.96
^{180}W	0.00	0.08	0.03	—	—	—

Table 5.1: Contributions to the solar–system abundances

	σ_{30keV}(mb)	$\Delta\sigma$(%)	$N_\odot$(atoms/10^6 Si)	$\Delta N_\odot$(%)	$\Delta(\sigma N_\odot p)$(%)
^{58}Fe	12.8	10.0	2.52×10^3	2.7	10.4
^{70}Ge	.90	5.8	24.4	9.6 [a]	12.2
^{76}Se	163	4.0	5.6	6.4	9.1
^{80}Kr	251	5.8	0.999	18.0	20.3
^{82}Kr	82	6.3	5.15	18.0	19.1
^{86}Kr	3.7	8.6	7.84	18.0	20.0
^{87}Rb	21	9.5	2.11	6.6	11.6
^{86}Sr	74	4.3	2.32	8.1	9.6
^{87}Sr	100	6.1	1.51	8.1	10.1
^{152}Gd	1010	6.4	6.6×10^{-4}	1.4	17.8
^{180}Ta	1728	11.0	2.48×10^{-6}	1.8	11.1

[a] See however discussion in the text.

Table 5.2: Physical inputs and their uncertainties

	MS	TOTAL
^{58}Fe	0.38	0.40
^{70}Ge	1.77	2.01
^{76}Se	2.16	2.55
^{80}Kr	5.46	5.71
^{82}Kr	2.64	3.19
^{86}Sr	2.55	3.27
^{87}Sr	2.45	3.21
^{152}Gd	0.19	0.97
^{180}Ta	0.11	1.05

Table 5.3: s–contributions when stars more massive than 50 $M_{\odot}$ are included

	KBW89			BWK91	
	main	weak (ee)	weak (sf)	main	weak (He+C)
^{58}Fe	0.02	1.12	0.17	0.03	0.28
^{70}Ge	0.11	0.51	0.72	0.15	0.84
^{76}Se	0.23	0.60	0.67	0.29	0.58
^{80}Kr	0.38	0.54	0.33	0.49	0.32
^{82}Kr	0.42	0.67	0.46	0.55	0.39
^{86}Kr	0.72	0.38	0.18	0.66	0.40
^{87}Rb	0.73	0.32	0.00	0.65	0.05
^{86}Sr	0.58	0.32	0.09	0.93	0.04
^{87}Sr	0.59	0.29	0.03	1.01	0.01

Table 5.4: The main and weak contributions according to the phenomenological approach

Chapter 6

BEHAVIOUR AS A FUNCTION OF METALLICITY AND INTERPRETATION OF OBSERVATIONAL TRENDS

6.1 INTRODUCTION

In the two previous Chapters we discussed the s–processing in massive stars, and how it can fit the weak s–component in the solar system: we found that the solar system distribution of the s–isotopes in the atomic mass range $60 < A < 90$ is satisfactorily reproduced when the contributions from a whole generation of massive stars, up to $\simeq 50$ $M_{\odot}$, are considered.

In order to analyze how massive stars can account for the weak component, we assumed that the s–process in massive stars follows a secondary behavior, as is generally believed. However, there are several points that need to be investigated when discussing the s–yields from generations of stars of different metallicities that we want to analyze here in more detail. First of all one must include the effect of the observed *enhancement of the so–called "α –nuclei"* (^{16}O, ^{20}Ne, ^{24}Mg, ^{28}Si, ^{32}S, ^{40}Ca, ^{48}Ti plus ^{39}K) with respect to iron at metallicities lower than solar (Luck and Bond, 1985; François, 1986; Magain, 1989; Bessell and Norris, 1987; Barbuy, 1988; Abia and Rebolo, 1989; Gratton, 1990). Indeed, the observations show that the abundances of these isotopes grow in the *disc* (the galactic phase currently characterized by [Fe/H]> -1) as the metallicity decreases, while in the *halo* (the more metal–poor galactic phase) they have a nearly flat overabundance in comparison to iron, the case of ^{16}O being probably a bit different The efficiency both of the ^{22}Ne neutron source (that depends on the initial CNO abundance), and of important neutron poisons is sensitive to this enhancement. Moreover, it is necessary to account for the operation of *primary poisons* such as ^{16}O, ^{20}Ne during He burning, and ^{20}Ne, ^{23}Na,

^{24}Mg during C burning, which take a predominant role in population II stars. In particular ^{16}O must be considered as the major neutron poison during He burning at low metallicities, despite its very low $< \sigma_{n,\gamma}^{30keV} >= 2 \times 10^{-4}$ mb (quoted in Bao and Käppeler, 1987). Actually, one has to notice that this value is probably underestimated and that Beer, Voß and Winters (1991) suggest a value up to a factor 10 higher. The enhancement of the α–nuclei and the behavior of neutron absorbers determine the way in which massive stars production of s–isotopes evolves in time.

The next step is to deduce (starting from a fit to the solar system composition like the one performed in Chapter 5) the s– and e– or r–contributions to each isotope of interest and hence to the elements as a whole. In this way, an indication is obtained of how different production mechanisms played in building up the elements considered.

An interpretation of the observed trends of heavy elements versus metallicity can eventually be attempted, while a more detailed analysis needs a complete model for the chemical evolution of the Galaxy.

In § 6.2 we briefly illustrate the procedure we adopted to obtain our results. These are discussed in § 6.3, where also a comparison with recent results is made. § 6.4 deals about the debated problem of the primary or secondary nature of the s–process, while § 6.5 faces the question of an interpretation of the abundance observations in stars of different metallicity. Finally, in § 6.6, improved calculations for Cu and Zn with a proper model for the chemical evolution of the Galaxy are presented.

6.2 COMPUTATIONS

In order to perform nucleosynthesis calculations in stars of different metallicities, we used stellar models originally computed for a solar composition. This is an acceptable approximation, since the fundamental evolutionary parameters affecting the result of the s–processing, such as the central temperature and the central density near the end of core He burning, or the relative C/O amount at that stage, do not vary much with the metal content. To verify this point, Table 6.1 shows the results of two evolutionary computations of a 25 $M_\odot$ star with solar and 1/20 of solar metallicity. The data refer to the end of core He burning, and were obtained by us using the FRANEC evolutionary code. M_α is the H–depleted core, while M_{CO} is the He–depleted one. As can be seen, the effect of metallicity is quite low, and the same would stand true for the subsequent carbon burning, as well as for the final presupernova model.

The numerical procedure we adopted to calculate the neutron captures and the input nuclear parameters we chose were the same as described in Chapter 4. We briefly remind that the thermonuclear reaction rates are taken from Caughlan et al. (1985); the weak interaction rates are derived from Takahashi and Yokoi (1987), except for ^{79}Se, for which the temperature–dependent β–decay rate by Klay and Käppeler (1988) is adopted. The neutron capture cross sections are mostly taken from Bao and Käppeler (1987) and Beer and Macklin (1989). The $< \sigma_{n,\gamma}^{30keV} >$ of ^{84}Kr was put equal to its lower experimental limit of 30 mb, while for ^{22}Ne we adopted $< \sigma_{n,\gamma}^{30keV} >$=0.06 mb, according to Beer et al. (1989). We also included the not–$1/v$ behavior of many important $\sigma_{n,\gamma}$, that can especially affect the neutron poisoning action by light nuclei, and the neutron capture on ^{56}Fe.

The nucleosynthetic calculations were started taking into account that the so called "α–rich nuclei" have shown to be overabundant with respect to iron in stars with metallicity less than solar. The choice we made for this "α–enhancement" was based on the observations (see Figure 6.1), and different prescriptions should be adopted in order to cover the whole spread of observational data. In particular, if we consider oxygen (the most important of the α–nuclei), a linear increase of its abundance can be assumed from [Fe/H]=0.0 down to [Fe/H]=–1, being followed by a flat enhancement in the halo by about 0.3–0.4 dex (Sneden, Lambert and Whitaker, 1979; Gratton and Ortolani, 1986; Barbuy, 1988; Gratton, 1990). We recall that in the standard spectroscopic notation [el/Fe] = log(el/Fe)$_\star$ - log(el/Fe)$_\odot$. The possibility is open for a stronger enhancement of [O/Fe] in the most metal poor stars with [Fe/H]<–2.5, as suggested by observations of Bessell and Norris (1987), while the linear increase of [O/Fe] for decreasing [Fe/H] down to [Fe/H]$\sim$–2, as suggested by Abia and Rebolo (1989), has recently been questioned (see Pagel, 1991). Figure 6.2 shows the [O/Fe] versus [Fe/H] ratios derived by Abia and Rebolo (1989) (filled circles), together with those obtained by other authors: the disagreement becomes particularly evident at the lower metallicities.

Notice that the increase of the O abundance implies a proportional increase of

the ^{22}Ne neutron source, since ^{22}Ne is produced by α–captures starting from ^{14}N, to which the CNO initial content is processed in the H burning phase. At the same time, having more ^{22}Ne, we also get more ^{25}Mg, which is a very efficient neutron poison if the metallicity is not too low. The enhancement of the other α–nuclei implies a growth of the neutron absorbers too. However, for metal poor stars the main neutron poison in the core He burning phase is primary ^{16}O, largely produced by the operation of the $^{12}C(\alpha,\gamma)^{16}O$ reaction. A full discussion on the relative importance of the neutron poisons is performed in the next section.

6.3 RESULTS

6.3.1 Core He Burning

Table 6.2 shows the results of the s–processing in a 25 $M_\odot$ star at the end of core He burning, for different metallicities. Column 1 gives the assumed amount of initial oxygen enhancement, while column 2 gives the corresponding adopted enhancement of the other α–nuclei. In order not to introduce too many parameters, we consider the same overabundance with respect to iron for all of these nuclei, even if some differences in their behavior as a function of [Fe/H] are possibly observed (see Lambert, 1989). In Table 6.2 the number of neutrons captured per iron seed nucleus n_c is presented as a function of metallicity [Fe/H]. Some of the results of Table 6.2 are also dispayed in Figure 6.3, where the curves labelled 1 are obtained with no enhancement of the α–rich nuclei, while the ones labelled 2 are the result of a linear increase of the enhancement down to [Fe/H]=–1, followed by a constant [α/Fe] = 0.3 at lower metallicities. In the Figure the label "$\sigma_{16} = 2M4$" means that the Bao and Käppeler (1987) value of 2×10^{-4} mb was adopted for the $< \sigma_{n,\gamma}^{30keV} >$ of ^{16}O; but cases are also presented with this $< \sigma_{n,\gamma}^{30keV} >$ put to zero (see discussion below). In case 2–$\sigma_{16} = 2M4$ (our standard case), n_c stays within 20 % of the value obtained for a solar metallicity down to [Fe/H]$\sim$–1.8. The corresponding variation of the overabundances can be seen in Figure 6.4; the increase in the disc is due to the rise of the neutron source down to [Fe/H]=–1. Then, after the peak, the effect of the poisons plays the dominant role, and the overabundances begin to decrease. Anyway, since this variation is much smaller than the change in metallicity, we can conclude that *a secondary–like behavior characterizes the s–process in massive stars down to [Fe/H]$\sim$–2.* Beyond that point the efficiency of the process is very low, because of the neutron absorption by the primary light nuclei, first of all ^{16}O.

In order to recognize the importance of ^{16}O as a neutron poison, we show in Figure 6.3 what happens to n_c when this nucleus is prevented from capturing neutrons (cases with $\sigma_{16} = 0$). It is clear that the importance of ^{16}O grows when [Fe/H] is low because the other poisons that depend on metallicity (mainly ^{25}Mg) are greatly reduced. As for the poisoning action of ^{12}C, it is rubbed out by an almost complete effect of instantaneous neutron recycling on this nucleus, since the reaction ^{12}C(n,γ)^{13}C is immediately followed by ^{13}C(α,n)^{16}O (see also Gallino, 1989) which, at the temperatures typical of He burning, is very efficient.

To discuss in more details how the poisons behave as a function of metallicity, we plotted in Figure 6.5 the σY values of the most important light neutron absorbers, as a function of time. The two cases that are shown were calculated considering an α–enhancement of a factor 2 for both the oxygen and the other α–rich nuclei; as for the metallicity, in panel a) it is [Fe/H]=–1.3, while in panel b) it is [Fe/H]=–2.3. The discontinuities of the σY curves in the case of ^{24}Mg, ^{17}O, and ^{56}Fe are artificial; they are due to the fact that the n–capture cross sections of these isotopes do not follow the common $1/v$ law, so that their value changes with increasing temperature.

Since we took account of the variation of the temperature using three successive nuclear networks, we have formally two points of discontinuity when we pass from one network to the other. From Figure 6.5 we can easily recognize some features:

- $\sigma Y(^{16}O)$ and $\sigma Y(^{20}Ne)$ are essentially constant with metallicity, because ^{16}O and ^{20}Ne are primary products of the star;
- in the case [Fe/H]=–1.3 the most important n–absorber at the beginning of the process is ^{56}Fe; but soon ^{25}Mg, whose abundance grows very rapidly due to the operation of the $^{22}Ne(\alpha,n)^{25}Mg$ reaction, takes the dominant role. Then we have quite an important n–poisoning effect by ^{16}O, that only at the very end of core He burning is overcome by ^{24}Mg and ^{20}Ne, that are efficiently produced by α–captures on ^{20}Ne and ^{16}O respectively. However, the importance of one nucleus as a neutron poison is determined by the integral of the σY curve, and not by the mere final value;
- if we now analyze the case with [Fe/H]=–2.3 we see that ^{16}O is the major n–poison, ^{25}Mg still giving a consistent contribution at the end of the process. This contribution will be lost in stars of lower metal content, owing to the ^{25}Mg–dependence on metallicity.

If we now come back to Table 6.2 and consider cases that have been run with higher O–enhancements with respect to the scenario outlined so far, we see that the efficiency of the s–process rises. It is interesting to notice that a sequence with $n_c \simeq$ constant down to very low metallicities could in principle be found, but in order to have $n_c \sim 6$ at [Fe/H]=–3.3, [O/Fe] should be as large as 1.6, which seems quite unlikely at present. We conclude that the s–process efficiency must fall in the extreme halo. However, at these low metallicities, another contribution to the s–nucleosynthesis could come from the operation of the $^{13}C(\alpha,n)^{16}O$ reaction, that becomes effective at the end of core hydrogen burning. This possibility has recently been investigated by El Eid and Baraffe (1990), who found that in very metal poor stars s–nuclei in the atomic range 60–90 are efficiently produced through this mechanism.

6.3.2 Shell C Burning

Table 6.3 shows the final n_c values at the end of shell C burning as a function of metallicity [Fe/H]. As can be seen, the contributions coming from C burning rapidly decrease with metallicity, their effect being important in the disc, but not in the halo. The fall of the additional neutron exposure at low [Fe/H] is easy to understand since the neutron source is essentially provided by the same $^{22}Ne(\alpha,n)^{25}Mg$ reaction that was already responsible for the neutron release in the previous central He burning phase. Going to low metallicities, the ^{22}Ne content rapidly falls, so that it is completely consumed during He burning. Figure 6.6 gives the efficiency of

the s–process in stars of 25 $M_\odot$ and different metal contents, at the end of shell C burning. As in Figure 6.3, the curve labelled 1 is obtained with no α–enhancement, while that labelled 2 is the result of our standard choice for the enhancement.

The neutron poisons acting during shell C burning are essentially ^{20}Ne, ^{24}Mg and ^{23}Na, all of them being of primary nature, with a not negligible contribution by ^{25}Mg in the disc only [see Figure 6.7, where panel a) is for solar metallicity, and panel b) for [Fe/H]=–1.6].

We can wonder how the operation of shell C burning can modify the previous discussion about the secondary origin of the s–process in massive stars, taking into account that in a 25 $M_\odot$ star the carbon burning shell spreads over almost all the previous He processed region. An inspection of our results at the end of shell C burning leads to the conclusion that the overabundances of the s–isotopes belonging to the weak component do not depend so much on metallicity in the disc (see Figure 6.8): this means that the secondary–like behavior is satisfactorily preserved.

6.3.3 Enhancement of the $\sigma_{n,\gamma}$ of ^{16}O

We have just seen the importance of ^{16}O as a neutron poison during core He burning, especially when stars of low metallicity are considered. The major role played by ^{16}O relies on a very small neutron capture cross section at 30 keV of only 2×10^{-4} mb, as quoted in Bao and Käppeler (1987), who refer to the evaluation by Allen and Macklin (1971). We used this choice up to now. However, Beer, Voß and Winters (1991) have recently found that by properly treating the 434 keV resonance, the $< \sigma_{n,\gamma}^{30keV} >$ of ^{16}O can be up to 10 times higher than the value accepted by Bao and Käppeler.

To investigate the consequence on the s–process taking place in massive stars, we performed calculations with the ^{16}O cross section $< \sigma_{n,\gamma}^{30keV} >= 2 \times10^{-3}$ mb. In this case the efficiency of the s–process in the disc is slightly reduced, the overall pattern still remaining roughly secondary–like. In particular, the reproduction of the solar weak component is still satisfactory for all the s–only isotopes but ^{70}Ge, whose solar abundance is however badly determined. On the contrary, in the halo n_c is so small that pratically no s–process contributions are expected at low metallicities.

Figure 6.9 gives the n_c values as well as the overabundances as a function of [Fe/H] in the case we are dealing with. The fall of the curve in the halo is evident.

We must stress that the present uncertainty on the n–capture cross section of ^{16}O is high, so that an experimental determination is strongly needed before concluding that the weak component does not work in the halo.

6.3.4 Comparison With Previous Results

In a recent paper, Prantzos, Hashimoto and Nomoto (1990, hereafter PHN90) discussed the s–process in massive stars of different masses and composition, taking

into account that the observed enhancement in α–nuclei is affected by a large scatter, and made calculations considering three cases (see their Figure 1): case A, with no enhancement; case B, in which [Fe/O] linearly increases with [O/H], and case C, where it is [Fe/O]=–0.3 up to [O/H]=–1, rising afterward to the solar content. We show the results they obtained in their cases A and C in Figure 6.3, to make a comparison with our results easier.

In order to understand the differences, let us underline some points:

- the poisoning effect of ^{16}O was not considered by PHN90, and this means that their n_e values are always higher than ours, especially at the lower metallicities;

- a number of neutron capture cross sections are different: in particular, we take into account the deviations from the simple $1/v$ law for the cross sections of many important isotopes. As already mentioned, in our computations three nuclear networks are read by the program when the central temperature is equal to 2.5, 3.0, and 3.5 $\times 10^8$ K respectively. Table 6.4 compares our cross sections with the ones adopted by PHN90: as can be seen, some of them are strongly sensitive to the variation of the temperature. When the PHN90 set of neutron capture cross sections is adopted, the efficiency of the s–process is slightly reduced;

- PHN90 have a strong neutron poisoning effect by primary ^{12}C and ^{20}Ne. But one has to take into due consideration the neutron recycling effect by ^{12}C; as for ^{20}Ne, following Winters and Macklin (1988) we have a 50 times lower neutron capture cross section for this isotope, so that its importance as a neutron poison has been heavily reduced;

- as for the "α–nuclei", not only the enhancements of ^{16}O, ^{20}Ne, ^{24}Mg and ^{28}Si, but also those of ^{32}S, ^{39}K, ^{40}Ca and ^{48}Ti must be included. In order to check this point, we performed calculations of neutron captures in a [Fe/H]=–1 star, choosing a factor–of–2 enhancement for all the α–nuclei. In Table 6.5 column 2 shows the results at the end of core helium burning, while in column 3 we present the corresponding results when S, K, Ca and Ti are simply scaled to their solar values. The Table gives, besides the n_e values, the neutron exposures τ at 30 keV, the maximum value of the average neutron density, and the overabundances with respect to the initial ones (i.e. the solar abundances properly scaled according to the Fe content) for the most interesting isotopes. The Table clearly demonstrates the importance of S, K, Ca and Ti as neutron poisons. In particular, the mean neutron density is slightly reduced in the case shown in column 2, and this affects the production of such branching–dependent isotopes as ^{80}Kr and ^{82}Kr: their overabundances decrease from 1202 to 908 and from 558 to 413 respectively. The same effect is felt by the two s–only isotopes of Sr: ^{86}Sr goes from 444 to 312 and ^{87}Sr from 395 to 276.

In conclusion, though a comparison of our results with PHN90 is not easy to accomplish, we think that such an increase of n_c values as they found for intermediate metallicities (in both their cases B and C), is mainly due to their neglecting the poisoning action of ^{16}O.

6.4 THE PRIMARY/SECONDARY NATURE OF THE *s*–PROCESS

The results of the previous section can provide us a critical tool to discuss in a deeper way the behaviour of the heavy elements as a function of metallicity. In the history of the Galaxy, the chemical enrichment of the interstellar medium depends on the way successive generations of stars have been contributing. A commonly used rough approach to the study of abundance buildup is the so–called Simple Model of galactic evolution (Talbot and Arnett, 1973; Tinsley, 1980; Chiosi and Matteucci, 1984), in which the instantaneous recycling approximation is made, that is the time scale of stellar evolution is considered as negligible with respect to the age of the Galaxy. A further assumption is that the yield of a stellar generation is constant for primary species, and proportional to Fe for secondary ones. In this framework, the elemental abundances in the interstellar medium are given by [el/Fe]=const for a primary element, and by [el/Fe]=[Fe/H] for a secondary one.

The "primary" or "secondary" nature of the *s*–elements is a still debated problem; since neutron captures on heavy nuclei depend on initial Fe, in principle one would expect a secondary origin for them, and consequently to observe a linear increase of [el$_s$/Fe] versus [Fe/H] in metal–poor stars. However, the true scenario is much more complicated. Indeed, the instantaneous recycling approximation is commonly accepted for massive stars, at least in the disc, but is no valid for low mass stars with long lifetimes. Moreover, our results of § 6.3 indicate how the yield from a stellar generation to a given element depends on the metallicity in a complex way, due to the differential effect of primary or secondary neutron poisons and to the increase of the $^{22}Ne/^{56}Fe$ abundance ratio in stars of metallicity lower than the solar one. As a consequence, the correlation between the nucleosynthetic process due to a whole generation of stars and the chemical enrichment of the Galaxy must be examined with extreme caution, and for every element.

Observations of *s*–abundances in the atmospheres of dwarf stars with different metal content clearly put into discussion the predictions by the Simple Model, showing that in the disc phase it is [el$_s$/Fe]$\simeq$const, while in the halo we must distinguish between the heavy "*s*–elements" (as Ba) and the lightest ones (as Sr or Y), both being underabundant with respect to iron, but with different trends (Spite and Spite, 1978, 1985; Magain, 1989; Zhao and Magain, 1990). Figure 6.10 shows a collection of observational data for [Sr/Fe], [Y/Fe] and [Ba/Fe] versus [Fe/H] taken from Pagel (1991).

Before entering the problem of the evolutionary behaviour of *s*–species, we must stress two fundamental points:

- First, what we observe is the elemental abundance, and generally it is not possible to get information on isotopic ratios. Moreover, when we speak about an "*s*–element", we refer to something that in the solar–system is mainly supplied

by the s–process, but that can also receive minor contributions from other sources: the e–process (that we define as a combination of nuclear statistical equilibrium processing and explosive nuclear burning) or the r–process, both processes being currently assumed of primary nature. This is particularly true in the atomic mass range $60 < A < 90$. Each of the mechanisms at work will leave a signature on the element's production as a function of metallicity, so that a comparison between the theoretical results and the observations is not easy to perform.

- Furthermore, we saw that there is not a unique site for the s–process. In fact, we have to deal with the weak and the main component, that behave in a different way as a function of [Fe/H]. The atomic mass region from Fe to Zr sees an overlapping of the two contributions; actually, all the s–isotopes produced by the weak component are more or less affected by the main component (see Chapter 5).

  In massive stars, the neutron source is provided by the ^{22}Ne(α,n)^{25}Mg reaction and is of secondary origin, its efficiency depending on the initial CNO content of the star. According to the results obtained § 6.3, the s–process in such stars behaves as "secondary" down to [Fe/H] ~ -2. On the other hand, as we saw in Chapter 3, the main component is ascribable to the s–processing occurring in low mass stars during He thermal pulses on the Asymptotic Giant Branch, mainly through the operation of the ^{13}C(α,n)^{16}O neutron source. As pointed out by Clayton (1988), this n–source is in principle of primary nature, since the ^{13}C is synthesized from proton–captures on ^{12}C, that is produced by He burning in the star. Also from an observational point of view, the fact that [Ba/Fe]$\simeq$0 in the disc, and in general the constancy of r/s trends, must be interpreted in the light of a combined effect of the not instantaneous recycling approximation and of a varying efficiency of the neutron poisons with metallicity. Other important and poorly known factors do play a critical role, such as the efficiency of the ^{13}C–pocket, the effect of the variations of the overlapping factor between subsequent pulses, and of dredge–up mechanisms (Gallino et al., 1990b).

  The double site of the s–process implies a differential evolutionary history for the weak and the main component. Indeed, while massive stars contribute to the chemical enrichment of the Galaxy in the halo, low mass stars are currently believed to participate only to the chemical enrichment of the disc, because of their longer lifetimes. Consequently, when we are dealing with the weak component in the disc, we must take into account that there is an interference from the main component.

6.5 COMPARISON WITH OBSERVATIONS

The main check on the predictions of our results has to be looked for through a comparison with the observational data coming from stars of different metallicity. In order to do that, we need first to evaluate the e–, r–, s–weak and s–main contributions to the solar system chemical composition. In particular, being the s–process (despite all its uncertainties) the best known among the quoted mechanisms, we can evaluate the e– or r–contributions as: $N_{e,r} = N_{\odot} - (N_s^{weak} + N_s^{main})$. Furthermore, if we want to examine halo stars, it is also important to have an estimate of the relative e–contribution from type II (short–lived stars) and type I (long–lived stars) supernovae. For this purpose, we adopted the Thielemann, Nomoto and Hashimoto (1990) yields for the nucleosynthesis products ejected by a 20 $M_{\odot}$ star, assumed to be a typical SNII. Indeed, a fair consistency is found between their theoretical expectations and observations for what concerns the enhancement of the α–nuclei with respect to Fe. As for the yields provided by models of various types of SNI, they are affected by much larger uncertainties (see Thielemann et al., 1989, and Matteucci, 1988). Anyhow, the subdivision of e–contributions from SNI and SNII must be taken as only indicative.

Table 6.6 shows the massive star s–contribution (columns 3 and 7) to the solar abundance of elements from Co to Zr, assuming that in the disc the s–process in massive stars is secondary–like. The method we adopted to obtain these numbers is the same as in the previous Chapter. From Table 6.6 we see that the elements most contributed from the weak s–component are Ga and Ge (by less than 50 % anyway). Unfortunately, we have no observational data concerning these two elements at different metallicities. In all the remaining cases, other nucleosynthetic mechanisms are more efficiently working, so that the secondary imprinting due to the weak component is smaller. In particular, we expect important e–contributions to Co, Ni, Cu, and Zn, while the heavier elements must be totally understood in terms of s– and r–processes (with low contributions from the p–process). The s–main contributions from TP–AGB stars of low mass are given in columns 4 and 8 of Table 6.6 (from Gallino et al., 1990b, with an updated revision for ^{86}Kr and ^{87}Rb).

Table 6.7 shows the elemental contributions to the solar abundances of interesting chemical species, coming from the weak and the main s–process (column 2 and 3 respectively) and from SNII (column 4). In the last column our predictions for SNI, that are simply given by: $1 - (N_s^{weak} + N_s^{main} + N^{SNII})/N_{\odot}$, are presented. In the Table we made the further assumption that the r–process is coming from type II SN only, probably from the less massive star range ($\sim$ 10 $M_{\odot}$), with longer evolutionary times (Mathews and Cowan, 1990). This is not in contradiction with recent computations of nucleosynthesis products of the propagating shock wave during the supernova explosion in a 20 $M_{\odot}$ star (Thielemann, Nomoto and Hashimoto, 1990), where no signature of an incoming r–process has been found.

The question is open about the behavior of the r–process in the halo. As a matter of fact, the observations of a typical r–element such as Eu as a function

of [Fe/H] seem to show a roughly flat overabundance, with a possible decreasing trend at metallicities [Fe/H]$\leq$−2.5 (Cowan, Thielemann and Truran, 1991). The fall could be explained in the light of a not instantaneous recycling approximation scenario, where the bulk of Fe is produced by stars more massive than those that are responsible for the *r*–process. In such a hypothesis, the same decreasing pattern at very low metallicities should characterize all the heavy elements, that in Table 6.7 are seen to have even a small *r*–contribution (Rb, Sr, Y, Zr).

In order to deduce information from the data of Table 6.7, we must recall that Fe is currently assumed to be produced up to $\sim$ 30 % of its solar value by SNII, the remaining percentage being ascribable to long lived SNI. Moreover, we must keep in mind that the *s*–contributions coming from massive stars cannot play any role during the halo phase, in comparison to even a small primary *r*–contribution. The observed patterns at low metallicities must be essentially understood in terms of primary nucleosynthesis only (Truran, 1981; Cowan, Thielemann and Truran, 1991).

Starting from the above considerations, the results of Table 6.7 allow us to conclude that, *in the halo*:

- Co should be slightly underabundant with respect to Fe, as confirmed by the observations of Gratton and Sneden (1991);

- Ni should be more than a factor 2 higher than Fe, which is in contrast with the observed trend recently derived by Gratton and Sneden (1991), who found that [Ni/Fe]$\simeq$0. However, the estimated yield of this element from type II SN is strongly dependent on the position of the mass cut in SNII, that is a very debated point (Thielemann, Nomoto and Hashimoto, 1990, see also § 2.2);

- Cu receives only a small *e*–contribution from SNII, so that it must be underabundant. Sneden, Gratton and Crocker (1991) did find an underabundance of Cu, but also a linear increase with [Fe/H], with [Cu/Fe]$\simeq$−0.2 at [Fe/H]=−1 (see Figure 6.11). They interpret this trend by assuming a very large *s*–process contribution from massive stars. But, according to the present knowledge of nuclear cross sections, this explanation appears unlikely, and we would rather think in term of a differential production of Cu and Fe by type I SN;

- Zn can be reconciled with the observed flatness (Sneden, Gratton and Crocker, 1991; see Figure 6.12) inside the range of present uncertainties;

- Rb is efficiently produced by the *r*–process, so that we expect it to be overabundant in comparison to Fe, with a typical [Rb/Zr]=+0.3;

- Sr should roughly go as Fe, being possibly underabundant; for this element the existing observational data are affected by a large spread, but nonetheless a decrease at [Fe/H]$\sim$−2.5 is evident (Cowan, Thielemann and Truran, 1991;

see Figure 6.10), confirming our opinion that the instantaneous recycling approximation does not work also at very low metallicities;

- Y shows about the same features as Sr, and the predicted trend is in reasonable agreement with the observations (Spite and Spite, 1978; Pagel, 1991; see Figure 6.10);
- Zr should behave approximatively as Fe, the overabundance of this element observed by Magain (1989) being probably due to an underestimate of Fe (see discussion in Gratton and Sneden, 1991), with a possible decrease at [Fe/H]$\leq$−2.5

6.6 IMPROVED CALCULATIONS OF GALACTIC CHEMICAL EVOLUTION

The next step is to insert our theoretical prescriptions for the elemental yields in a detailed model for the chemical evolution of the Galaxy. In this way, we can follow the element's behaviour as a function of time also from a quantitative point of view, and perform a better comparison with observations.

We are now entering the problem for Cu and Zn, for which new results have been recently derived by Sneden, Gratton and Crocker (1991), based on high resolution spectroscopy. Figure 6.11 is taken from their paper, and gives the behaviour of Cu as a function of $[M/H]_{avg}$, i.e. the mean of the abundances of Fe and Ni, weighted by the number of lines observed for each species. They chose to combine Fe and Ni abundances in order to increase the number of transitions used in the metallicity estimate, and thus to reduce the scatter. From the data in the Figure, a linear relation can be identified between [Cu/M] and $[M/H]_{avg}$; according to the authors:

$$[Cu/M] = +0.38[M/H]_{avg} + 0.15.$$

As for Zn, its trend as a function of metallicity is shown in Figure 6.12. The solid horizontal line is placed at the mean Zn abundance, [Zn/M]=+0.04. These data strongly suggest that Zn exists in solar ratio in stars of all metallicity down to $[M/H]_{avg} \sim -3$.

The code used to make calculations of galactic chemical evolution is essentially the one described in Matteucci and Francqis (1989), that has proved to well reproduce the observations of the α–elements (O, Ne, Mg, Si, and S). The galactic model assumes two components: the *halo* and the *disc*. The first one is treated as an homogeneous sphere of primordial gas, where instantaneous mixing of gas but not its instantaneous recycling is assumed. The disc is formed out of the residual gas from the halo through infall of primordial material on timescales of the order of 1 Gyr (but the possibility of infall of chemically enriched material can also be considered). The halo phase is rapid and when the iron content of the Galaxy reaches [Fe/H]=–1, the disc phase begins. The Star Formation Rate is a function of the gas density, and the rate of type I SN is computed taking into account the evolutionary time of the progenitor stars.

In order to follow the chemical evolution of the element i, we must insert into the code the nucleosynthetic yields in terms of mass in i that is ejected by stars of different masses of the same generation. Furthermore, we must know the behaviour of the element as a function of metallicity, i.e. if it has a primary or a secondary nature.

As for *massive stars*, we calculated such values using our results in the case of solar composition. The results are shown in Table 6.8. As can be seen, the contributions from a 15 $M_{\odot}$ star are much lower than those from a 25 or a 35

$M_\odot$ star: this is due to the fact that in a 15 $M_\odot$ star only a small fraction of the He–processed core does not suffer photodisintegration of the *s*–nuclei, as discussed in § 5.2. According to our previous analysis of § 6.3 we can assume that in such stars Cu and Zn follow a secondary–like trend down to [Fe/H]~ -2; then, for lower metallicities, their production falls because of the primary neutron poisons.

But massive stars can also give *e*–process contributions coming from equilibrium processes or explosive burning. We took the corresponding yields from the calculations of a 20 $M_\odot$ supernova model by Thielemann, Nomoto and Hashimoto (1990), that are shown in Table 6.8. They are assumed constant for all massive stars. Two sets of data corresponding to different choices for the mass cut are presented : M_{cut} = 1.63 $M_\odot$ (SNIIa), and M_{cut} = 1.59 (SNIIb). In the case of a mass cut at 1.63 $M_\odot$, one can derive:
$(Cu/Fe)/(Cu/Fe)_\odot = 0.08$
$(Zn/Fe)/(Zn/Fe)_\odot = 0.30$.

If we now believe in the standard prescription that $\sim$ 30 % of $Fe_\odot$ comes from type II SN,
$Cu/Cu_\odot = 0.03$
$Zn/Zn_\odot = 0.10$

We can now estimate the *s*–yields coming from *TP–AGB stars*, referring to the best–fit model of Gallino et al. (1990b), that is valid for stars in the mass range 1–3 $M_\odot$. The metallicity of this typical star in order to reproduce the solar–system main component is $\sim 1/3$ of the solar one. The major problem here is to evaluate how much *s*–enriched material from the He shell is mixed up to the envelope trough the dredge–up episodes and is subsequently ejected by mass loss.

The problem is not so easy, since the envelope enrichment is a gradual process and one has to take into account that the He shell is moving outward in time, the pulses overlap and the chemical composition changes, while the envelope is reduced by stellar winds.

As a first approximation we can calculate the amount of matter that must be brought to the surface to make the star become a carbon star (that is: with a surface ratio C/O=1). Since carbon comes from the same production region where also the *s*–nuclei come from, this evaluation will tell us how much *s*–enriched material is saved in the envelope and thus dispersed in the interstellar medium.

We obtained M= 1.6 $\times 10^{-2}$ $M_\odot$ as the ejected *s*– and C–enriched matter from the typical TP–AGB star which accounts for the main component. Consequently, if we take the *s*–abundances obtained by Gallino et al.(1990b) for such a star, we get the data in Table 6.8. These yields from low mass stars are much smaller than the ones from massive stars, but we must remember that an integration over the Initial Mass Function has to be performed, that gives more weight to the less massive stars. As a consequence, the contribution coming from massive stars and from low mass stars inside the same stellar generation is comparable. The behaviour of Cu and Zn synthesized by the *s*–process in low mass stars is secondary–like.

The last production site we have to consider is *type I SN*, where in principle some Cu and Zn can be formed. The yields, taken by Thielemann, Nomoto and Yokoi (1986), are shown in Table 6.8 (the case labelled SNIc). As for the ratios with respect to the solar values, we have:
$(Cu/Fe)/(Cu/Fe)_{\odot} = 0.02$
$(Zn/Fe)/(Zn/Fe)_{\odot} = 0.05$
that means:
$Cu/Cu_{\odot} = 0.01$
$Zn/Zn_{\odot} = 0.03$.

These results are quite lower than according to our prescriptions (the case SNId in Table 6.8), that are based on a global fit of the solar–system composition. But as we have already stressed, the results of nucleosynthesis calculations in type I SN are affected by large uncertainties.

The results that we have obtained so far by inserting the data contained in Table 6.8 inside the code for the calculation of the galactic chemical evolution are very preliminary. The main problem is that Cu and Zn tend to show a similar behaviour as a function of metallicity, at odd with the observations. However, the theoretical curves are very near to the observational trends, and we expect that with a bit of effort to improve the whole picture, a final agreement will be found.

	Z=0.02 Y=0.28	Z=0.001 Y=0.25
M_α ($M_\odot$)	8.876	9.142
M_{CO} ($M_\odot$)	6.295	6.359
logT_c (K)	8.539	8.542
logρ_c (g cm^{-3})	3.524	3.520
X_C	0.17	0.15
X_O	0.80	0.84

Table 6.1: End of core He burning in a 25 $M_\odot$ star of different chemical compositions

α-enh.		[Fe/H]								
O	α	0.0	-0.3	-0.6	-1.0	-1.3	-1.6	-2.3	-2.6	-3.3
1	1	**5.7**	5.8	5.7	5.4	4.9	4.2	1.9	1.2	0.3
1.2	1.2		**6.1**							
1.5	1.5		6.5	**6.4**						
2	2		7.0	7.0	**6.8**	**6.3**	**5.5**	**2.8**	**1.8**	**0.4**
3	2				8.9	8.4	7.4	3.8		
5	2					12.1	10.8	5.7		
8	2							8.4	5.4	

Table 6.2: n_c values at the end of core He burning

α-enh.		[Fe/H]								
O	α	0.0	-0.3	-0.6	-1.0	-1.3	-1.6	-2.3	-2.6	-3.3
1	1	**8.0**	7.2	6.5	5.8	5.1	4.3	1.9	1.2	0.3
1.2	1.2		**7.7**							
1.5	1.5			**7.6**						
2	2				**7.4**	**6.6**	**5.7**			
3	2									
5	2							5.8		
8	2								5.5	

Table 6.3: n_c values at the end of shell C burning.

	THIS WORK			PHN90
	T_8=2.5	T_8=3.0	T_8=3.5	
^{20}Ne	7.7E-2	7.7E-2	7.7E-2	1.4
^{21}Ne	0.1	0.1	0.1	1.5
^{24}Mg	2.4	3.1	3.8	4.1
^{25}Mg	6.5	6.5	6.5	4.7
^{26}Mg	5.9E-2	7.0E-2	8.0E-2	8.4E-2
^{28}Si	2.1	2.4	2.8	2.9
^{29}Si	8.9	8.3	7.9	7.8
^{30}Si	10.1	8.0	6.7	6.3
^{56}Fe	11.1	12.0	12.8	13
^{57}Fe	40.4	37.6	35.6	35

Table 6.4: Neutron capture cross sections (mb) in He burning conditions

	a	b
n_c	6.76	7.35
τ (mb^{-1})	0.233	0.246
$\overline{n}_n^{max}$ ($\times 10^6$cm^{-3})	0.816	0.831
^{58}Fe	72	66
^{70}Ge	388	464
^{76}Se	379	479
^{80}Kr	908	1202
^{82}Kr	413	558
^{86}Sr	312	444
^{87}Sr	276	395

(a) standard choice
(b) excluding ^{32}S, ^{39}K, ^{40}Ca and ^{48}Ti enhancement

Table 6.5: Results at He exhaustion for [Fe/H] = -1

	Sun	MS_s	LMS_s		Sun	MS_s	LMS_s
Co59	1.00	6	1				
				Se 76	0.09	71	29
Ni58	0.68	0	0	77	0.08	27	13
60	0.26	1	0	78	0.24	45	20
61	0.01	11	2	80	0.50	12	17
62	0.04	7	1	82	0.09	0	0
64	0.01	33	9	Se	1.00	25	13
Ni	1.00	1	0.2				
				Br79	0.51	10	18
Cu63	0.69	19	6	81	0.49	11	13
65	0.31	32	5	Br	1.00	11	16
Cu	1.00	22	6				
				Kr80	0.02	83	10
Zn64	0.49	6	0.2	82	0.12	51	52
66	0.28	19	3	83	0.12	16	18
67	0.04	28	5	84	0.57	13	25
68	0.19	34	7	86	0.17	17	94
70	0.01	0	0.8	Kr	1.00	19	37
Zn	1.00	8	2				
				Rb85	0.72	11	23
Ga69	0.60	45	10	87	0.28	22	81
71	0.40	43	15	Rb	1.00	14	39
Ga	1.00	44	12				
				Sr86	0.10	21	66
Ge70	0.20	57	14	87	0.07	13	76
72	0.27	64	16	88	0.83	7	80
73	0.08	33	11	Sr	1.00	9	77
74	0.37	29	12				
76	0.08	0	0	Y89	1.00	4	85
Ge	1.00	43	12				
				Zr90	0.51	1	65
As75	1.00	17	7	91	0.11	3	90
				92	0.17	3	95
				94	0.18	2	100
				96	0.03	0	65
				Zr	1.00	2	78

Table 6.6: s–contributions from massive stars (MS_s) and from low mass stars (LMS_s) to the solar–system abundances. In columns 2 and 6 the atom percent of each species is given

	s–weak	s–main	SNII (e,r)	SNI (e)
Co	0.06	0.01	0.21	0.72
Ni	0.01	0.00	0.75	0.24
Cu	0.22	0.06	0.07	0.65
Zn	0.08	0.02	0.15	0.75
Rb	0.14	0.39	0.47	–
Sr	0.09	0.77	0.14	–
Y	0.04	0.85	0.11	–
Zr	0.02	0.78	0.20	–

Table 6.7: Contributions to the solar–system from different nucleosynthetic sites

$M/M_\odot$	$M(Cu)/M_\odot$	$M(Zn)/M_\odot$
	Massive Stars	
15	6.83(-7)	5.81(-7)
25	3.58(-4)	6.39(-4)
35	4.74(-4)	8.00(-4)
	TP–AGB Stars	
1–3	2.8(-7)	3.6(-7)
	Supernovae	
SNIIa	3.31(-6)	3.06(-5)
SNIIb	1.5 (-5)	9.74(-5)
SNIc	1.05(-5)	3.24(-5)
SNId	2.61(-4)	6.30(-4)

SNIIa–mass cut at 1.63 $M_\odot$ –from TNH90;
SNIIb–mass cut at 1.59 $M_\odot$ –from TNH90;
SNIc–from Thielemann et al.(1986);
SNId–according to our prescriptions

Table 6.8: Yields from a whole stellar generation

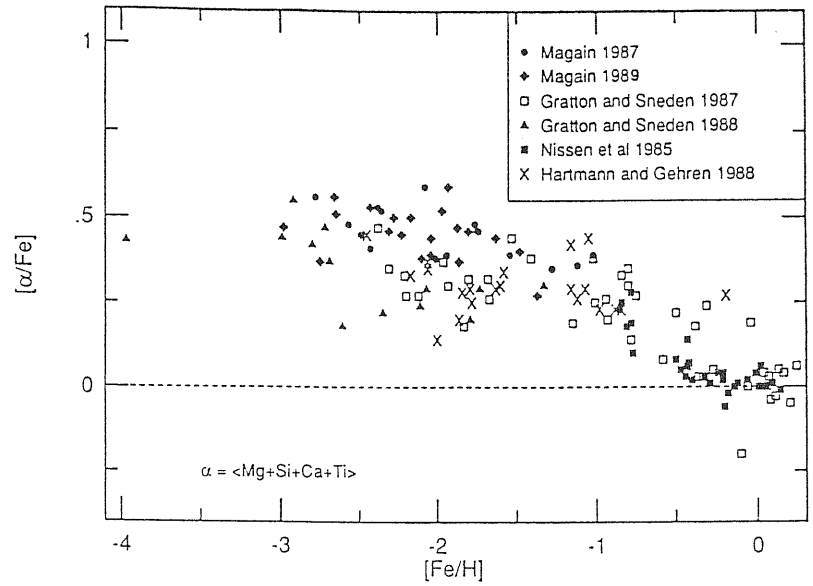

Figure 6.1: The average α-element abundances as a function of metallicity [Fe/H]; from Wheeler, Sneden, and Truran (1989)

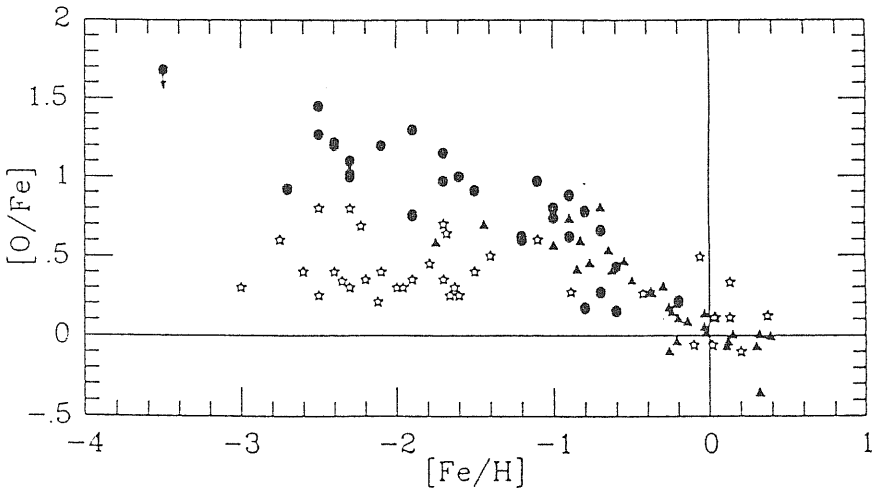

Figure 6.2: The [O/Fe] versus [Fe/H] trend as derived by Abia and Rebolo (1989) (filled circles), compared to other results from the literature

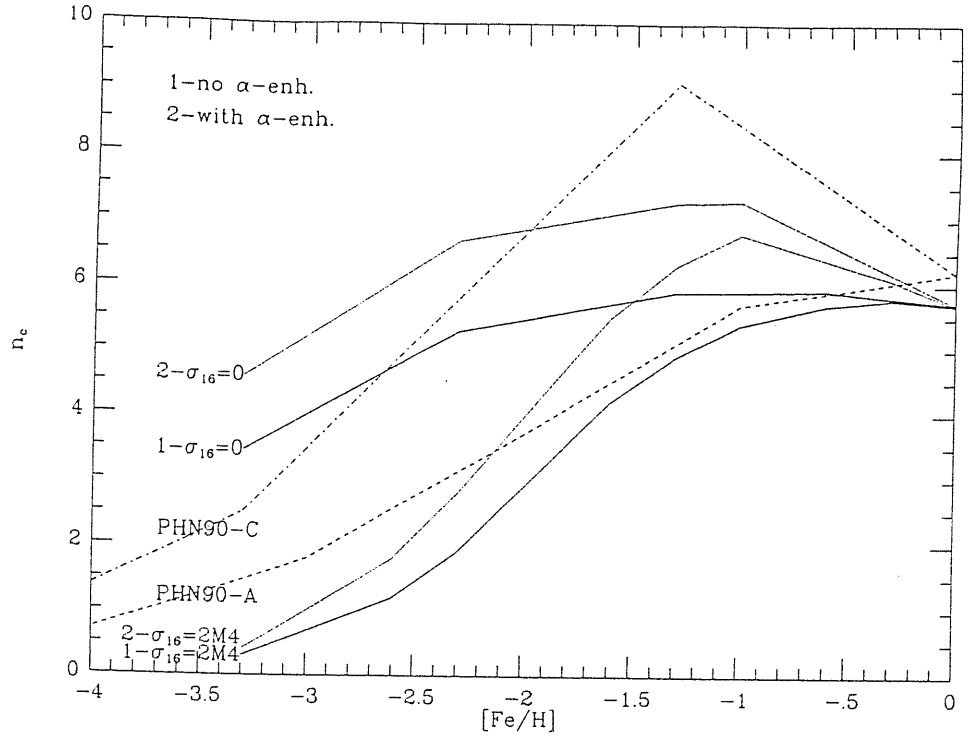

Figure 6.3: n_c values at the end of core He burning in stars of 25 $M_\odot$ and different metallicities

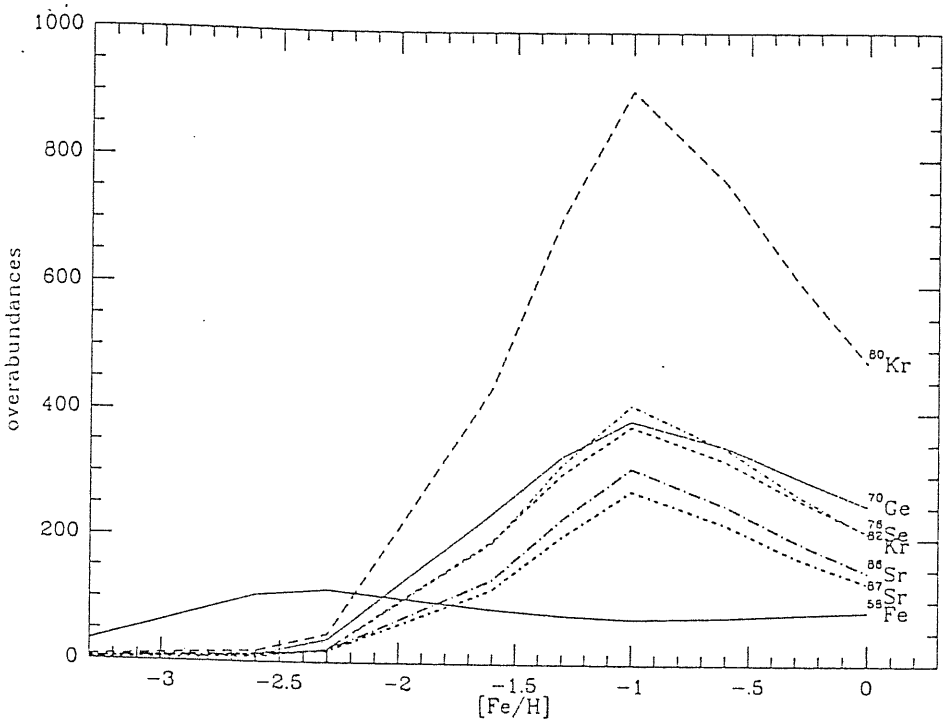

Figure 6.4: Overabundances as a function of [Fe/H] at the end of core He burning in a 25 $M_\odot$ star, for our standard choice of the α-enhancement (see the text)

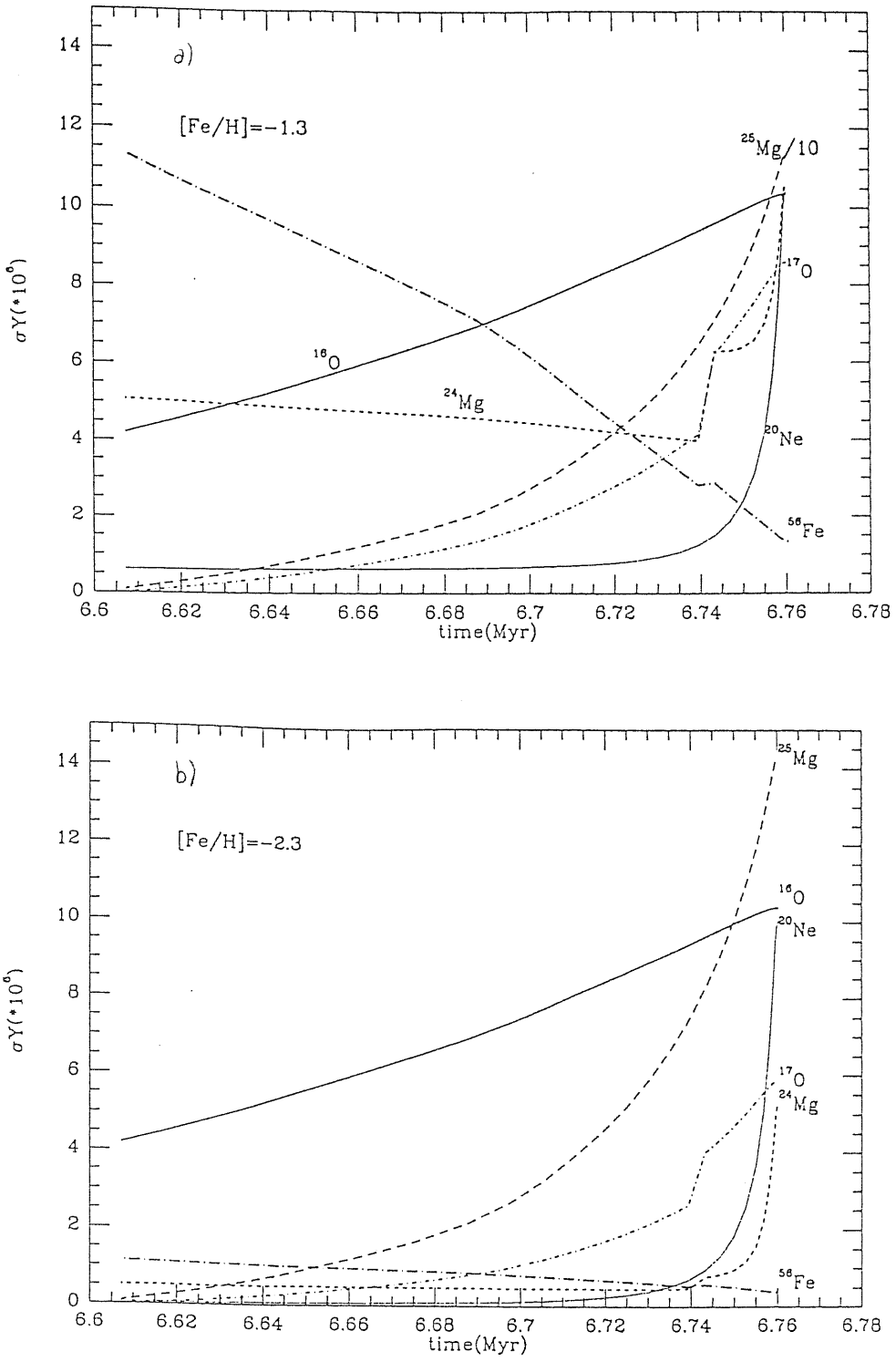

Figure 6.5: σY values of the main neutron absorbers as a function of time, during the last phase of core He burning. In panel a) the metal content is [Fe/H]=−1.3, while in panel b) it is −2.3

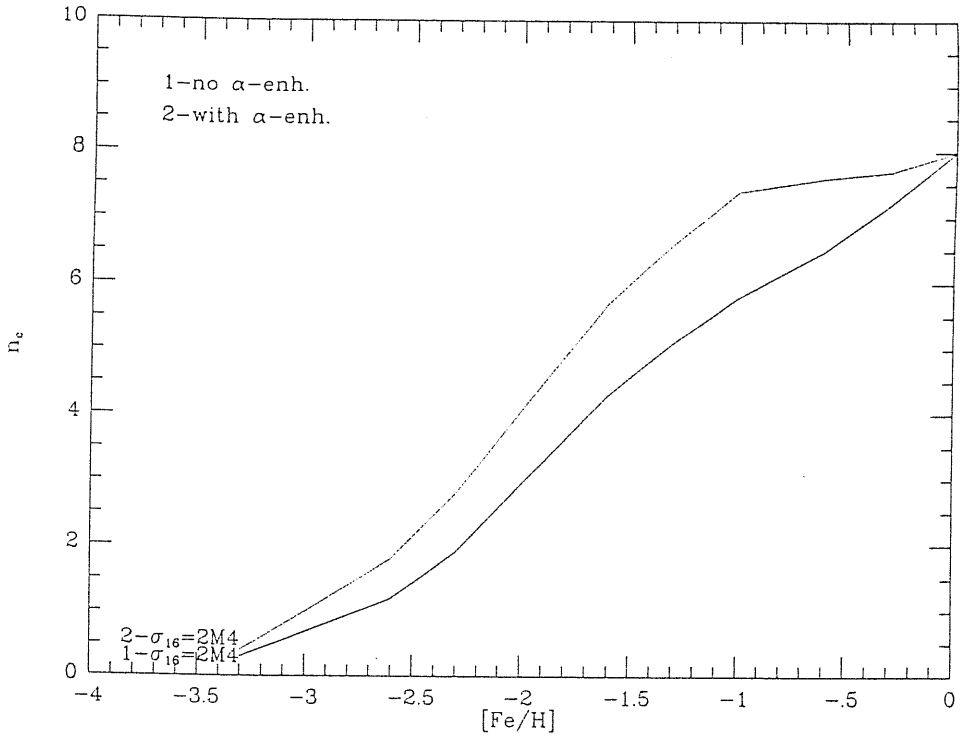

Figure 6.6: n_c values at the end of shell C burning in stars of 25 $M_\odot$ and different metallicities

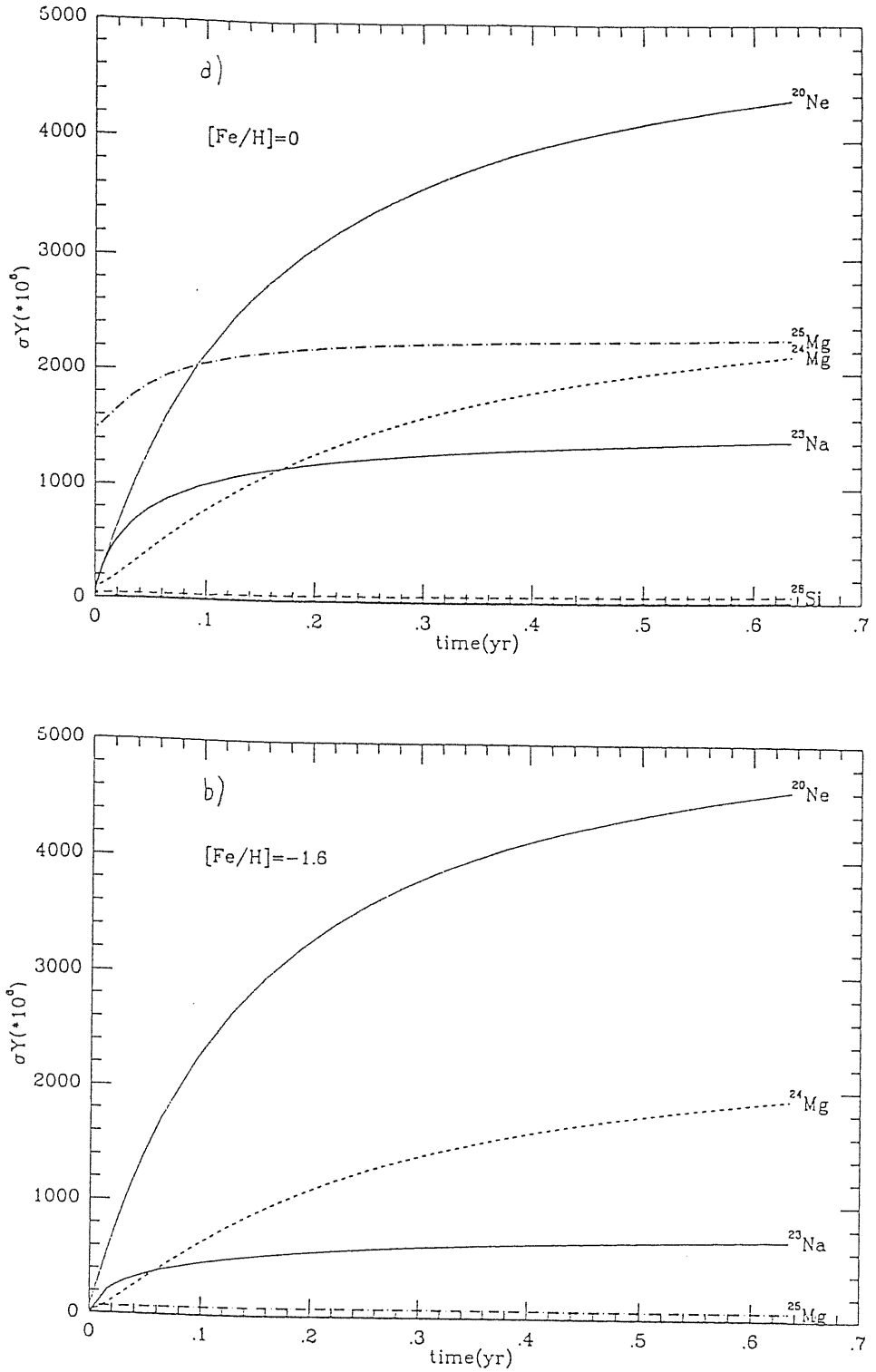

Figure 6.7: σY values of the main neutron poisons as a function of time, during shell C burning. Panel a) is for a solar metallicity, while panel b) is in the case [Fe/H]=−1.6.

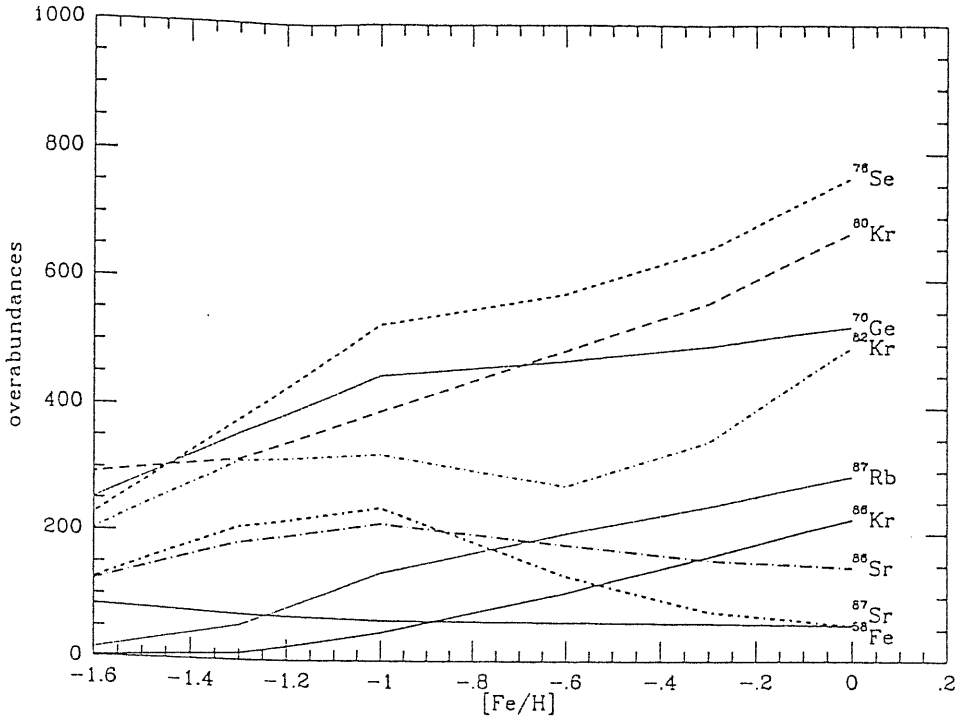

Figure 6.8: Overabundances at the end of shell C burning as a function of metallicity for our standard choice of the α-enhancement.

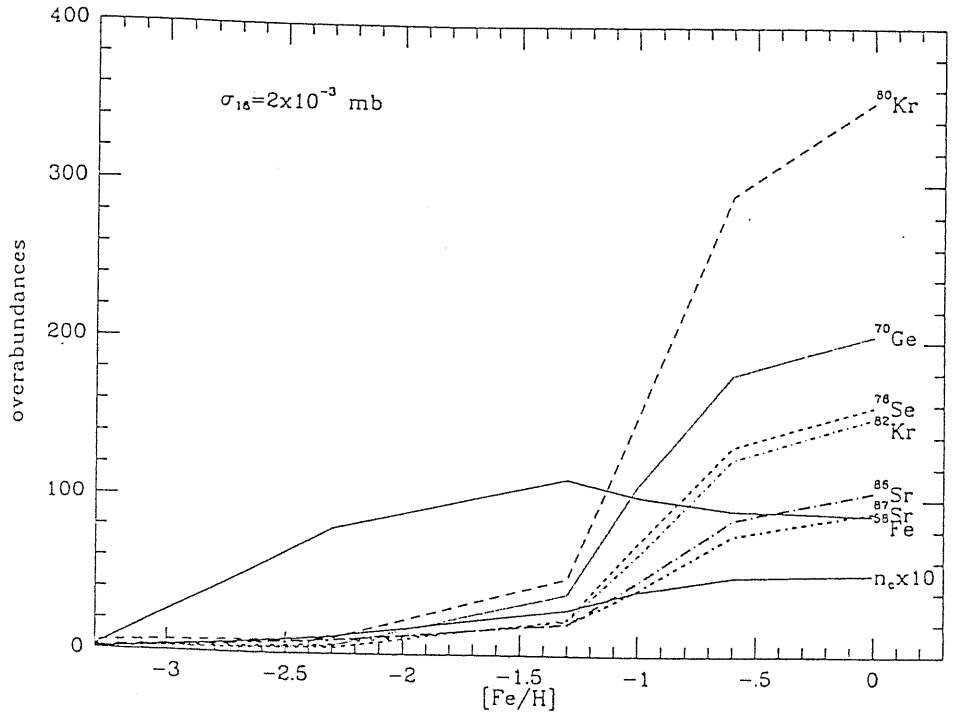

Figure 6.9: n_c values (x10) and overabundances at the end of core He burning as a function of [Fe/H] with the choice $< \sigma_{n,\gamma}^{30keV} >= 2 \times 10^{-3}$mb for ^{16}O.

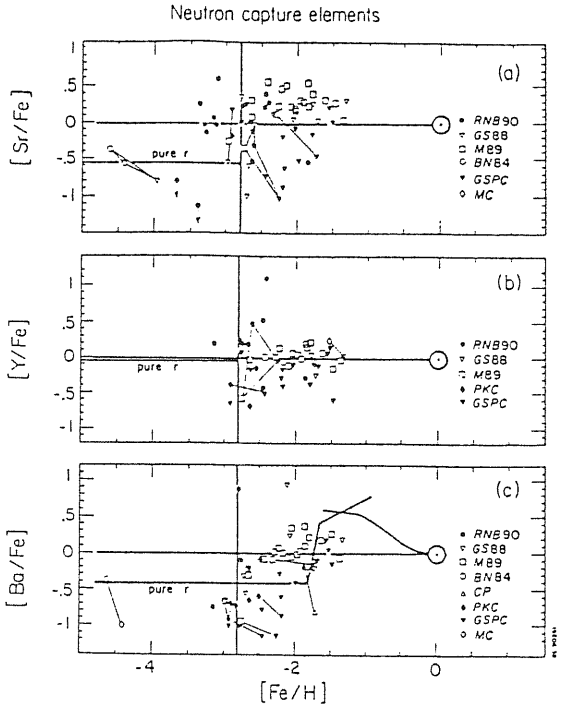

Figure 6.10: Relation between Sr, Y and Ba abundances and iron abundance; from Pagel (1991).

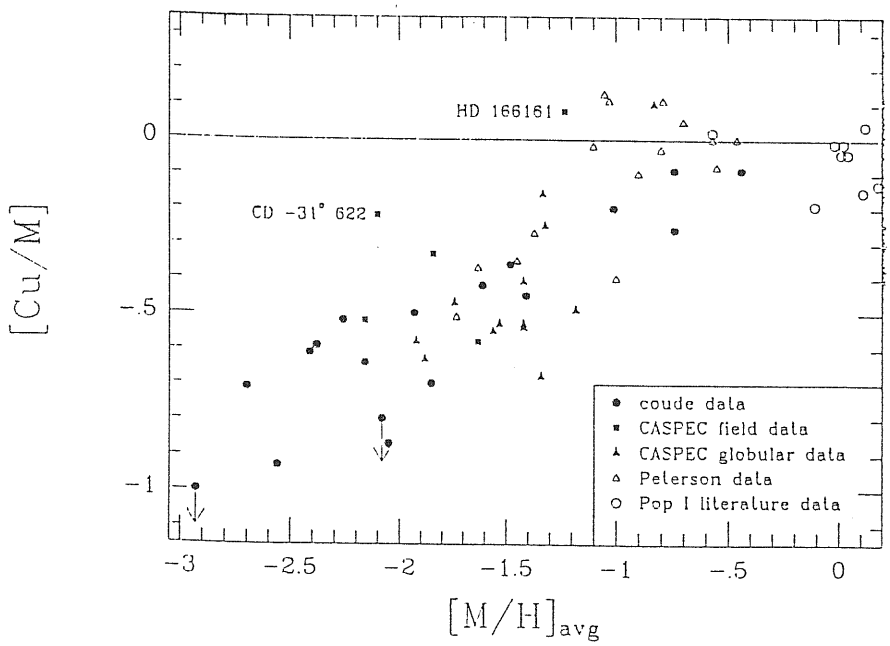

Figure 6.11: The behaviour of Cu as a function of metallicity; from Sneden, Gratton and Crocker (1991)

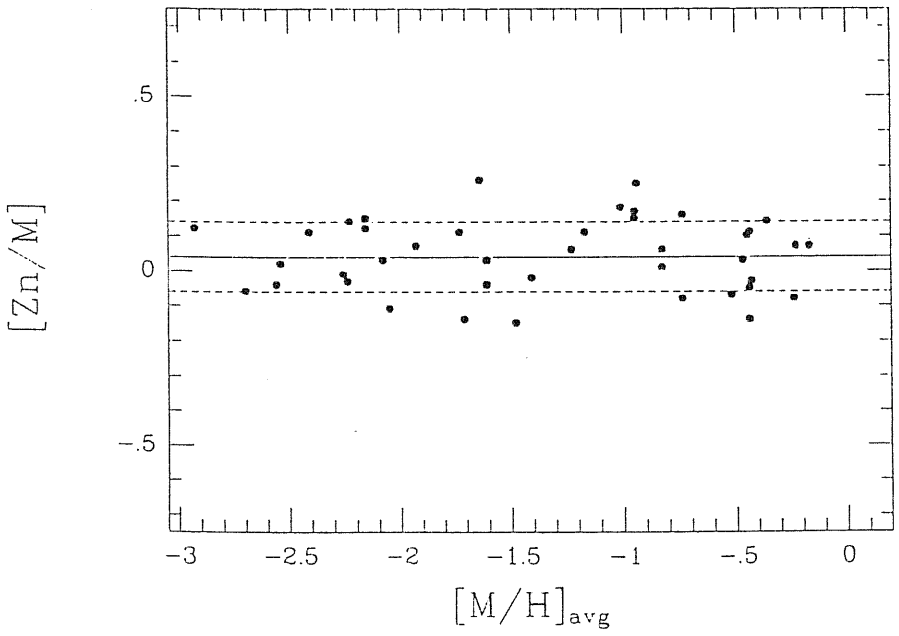

Figure 6.12: The trend of Zn with metallicity; from Sneden, Gratton and Crocker (1991)

Chapter 7

CONCLUSIONS

In this thesis we treated the problem of the origin of the *s*–elements, concentrating our attention on the atomic mass region from iron to strontium, where the weak component is believed to play the major role.

Since this component has long been ascribed to the nucleosynthesis occurring in massive stars, we reanalyzed the mechanism of *n*–captures in such stars with the most updated evolutionary models and nuclear inputs, in order to see whether it is possible to reproduce the solar–system distribution of the *s*–elements in the atomic mass region of interest.

We first ran evolutionary calculations of a typical massive star of 25 $M_\odot$ and solar composition, under canonical prescriptions. The *n*–capture process occurring during both core He–burning and shell C–burning was analyzed, studying the effects of variations within the present uncertainties of the $^{12}C(\alpha,\gamma)^{16}O$ and $^{22}Ne(\alpha,n)^{25}Mg$ rates as well as of other nuclear inputs.

The nucleosynthetic mechanism during core He burning is characterized by a low mean neutron density, which never exceeds 10^6 cm^{-3}. In agreement with previous investigations, we found a good production of the *s*–isotopes in the atomic mass range 70–90, the actual neutron exposure depending on some critical parameters such as the $^{12}C(\alpha,\gamma)^{16}O$ and $^{22}Ne(\alpha,n)^{25}Mg$ rates. Important contributions are found also for several light *n*–rich species and for the heavy rare isotopes ^{152}Gd and ^{180}Ta. Using the rates by CFHZ85, the process is characterized by a total neutron exposure $\tau = 0.206$ mb^{-1} and by a number of neutrons captured per ^{56}Fe seed $n_c = 5.665$.

A discussion of the nuclear stages following core He burning shows that during the He shell burning neutron captures do not occur, because of the too low temperature. On the contrary, a good contribution to the *s*–elements is given by shell carbon burning, that can spread convectively over almost all the CO core. The average neutron density here is very high at the beginning, (of the order of 10^{11} cm^{-3}), but then decreases rapidly, following an exponential law. Even if the neutron exposure in this phase is low ($\tau \approx 0.06$ mb^{-1}), nonetheless the final abundance

of the *s*–isotopes is noticeably affected.

The evaluation of the chemical composition of the stellar ejecta is not an easy task, and requires a very careful analysis of the evolutionary model in order to know how much He–processed and how much He+C–processed material is present. Moreover, one has to take into account that the subsequent Ne and O burning stages, by demanding high burning temperatures, lead to the photodissociation of the elements heavier than Fe. The same process is induced by the passage of the shock front during the supernova explosion.

The presupernova chemical structure however depends on the stellar mass, each star contributing in a different way to the chemical enrichment of the interstellar medium. This means that the *s*–yields from massive stars must be calculated by performing an integration over the Initial Mass Function of the contributions of a whole stellar generation. In order to estimate these yields, we assumed a Simple Model for the galactic chemical evolution, and required the solar abundance of ^{16}O to be reproduced, since oxygen is synthesized in massive stars in the same region as the *s*–isotopes. The calculation is performed in a scenario where stars more massive than 50 $M_\odot$ eject *s*–processed material only through stellar wind, while their cores collapse into black holes. This picture seems to be reliable according to the most recent observational works.

But the isotopes in the atomic mass range we are considering are also contributed by the *s*–process occurring in thermally pulsing AGB stars of low mass (which are responsible for the main component), and marginally by the *p*–process. When all the production mechanisms are included, we found that the solar–system distribution of *s*–isotopes is fairly reproduced, with an error which is largely explained by the uncertainties affecting the stellar models as well as the nuclear inputs. Hence we could conclude that, under the assumptions we made, *s–processing in massive stars is suitable to completely account for the weak component.*

The alternative picture, where stars with mass greater than 50 $M_\odot$ are allowed to successfully explode as supernovae, thus heavily contributing to the chemical enrichment of oxygen, leads to strong overproductions of the *s*–only isotopes in the atomic range 70–90 and must be discarded. In this sense, the *s*–process occurring in massive stars proves to be a useful tool to put constraints on the way the Galaxy has become metal rich.

We then investigated the process of nucleosynthesis occurring in massive stars of different metallicities, for the elements affected by the weak *s*–component. We found that a *secondary origin* for them is expected down to [Fe/H]$\simeq$–2, when the enhancement for the so–called α–nuclei is assumed to increase linearly in the disc and to remain flat at [α/Fe]=0.3 in the halo. For lower metallicities, the efficiency of the *s*–process sharply falls, due to the increasing strenght of the primary neutron poisons. The possibility of a higher neutron–capture cross section of ^{16}O, within a factor of 10 than currently assumed, would decrease even more the contribution from the *s*–process by massive stars in the halo, while preserving the secondary–like

behavior of the s–nuclei in the disc.

An observational check is not easy to undertake, since there is not a detectable element whose production is mainly ascribable to s–processing in massive stars. In fact, we have to distinguish among several nucleosynthetic mechanisms which must be responsible for the production of elements from Fe to Zr. Our predictions account satisfactorily for the observed trends, when the r–process is considered to be primary, and ascribed to type II supernovae, more likely of the lower mass range ($M \sim 10\ M_{\odot}$).

Finally, we presented some preliminary results for the chemical evolution of Cu and Zn, obtained with a detailed model for the chemical evolution of the Galaxy.

Many sources of uncertainty are still present in the kind of analysis we performed, chiefly related to the stellar models and to the input nuclear parameters. Presupernova models of different metallicities are missing; the models available show differences related to the particular evolutionary code that is used. As for the nuclear data, various neutron–capture cross sections are still poorly known. In particular, in the atomic mass region between Fe and Zr, cross sections are typically not known better than 10 %, while those characterizing unstable nuclei at branching points along the s–path are mainly calculated theoretically, with an uncertainty of 50 %. Moreover, the $^{12}C(\alpha,\gamma)^{16}O$ reaction rate is still given within a factor of 2, while that of $^{22}Ne(\alpha,n)^{25}Mg$ is affected by a large error at the low temperatures we are dealing with.

The way how carbon shell burning operates in stars of different masses needs further investigation too, and the amount by which the nucleosynthesis that occurs during the SN shock wave affects the results of hydrostatic He and C burning phases must be better defined, especially for the less massive stars, with $M \leq 20\ M_{\odot}$.

More refined computations of s–processing in massive stars, introducing recent improvements for the neutron capture cross sections of many isotopes, with a more complete analysis of $\sigma \neq 1/v$ trends, and a better estimate of the beta decay rates at the temperature typical for C burning are in progress.

The main results that I have obtained while working at this thesis have been already published, or are in course of publication. A list of the papers follows:

- Raiteri, C.M., Busso, M., Gallino, R., Picchio, G., and Pulone, L.: 1991, "s–Process Nucleosynthesis in Massive Stars and the Weak Component. I. Evolution and Neutron Captures in a 25 $M_{\odot}$ Star.", *Ap. J.* **367**, 228.

- Raiteri, C.M., Busso, M., Gallino, R., Picchio, G.: 1991, "s–Process Nucleosynthesis in Massive Stars and the Weak Component. II. Carbon Burning and Galactic Enrichment", *Ap. J.* **371**, 665.

- Raiteri, C.M., Gallino, R., and Busso, M.: 1991,"s–Processing in Massive Stars as a Function of Metallicity and Interpretation of Observational Trends", *Ap. J.*, submitted.

- Raiteri, C.M., Busso, M., Gallino, R., Picchio, G., and Pulone, L.: 1990, "s–Process in Massive Stars and the Weak Component", *Proceedings of the Elba Workshop on Chemical and Dynamical Evolution of Galaxies*, Marciana Marina, 3–13 September 1989, F. Ferrini, J. Franco, F. Matteucci (eds.), ETS, Pisa, p. 302-308.

- Raiteri, C.M., Busso, M., Gallino, R., and Picchio, G.: 1990, "Variations in the $^{12}C(\alpha,\gamma)^{16}O$ and $^{22}Ne(\alpha,n)^{25}Mg$ Reaction Rates and Their Consequences on the Stellar s–Process Nucleosynthesis", in *"Nuclei in the Cosmos"*, Baden/Vienna, 18–22 June 1990, p.281.

- Raiteri, C.M., Busso, M., Gallino, R., and Picchio, G. 1990, "s–process Yields from Type II Supernovae: Contributions to the Solar Composition from Iron to Zirconium", in *"SN1987A and Other Supernovae"*, Elba Workshp, Marciana Marina, 17–22 September 1990, in press.

- Raiteri, C.M., Gallino, R., and Busso, M.: 1991, "Galactic Enrichment of s–isotopes up to Zr", MPA Yellow Reports of the VI Workshop on *"Nuclear Astrophysics"*, Ringberg Castle (Germany), February 19–22, 1991, in press.

As a final comment I would like to thank Roberto Gallino for his continuous help and assistance, and Maurizio Busso for useful discussions.

Franz Käppeler and Hermann Beer are deeply acknowledged for a long–standing collaboration, that allows us always to deal with the most updated nuclear inputs.

I want also to thank Patrick François and Raffaele Gratton for many interesting discussions on the abundance observations, and Francesca Matteucci, who is working on our results with her code for the chemical evolution of the Galaxy.

Bibliography

[1] Abia, C., and Rebolo, R. 1989, *Ap. J.*, **347**, 186.

[2] Allen, B. J., and Macklin, R. L. 1971, *Phys. Rev C*, **3**, 1737.

[3] Almeida, J., and Käppeler, F. 1983, *Ap. J.*, **265**, 417.

[4] Alongi, M., Bertelli, G., Bressan, A., and Chiosi, C. 1991, *Astron. Astrophys.*, **244**, 95

[5] Anders, E., and Grevesse, N. 1989 (AG89), *Geochim. Cosmochim. Acta*, **53**, 197.

[6] Applegate, J. H., Hogan, C. J. and Scherrer, R. J. 1988, *Ap. J.*, **329**, 572

[7] Arcoragi, J.-P. 1986, in *Advances in Nuclear Astrophysics*, ed. E. Vangioni-Flam, J. Audouze, M. Casse, J. P. Chieze and J. Tran Thanh Van (Paris: Editions Frontières), p. 385.

[8] Arnett, W.D. 1972a, *Ap. J.* **176**, 681.

[9] Arnett, W.D. 1972b, *Ap. J.* **176**, 699.

[10] Arnett, W.D. 1977, *Ap. J.* **35**, 145.

[11] Arnett, W.D., and Truran, J.W. 1969, *Ap. J.***157**, 339.

[12] Arnett, W.D., and Thielemann, F.K. 1985, *Ap. J.* **295**, 589.

[13] Arnould, M. 1976, *Astron. Astrophys.*, **46**, 117

[14] Audouze, J., and Truran, J. W. 1975, *Ap. J.*, **202**, 204

[15] Bach, B., Oberhummer, H., Abele, H., and Staudt, G. 1990, in *From Miras to Planetary Nebulae: Which Path for Stellar Evolution?*, ed. E. O. Mennessier and A. Omont (Paris: Edition Frontières), p. 326

[16] Bao, Z. Y., and Käppeler, F. 1987, *Atomic Data and Nucl. Data Tables*, **36**, 411.

[17] Barbuy, B. 1988, *Astron. Astrophys.*, **191**, 121.

[18] Barnes, C. A., 1982, in *Essays in Nuclear Astrophysics*, ed. C. A. Barnes, D. D. Clayton, and D. N. Schramm (Cambridge: Cambridge University Press), p. 193.

[19] Beer, H. 1985, Kernforschungszentrum Karlsruhe Internal Report

[20] Beer, H. 1986, in *Advances in Nuclear Astrophysics*, ed. E. Vangioni-Flam, J. Audouze, M. Casse, J. P. Chieze and J. Tran Thanh Van (Paris: Editions Frontières), p. 375.

[21] Beer, H. 1991, *Ap. J.*, **375**, 823.

[22] Beer, H., and Macklin, R. L. 1988, *Ap. J.*, **331**, 1047.

[23] Beer, H., and Macklin, R. L. 1989, *Ap. J.* **339**, 962.

[24] Beer, H., Rupp, G., Voss, F., and Käppeler, F. 1989, *Proc. of Fifth Workshop on Nuclear Astrophysics*, Ringberg Castle, Bad Wiessee, p.20

[25] Beer, H., Voß, F., and Winters, F. F., 1991, "On the Calculation of Maxwellian Averaged Capture Cross Sections", preprint.

[26] Beer, H., Walter, G., and Käppeler, F. 1991, "Measurement of the ^{76}Se(n, γ) Capture Cross Section and Phenomenological *s*–process Studies: the Weak Component", preprint

[27] Bertelli, G., Bressan, A. G., and Chiosi, C. 1984, *Astron. Astrophys.* **130**, 279.

[28] Bertelli, G., Bressan, A. G., and Chiosi, C. 1985, *Astron. Astrophys.* **150**, 33.

[29] Bertelli, G., Bressan, A. G., Chiosi, C., and Angerer, K. 1986, *Astron. Astrophys. Suppl.* **66**, 191.

[30] Bessell, M. S., and Norris, J. 1987, *J. Astrophys. Astron.* **8**, 99.

[31] Boothroyd, A. I., and Sackmann, I.-J. 1988, *Ap. J.*, **328**, 632.

[32] Boothroyd, A. I., and Sackmann, I.-J. 1988, *Ap. J.*, **328**, 641.

[33] Boothroyd, A. I., and Sackmann, I.-J. 1988, *Ap. J.*, **328**, 653.

[34] Boothroyd, A. I., and Sackmann, I.-J. 1988, *Ap. J.*, **328**, 671.

[35] Bressan, A. G., Bertelli, G., and Chiosi, C. 1981, *Astron. Astrophys.*, **102**, 25.

[36] Brunish, W.M., and Truran, J.W. 1982a, *Ap. J.*, **256**, 247.

[37] Brunish, W.M., and Truran, J.W. 1982b, *Ap. J. Suppl.*, **49**, 447.

[38] Burbidge, G. R., Burbidge, E. M., Fowler, W. A., and Hoyle, F. 1957, *Rev. Mod. Phys.*, **29**, 547.

[39] Busso, M., and Gallino, R. 1985, *Astron. Astrophys.*, **151**, 205.

[40] Busso, M., Gallino, R., Picchio, G., and Chieffi, A. 1987, *Mem. S.A.It.*, **57**, 539.

[41] Busso, M., Picchio, G., Gallino, R., and Chieffi, A. 1988, *Ap. J.*, **326**, 196.

[42] Busso, M., Gallino, R., and Raiteri, C. M. 1991, Proc. of the *"VI Workshop on Nuclear Astrophysics"*, Ringberg Castle, Bad Wiessee, in press.

[43] Busso, M., Gallino, R., Lambert, D. L., Raiteri, C. M., and Smith, V. V. 1991, in preparation.

[44] Cameron, A. G. W. 1955, *Ap. J.*, **121**, 144.

[45] Cameron, A. G. W. 1973, *Space Sci. Rev.*, **15**, 121.

[46] Cameron, A. G. W. 1982, in *Essays in Nuclear Astrophysics*, ed. C. A. Barnes, D. D. Clayton and D. N. Schramm (Cambridge: Cambridge University Press), p. 23.

[47] Castellani, V., Giannone, P., and Renzini, A. 1971a, *Ap. Space Sci.*, **10**, 340.

[48] Castellani, V., Giannone, P., and Renzini, A. 1971b, *Ap. Space Sci.*, **10**, 355.

[49] Castellani, V., Chieffi, A., Pulone, L., and Tornambe', A. 1985, *Ap. J.*, **296**, 204.

[50] Caughlan, G. R., Fowler, W. A., Harris, M. J., and Zimmerman, B. A. 1985 (CFHZ85), *Atomic Data and Nucl. Data Tables*, **32**, 197.

[51] Caughlan, G. R., and Fowler, W. A. 1988 (CF88), *Atomic Data and Nucl. Data Tables*, **40**, 283.

[52] Chieffi, A., and Straniero, O. 1989, *Ap. J. Suppl.*, **71**, 47.

[53] Chiosi, C., and Maeder, A. 1986, *Ann. Rev. Astron. Astrophys.* **24**, 329.

[54] Chiosi, C., and Matteucci, F. 1984, in *Stellar Nucleosynthesis*, C. Chiosi and A. Renzini (eds.), D. Reidel Publ. Company, p.359.

[55] Chiosi, C., Bertelli, G., Bressan, A. 1988, *Astron. Astrophys.*, **196**, 84

[56] Chiosi, C., Bertelli, G., Meylan, G., Ortolani, S. 1989, *Astron. Astrophys.*, **219**, 167

[57] Clayton, D. D. 1988, *Mon. Not. Astr. Soc.* **234**, 1.

[58] Clayton, D. D., Fowler, W. A., Hull, T. E., and Zimmerman, B. A. 1961, *Ann. Phys.*, **12**, 331.

[59] Clayton, D. D., and Ward, R. A. 1974, *Ap. J.*, **193**, 397.

[60] Cosner, K., Iben, I., Jr., and Truran, J. W. 1980, *Ap. J. (Letters)*, **238**, L91.

[61] Cosner, K., and Truran, J. W. 1981, *Ap. Space Sci.*, **78**, 85.

[62] Couch, R. G., Schmiedekamp, A. B., and Arnett, W. D. 1974, *Ap. J.*, **190**, 95.

[63] Cowan, J. J., Thielemann, F–K., and Truran, J. W. 1991, *Phys. Rep*, in press.

[64] El Eid, M., and Baraffe, I 1990 Proc. Int. Symp. on Nuclear Astrophysics *"Nuclei in the Cosmos"*, H. Oberhummer and W. Hillebrandt (eds.), p.238.

[65] Fowler, W. A., Caughlan, G. R., and Zimmerman, B. A. 1967, *Ann. Rev. Astron. Astrophys.*, **5**, 525.

[66] Fowler, W. A., Caughlan, G. R., and Zimmerman, B. A. 1975 (FCZ75), *Ann. Rev. Astron. Astrophys.*, **13**, 69.

[67] Francçois, P. 1986, *Astron. Astrophys.*, **160**, 264.

[68] Fuller, G. M., Fowler, W. A., and Newman, M. J. 1982, *Ap. J. Suppl.*, **48**, 279.

[69] Gallino, R. 1989, in *Evolution of Peculiar Red Giant Stars*, Proc. IAU Coll. no. 106, ed. H. R. Johnson and B. Zuckerman (Cambridge: Cambridge Univ. Press), p. 176.

[70] Gallino, R., and Busso, M. 1985, in *From Nuclei to Stars*, ed. A. Molinari and R. A. Ricci (Amsterdam: North-Holland), p. 309.

[71] Gallino, R., Busso, M., Picchio, G., Raiteri, C. M., and Renzini, A. 1988, *Ap. J. (Letters)*, **334**, L45.

[72] Gallino, R., Busso, M., Picchio, G., and Raiteri, C. M. 1990a, *Nature*, **348**, 298

[73] Gallino, R., Busso, M., Picchio, G., and Raiteri, C. M. 1990b, in *"SN1987A and Other Supernovae"*, ESO Workshop, Marciana Marina, in press

[74] Gallino, R., Busso, M., Picchio, G., and Raiteri, C. M. 1990c, in *"Chemical and Dynamical Evolution of Galaxies"*, F.Ferrini, J. Franco, F. Matteucci (eds.), ETS, Pisa.

[75] Gallino, R., Beer, H., Busso, M., Corcione, L., and Raiteri, C. M. 1991, in *"VI Workshop in Nuclear Astrophysics*, Ringberg Castle, Bad Wiessee, in press

[76] Gratton, R. G. 1990, "Oxygen Abundances in Metal–Poor Stars from Permitted and Forbidden Lines", preprint.

[77] Gratton, R. G., and Ortolani, S. 1986, *Astron. Astrophys.*, **169**, 201.

[78] Gratton, R. G., and Sneden, C. 1991, *Astron. Astrophys.*, **241**, 501.

[79] Gustafsson, B.: 1989, *Ann. Rev. Astr. Ap.*, **27**, 701.

[80] Habets, G.M.H.J. 1986, *Astron. Astrophys.*, **167**, 61

[81] Hartmann, D., Woosley, S. E., and El Eid, M. F. 1985, *Ap. J.*, **297**, 837

[82] Hollowell, D. E., and Iben, I., Jr. 1988, *Ap. J. (Letters)*, **333**, L25.

[83] Hollowell, D. E., and Iben, I., Jr. 1989, *Ap. J.*, **340**, 966.

[84] Holmes, J. A., Woosley, S. E., Fowler, W. A., and Zimmerman, B. A. 1976, *Atomic Data and Nucl. Data Tables*, **18**, 305.

[85] Howard, W. M., Meyer, B. S., and Woosley, S. E. 1991, *Ap. J.*, **373**, L5

[86] Iben, I., Jr. 1975, *Ap. J.*, **196**, 549.

[87] Iben, I., Jr. 1982, *Ap. J.*, **260**, 821.

[88] Iben, I., Jr., and Renzini, A. 1982a, *Ap. J. (Letters)*, **259**, L79.

[89] Iben, I., Jr., and Renzini, A. 1982b, *Ap. J. (Letters)*, **263**, L23.

[90] Ikeuchi, S., Nakazawa, K., Murai, T., Hoshi, R., and Hayashi, C. 1971, *Progr. Theor. Phys.*, **46**, 1713.

[91] Käppeler, F., Beer, H., Wisshak, K., Clayton, D. D., Macklin, R. L., and Ward, R. A. 1982, *Ap. J.*, **257**, 821.

[92] Käppeler, F., Beer, H., Wisshak, K., 1989, *Reports on Progress in Physics*, **52**, 945.

[93] Käppeler, F., Gallino, R., Busso, M., Picchio, G., and Raiteri, C.M. 1990a, *Ap. J.* **354**, 630.

[94] Käppeler, F., Zhao, W.R., Beer, H., and Ratzel, U., 1990b, *Astron. Astrophys.*, **355**, 348.

[95] Kilston, S.: 1975, *PASP*, **87**, 189.

[96] Kippenhan, R., Weigert, A., and Hofmeister, E. 1967, in *Methods in Computational Physics* vol.7, Astrophysics Academic press, p.129.

[97] Klay, N., and Käppeler, F. 1988, *Phys. Rev. C*, **38**, 295.

[98] Lamb, S., Iben, I.Jr., and Howard, W.M. 1976, *Ap. J.*, **207**, 209.

[99] Lamb, S., Howard,W.M., Truran, J.W., and Iben, I.Jr. 1977, *Ap. J.*, **217**, 213.

[100] Lambert, D. L. 1985, in *Cool Stars with Excesses of Heavy Elements*, ed. M. Jaschek and P. C. Keenan, (Dordrecht: Reidel), p. 191.

[101] Lambert, D. L. 1989, in *"Cosmic Abundances of Matter"*, C. J. Weddington (ed.), New York, Amer. Inst. Phys., p.168.

[102] Lambert, D.L.: 1991, in *'Evolution of Stars: the Photospheric Abundance Connection'* ed. G. Michaud and A. Tutukov, p. 299.

[103] Lambert, D. L., Gustafsson, B., Erichsson, K., and Hinkle, K. H. 1986, *Ap. J. Suppl.*, **62**, 373

[104] Lamers, H. J. G. L. M. 1981, *Ap. J.*, **245**, 593.

[105] Langer, N. 1986a, Phd. Thesis, unpublished.

[106] Langer, N. 1986b, *Astron. Astrophys.*, **164**, 45.

[107] Langer, N., El Eid, M. F., and Fricke, K.J. 1985, *Astron. Astrophys.*, **145**, 179.

[108] Langer, N., Arcoragi, J.-P., and Arnould, M. 1989, *Astron. Astrophys.* **210**, 187.

[109] Lattanzio, J. C. 1989, in *" Evolution of Peculiar Red Giant Stars"*, H. R. Johnson and B. Zuckerman (eds.) (Cambridge: Cambridge University Press), p.131

[110] Lewis, R.S., Amari, S. and Anders, E.: 1990, *Nature*, **348**, 293.

[111] Luck, R. E., and Bond, H. E. 1985, *Ap. J.*, **292**, 559.

[112] Maeder, A. 1981a, *Astron. Astrophys.* **101**, 385.

[113] Maeder, A. 1981b, *Astron. Astrophys.* **102**, 401.

[114] Maeder, A., and Meynet, G. 1987, *Astron. Astrophys.* **182**, 243.

[115] Maeder, A., and Meynet, G. 1989, *Astron. Astrophys.* **210**, 155.

[116] Magain 1989, *Astron. Astrophys.*, **209**, 211.

[117] Malaney, R. A., and Fowler, W. A. 1988, *Ap. J.*, **333**, 14

[118] Malaney, R. A., and Lambert, D. L. 1988, *M.N.R.A.S.*, **235**, 695.

[119] Mathews, G. J., and Cowan, J. J. 1990, *Nature*, **345**, 491.

[120] Matteucci, F. 1986, *Mon. Not. R. Astron. Soc.*, **221**, 911.

[121] Matteucci, F. 1988, in *"Origin and Distribution of the Elements"*, G. J. Mathews (ed.), World Scientific, p. 186.

[122] Matteucci, F., anf François, P. 1989, *Mon Not. R. astr. Soc.*, **239**, 885

[123] Nomoto, K., and Hashimoto, M. 1988 (NH88), *Phys. Reports*, **163**, 13.

[124] Olive, K.A., Thielemann, F-K, and Truran, J.W. 1987, *Ap. J.*, **313**, 813.

[125] Pagel, B. E. J. 1991, "Abundances in Galaxies", preprint.

[126] Prantzos, N., Arnould, M., and Arcoragi, J.P. 1987, *Ap. J.* **315**, 209.

[127] Prantzos, N., Hashimoto, M., and Nomoto, K. 1990, *Astron. Astrophys.* **234**, 211.

[128] Ratynski, W., and Käppeler, F. 1988, *Phys. Rev. C*, **37**, 595.

[129] Rayet, M., Prantzos, N., and Arnould, M. 1990, *Astron. Astrophys.*, **227**, 271

[130] Reeves, H. 1966, *Ap. J.*, **146**, 447.

[131] Reimers, D. 1975, *Mem. Soc. Roy. Liege 6th. Ser*, **8**, 369.

[132] Schwarzschild. M. 1958, in *Structure and Evolution of Stars*, (New York: Dover Publ. Inc.), p.167.

[133] Seeger, P. A., Fowler, W. A., and Clayton, D. D. 1965, *Ap. J. Suppl.*, **11**, 121.

[134] Smith, V. V., and Lambert, D. L. 1985, *Ap. J.*, **294**, 326.

[135] Smith, V. V., and Lambert, D. L. 1986, *Ap. J.*, **311**, 843.

[136] Sneden, C., Gratton, R. G., and Crocker, A. 1991, *Astron. Astrophys.*, **246**, 354.

[137] Sneden, C., Lambert, D. L., and Whitaker, R. W. 1979, *Ap. J.*, **234**, 684.

[138] Spite, M., and Spite, F. 1978, *Astron. Astrophys.*, **67**, 23.

[139] Spite, M., and Spite, F. 1985, *Ann. Rev. Astron. Astroph.*, **23**, 225.

[140] Straniero, O. 1989, *Astron. Astrophys. Suppl.* **76**, 157.

[141] Takahashi, K., and Yokoi, K. 1987, *Atomic Data and Nucl. Data Tables*, **36**, 375.

[142] Talbot, R.J.Jr, and Arnett, W.D. 1973, *Ap. J.*, **186**, 51.

[143] Tang, M., and Anders, E. 1988, *Geochim. Cosmochim. Acta*, **52**, 1235.

[144] Thielemann, F.-K. 1989, in *"Nuclear Astrophysics'*, Lorano, M., Gallardo, M. I, and Arias, J. M. (eds.), Springer Verlag, p. 106

[145] Thielemann, F.K., and Arnett, W.D. 1985, *Ap. J.*, **295**, 604.

[146] Thielemann, F.-K., Nomoto, K., and Yokoi, K. 1986, *Astron. Astrophys.*, **158**, 17

[147] Thielemann, F.-K., Hashimoto, M., and Nomoto, K. 1990, *Ap. J.*, **349**, 222.

[148] Thielemann, F.-K., Nomoto, K., and Hashimoto, M. 1990, *Chemical and Dynamical Evolution of Galaxies*, F. Ferrini, J. Franco, F. Matteucci (eds.), ETS, Pisa, p.373.

[149] Thielemann, F.-K., Hashimoto, M., Nomoto, K., and Yokoi, K. 1989, in *"Supernovae"*, S. E. Woosley (ed.), Springer Verlag, New York, in press

[150] Tinsley, B. M. 1980, *Fundam. of Cosmic Phys.*, **5**, 287.

[151] Truran, J. W. 1981, *Astron. Astrophys.*, **97**, 391.

[152] Truran, J. W., and Iben, I., Jr. 1977, *Ap. J.*, **216**, 797.

[153] Twarog, B. A., and Wheeler, J. C. 1987, *Ap. J.*, **316**, 153.

[154] Ulrich, R. K. 1973, in *Explosive Nucleosynthesis*, ed. D. N. Schramm and W. D. Arnett (Univ. of Texas: Austin), p. 139.

[155] Utsumi, K. 1985, in *Cool Stars with Excesses of Heavy Elements*, ed. M. Jaschek and P. C. Keenan, (Dordrecht: Reidel), p. 243.

[156] Walker, T. P., Mathews, G. J., and Viola, V. E. 1985, *Ap. J.*, **299**, 745

[157] Wallerstein, G., Dominy, J. F. 1988, *Ap. J.*, **330**, 937.

[158] Walter, G., and Beer, H. 1985, *Astron. Astrophys.*, **142**, 268.

[159] Ward, R. A., Newman, M. J., and Clayton, D. D. 1976, *Ap. J. Suppl.*, **31**, 33.

[160] Ward, R. A., and Newman, M. J. 1978, *Ap. J.*, **219**, 195.

[161] Weaver, T.A., Zimmerman, G.B., and Woosley, S.E. 1978, *Ap. J.* **225**, 1021.

[162] Wheeler, J. C., Sneden, C., and Truran, J. W. Jr. 1989, *Ann. Rev. Astron. Astrophys.*, **27**, 279

[163] Winters, R. R., and Macklin, R. L. 1988, *Ap. J.*, **329**, 943.

[164] Wolke, K., Harms, V., Becker, H.W., Hammer, J.W., Kratz, K.L., Rolfs, C., Schröder, U., Trautvetter, H.P., Wiescher, M., and Wöhr, A., 1989, *Z. Phys. A*, **334**, 491.

[165] Woosley, S. E. 1986, in *Nucleosynthesis and Chemical Evolution*, B. Hauck, A. Maeder, and G. Meynet (eds.), Geneva Obs., Sauverny, Switzerland, p.1.

[166] Woosley, S.E., and Weaver, T.A. 1986, in *"Nucleosynthesis and its Implications on Nuclear and Particle Physics"*, Audouze, J. and Mathieu, N. (eds.), p.145.

[167] Woosley, S.E., and Weaver, T.A. 1988, *Phys. Reports*, **163**, 79.

[168] Woosley, S. E., and Howard, W. M. 1978, *Ap. J.* Suppl., **36**, 295

[169] Zhao, G., and Magain, P. 1990, *Astron. Astrophys.*, **238**, 242.

[170] Zinner, E., Tang, M., and Anders, E. 1987, *Nature*, **330**, 730

[171] Zinner, E., Tang, M., and Anders, E. 1989, *Geochim. Cosmochim. Acta*, **53**, 3273

[172] Yang, J., Turner, M. S., Steigman, G., Schramm, D. N., and Olive, K. A. 1984, *Ap. J.*, **281**, 493

[173] Yokoi, K., and Takahashi, K. 1983, *Nature*, **305**, 198.

List of Tables

List of Figures